Ontario Hydro

COMPLIMENTARY COPY
Please Credit Ontario Hydro Research if
Reproduced In Whole or In Part

Memorandum To DISTRIBUTION

Date May 1, 1986

Location or Dept

File 827.2(T)

Subject Preliminary Evaluation of the Corrosion Performance of Materials for Lake Water Cooled Nuclear Heat Exchanger (HX) Tube Applications (Report No 86-86-K)

The attached report by B. Warr and S. Thorpe of the Corrosion and Tritium Technology Section was initially produced in draft form about a year ago. Review comments were sought from clients and those having a need to know. There was an urgent need at that time and throughout 1985, by designers and operations staff, to assess materials selection needs and rationale for replacement HX's in moderators and shutdown coolers at PNGS and DNGS. This stimulated vigorous and productive discussions of the material in this report and contributed to important materials input required. It also contributed to a competition for resources required to extend and expand the support R&D work in this area such as pit propagation testing and construction of a HX test rig. These factors combined with S. Thorpe moving to the Massachusettes Institute of Technology (MIT) for Post Doctoral studies beginning in the Summer of 1985, and the necessity to move B. Warr, full time, into the high priority Zr corrosion area beginning in May 1985, have resulted in delays in issuing this report.

This report represents an attempt at combining the laboratory assessment of corrosion performance in a substantial number of HX alloys in simulated environments with a conservative interpretation and prediction of long term performance. It is important to note the following in using this material:

- The tests carried out so far have been necessarily limited in number and scope. This was a result of urgent client needs to get basic answers as quickly as possible.

- The conclusions drawn are based on our best materials assessment at that time. Other criteria including site performance and financial evaluations must be integrated with this to provide specific materials selection decisions.

DISTRIBUTION

May 1, 1986

- More detailed programs (already underway) are required to give more fully quantitative predictive evaluations of long term performance.

- Because of the above, the conclusions are in our opinion prudently conservative.

- The material contained in this report represents valuable reference documentation. The large amount of detail and complexity in some of the data require a great deal more interpretation and understanding. For example, as our understanding of CPP plots deepens through more fundamental work (in progress), those data contained in this report may provide even more understanding.

- This report represents part of a large ongoing work area in HX corrosion performance. Samples used are archived so that additional evaluation (for example more detailed metallography) may be performed if required in the future. The results as reported here are an interim presentation of the basic features of the work as selectively detailed by the authors.

- Recent work (not contained in this report) providing estimates for pit propagation rates in I825 and S28 materials have provided additional data giving increased confidence in the use of these materials for HX life extension over the historical experience with I800.

Recent progress in all on-going HX research programs, and updates to the work described in the attached report, are contained in a report being written by P. King of this section.

P.C. Lichtenberger
Supervising Scientist
Corrosion & Tritium Technology
(Ext 122+6175)

PCL:md

91602
new 82-10

ontario hydro
research division

PRELIMINARY EVALUATION OF THE CORROSION PERFORMANCE OF MATERIALS FOR LAKE WATER-COOLED NUCLEAR HEAT EXCHANGER TUBE APPLICATIONS

Report No 86-86-K

B. Warr - Engineer
Metallurgical Research Dept

S. Thorpe
NATO Science Fellow
Massachusetts Institute of Technology

ABSTRACT

Electrochemical and immersion tests have been conducted in the laboratory to evaluate the corrosion performance of materials for lake water-cooled nuclear heat exchanger tube applications. Pitting corrosion was observed in all the materials tested with the exception of Titanium and Inconel 625. Based on these results, and the good external experience with Titanium, it is expected to be immune to pitting corrosion in lake water-cooled heat exchangers. Similarly, it is highly likely that Inconel 625 will perform adequately for a full design life (typically 30 years), although practical experience with this material is limited. Of the remaining materials tested, AL6X in particular, and 904L appear to be somewhat superior, although pits were observed on both these materials. The tests carried out so far have been limited in number and scope and a more detailed program of work currently underway is required to give a fully quantitative predictive evaluation of long term peformance. However these simulated tests provide a basic conservative materials assessment. Using this criteria and, based on their high propensity for pit initiation when compared to Incoloy 800,

job	file	date	report no.
740682-145-552	827.2	May 1, 1986	86-86-K

the materials Sanicro 28 and Incoloy 825 are not recommended tor heat exchanger service since the rate of pit propagation in these materials is currently unknown. The Copper-Nickel alloys Monel 400 and 70-30 Copper-Nickel showed poor resistance to general corrosion and pitting attack. This is consistent with the performance history of Monel 400 heat exchangers at Pickering B, but inconsistent with the generally good performance ot 70-30 Copper-Nickel heat exchangers in service. This report provides a preliminary laboratory materials' evaluation of currently used and potentially candidate heat exchanger materials for lakewater service. Additional site performance, and cost benefit criteria may be required for specification of individual materials selection decisions. The material contained in this report also provides extensive reference metallographic data that can be used as a basic guide to compare, focus and extend future required work in this area.Suggested areas for further work include on-site heat exchanger test rig materials testing, and laboratory tests to provide a fundamental understanding of the corrosion processes, and further quantify the pit initiation probabilities and propagation rates (and their variability) for the materials tested.

91602
new 82-10

ontario hydro
research division

EXECUTIVE SUMMARY

PRELIMINARY EVALUATION OF THE CORROSION PERFORMANCE OF MATERIALS FOR LAKE WATER-COOLED NUCLEAR HEAT EXCHANGER TUBE APPLICATIONS

B. Warr
Corrosion and Tritium Technology
Metallurgical Research Department

S. Thorpe
NATO Science Fellow
Massachusetts Institute of Technology

Corrosion of lake water-cooled nuclear plant heat exchanger tubes have resulted in economic losses to Ontario Hydro estimated to date at 100 M$. Failures of Moderator heat exchangers and Shutdown Coolers at Pickering B, attributed to under-deposit pitting corrosion, resulted in the need to replace their tube bundles with materials more resistant to pitting corrosion. The objective of this work, therefore, is to help provide a basis for material selection. Electrochemical and immersion tests have been conducted in the laboratory to evaluate the corrosion performance of heat exchanger tube materials in low temperature Lake Ontario water environments. A limitation of these tests arises from the inability to simulate continuous flow of lake water. This can produce local environments at the tube surface which are more concentrated in trace chemical impurities and contain a different biological make-up compared to stagnant water.

Materials tested were Titanium, Inconel 625, AL6X, 904L, Sanicro 28, Incoloy 825, Incoloy 800, and the Copper-Nickel alloys Monel 400, and 70-30 Copper-Nickel. Pits were observed in all materials with the exception of Titanium and Inconel 625. Titanium showed the greatest resistance to pitting corrosion. Based on these results and the excellent external service experience with this material, it is expected to be immune to pitting corrosion in lake water-cooled heat exchangers. Inconel 625 also exhibited high resistance to pitting attack in our tests. Although practical service experience with this material is

job	file	date	report no.
740682-145-552	827.2	May 1, 1986	86-86-K

limited, it is highly likely that it will also perform adequately in lake water service. The materials AL6X and 904L were somewhat superior to the remaining materials tested although pits were observed following testing (especially in 904L) indicating their propensity tor pit initiation. There is some indication that the presence of molybdenum in these alloys may inhibit pit growth; further work is required to quantitatively assess this. The materials Sanicro 28, Incoloy 825 and Incoloy 800 displayed a high susceptibility to pitting corrosion. In certain electrochemical tests, more pits were observed in Sanicro 28 and Incoloy 825 than in Incoloy 800. In view ot the poor service performance of Incoloy 800, these materials are not recommended tor use in heat exchanger service applications since the rate of propagation of pits in these materials is currently unknown, and the nucleation propensity ot pits in these materials is higher in these tests than for Incoloy 800. Finally, both Copper-Nickel alloys, Monel 400 and 70-30 Copper-Nickel, showed poor resistance to both general corrosion and pitting attack in the present tests. These materials have, however, shown good service performance in Pickering A heat exchangers and should not be ruled out as future candidate materials.

Further work should be directed primarily towards field testing of materials using a heat exchanger test rig. Laboratory studies are also proposed to provide a fundamental understanding of the corrosion processes, allow for increased confidence in extrapolating data obtained in laboratory tests to the field, and to further establish pit initiation probabilities and propagation rates for the materials tested.

This report provides a preliminary laboratory materials' evaluation of currently used and potentially candidate heat exchanger materials for lakewater service. The results and conclusions have been drawn from tests limited in number and scope and provide an initial basic conservative materials' assessment. More detailed testing and simulation of real heat exchanger operating conditions (in progress) are required to give a more fully quantitative predictive evaluation of expected long term site performance. Additional site performance and cost benefit criteria may be required for specification of individual materials' selection decisions.

The material contained in this report also provides extensive reference metallographic data that can be used as a basic guide to compare, focus, and extend future required work in this area.

TABLE OF CONTENTS

		Page
1.0	INTRODUCTION	1
	1.1 Program Objectives	1
	1.2 Historical Perspective of Heat Exchanger Failures	1
	1.3 Pitting Corrosion	3
	1.4 Interpretation of Potential-Current Relationships	5
	1.5 Materials	7
2.0	EXPERIMENTAL PROCEDURE	7
	2.1 Materials	8
	2.2 Electrochemical Testing	8
	2.3 Immersion Testing	10
	2.3.1 Heat Flux Immersion Testing	10
	2.3.2 Isothermal Immersion Testing	10
3.0	RESULTS	10
	3.1 Materials Tested	10
	3.2 Electrochemical Tests	11
	3.2.1 Cyclic Potentiodynamic Polarization (CPP)	11
	3.2.2 Potentiostatic Polarization (PP)	13
	3.3 Immersion Tests	13
4.0	DISCUSSION	14
	4.1 Materials	14
	4.2 Electrochemical Tests	15
	4.2.1 Cyclic Potentiodynamic Polarization	15
	4.2.2 Pit Induction Testing	18
	4.2.3 Metallographic Analysis of Samples Following Electrochemical Testing	19
	4.3 Immersion Tests	21
	4.4 Limitations	22
5.0	CONCLUSIONS	22
6.0	RECOMMENDATIONS	23
ACKNOWLEDGEMENTS		25
TABLES		26
FIGURES		35
REFERENCES		85
APPENDIX 1		87
DISTRIBUTION		last page

LIST OF TABLES

Table		Page
1	Ontario Hydro Nuclear Plant Heat Exchanger Data	26
2	Ranking of Austenitic Stainless Steels in Seawater by Pitting Temperature (°C) and Pitting Index (wt% Cr + 3.3 wt% Mo)	27
3	(a) Materials for Test Program	28
	(b) Detailed Analyses of Materials Tested	29
4	Charge Difference (ΔQ) (in Lake Water at 40°C) for Various Combinations of Scan Rate and Material Surface Condition	30
5	Pitting Potentials (in Lake Water at 40°C) for All Materials Using a Scan Rate of 1.2 V/h and Initial Surface Condition of 600 grit	31
6	Observations of Surface Appearance of Samples Following CPP Testing	32
7	Summary of Results of Isothermal and Heat Flux Immersion Testing	33
8	Summary of Results of EDX Analyses Within Pits	34

LIST OF FIGURES

Figures		Page
1	Tubes, Deposits and Evidence of Underdeposit Corrosion in Tube Bundles Removed from Pickering GS 'A' Unit 3 Moderator HX	35
2	Stages in Crevice Corrosion	36
3	Schematic of E vs log i Response for Stainless Steels in Acidic Media	37
4	Method of Determination of Pit Incubation Time (t_{inc}) where t_{inc} = Global minima in plot of i versus t at constant potential	38
5	Electrochemical Test Apparatus - Schematic	39
6	Heat Flux Immersion Test Apparatus - Schematic of One Test Cell	40
7	Heat Flux Immersion Test Program Schedule	41
8	Isothermal Immersion Test Apparatus - Schematic	42
9	OHRD Isothermal (40°C) Immersion Test Schedule (All Materials)	43
10	Isothermal Immersion Test Program at AECL-CRNL	44
11	Tube Through-Wall Composite Microstructure (a) Ti, (b) I625, (c) AL6X	45
12	Tube Through-Wall Composite Microstructure (a) 904L, (b) S28, (c) I825	46
13	Tube Through-Wall Composite Microstructure (a) I800, (b) M400, (c) 70/30	47
14	Cyclic Potentiodynamic Polarization (CPP) Forward Plots for Ti, I625, AL6X, 904L, S28, I825 and I800 for all Combinations of Scan Rate and Surface Condition	48-51
15	Cyclic Potentiodynamic Polarization (CPP) Forward Plots for M400 and 70/30 for all Combinations of Scan Rate and Surface Condition	52-55

LIST OF FIGURES (cont'd)

Figures		Page
16	95% Confidence Intervals for Four CPP Tests for I825-Forward Scan (Scan Rate 0.25 V/h, 600 grit)	56
17	CPP (Forward Scan) for I825 at an Initial Surface Condition of 600 grit, Showing Effect of Scan Rate	57
18	CPP (Forward Scan) for I825 at a Scan Rate of 0.25 V/h Showing Effect of Initial Surface Condition	58
19	CPP Plots for a Scan Rate of 0.25 V/h and Initial Surface Condition of 600 grit. All Materials	59-67
20	Temperature Dependence of ΔQ for I800, 904L, S28, I825 and I625 (Scan Rate 1.2 V/h, As-Received Condition)	68
21	Surface Appearance of Ti Tube Sample Following CPP Testing at a Scan Rate of 0.25 V/h and Initial Surface Condition of 600 grit	69
22	Surface Appearance of I625 Tube Sample Following CPP Testing at a Scan Rate of 0.25 V/h and Initial Surface Condition of 600 grit	70
23	Surface Appearance of AL6X Tube Sample Following CPP Testing at a Scan Rate of 0.25 V/h and Initial Surface Condition of 600 grit	71
24	Surface Appearance of 904L Tube Sample Following CPP Testing at a Scan Rate of 0.25 V/h and Initial Surface Condition of 600 grit	72
25	Surface Appearance of S28 Tube Sample Following CPP Testing at a Scan Rate of 0.25 V/h and Initial Surface Condition of 600 grit	73
26	Surface Appearance of I825 Tube Sample Following CPP Testing at a Scan Rate of 0.25 V/h and Initial Surface Condition of 600 grit	74
27	Surface Appearance of I800 Tube Sample Following CPP Testing at a Scan Rate of 0.25 V/h and Initial Surface Condition of 600 grit	75

LIST OF FIGURES (cont'd)

Figures		Page
28	Surface Appearance of M400 Tube Sample Following CPP Testing at a Scan Rate of 0.25 V/h and Initial Surface Condition of 600 grit	76
29	Surface Appearance of 70/30 Tube Sample Following CPP Testing at a Scan Rate of 0.25 V/h and Initial Surface Condition of 600 grit	77
30	Detailed Examination of Pits Arising from Cyclic Potentiodynamic Polarization Testing (Scan Rate 0.25 V/h, 600 grit)	78
31	Pit Incubation Times (t_{inc}) vs Applied Potential (E) for I800, I825 and AL6X	80
32	Detailed Examination of Sample Surfaces Following Immersion Testing	81
33	Nickel and Chromium Equivalents for Fe-Ni-Cr-Mo Austenitic Alloys Tested	83
34	Binary Phase Diagram, Ni-Cu System	84

91601
new 82-10

ontario hydro
research division

To Mr. B. Monttord
Manager Chemistry & Metallurgy Department
Central Nuclear Services
Technical & Training Services Division

PRELIMINARY EVALUATION OF THE CORROSION PERFORMANCE OF MATERIALS FOR LAKE WATER-COOLED NUCLEAR HEAT EXCHANGER TUBE APPLICATIONS

1.0 INTRODUCTION

1.1 Program Objectives

The major objective of the work reported here is to provide a basis for material selection for low temperature heat exchanger (HX) tube applications in Lake Ontario water/1,2/. This work has been requested and supported by TTSD-CNS, primarily as a result of the need to specify replacement materials for Moderator HXs and Shutdown Coolers at Pickering and Darlington. Given the large number of tube corrosion failures in lake water cooled HXs, however, it is likely that the results of this program will have a wider application within the corporation, in the selection of HX tube materials for lake water service.

The work reported here was directed towards providing an initial assessment of:

(i) the general corrosion resistance,

(ii) the localized corrosion resistance,

(iii) the temperature sensitivity of the corrosion behaviour,

(iv) the effect of deposits on the corrosion behaviour, and

(v) the effect of heat flux on the corrosion behaviour ot candidate materials.

1.2 Historic Perspective of Heat Exchanger Failures

Nuclear plant HXs transfer heat trom one station system or component to another. The majority of HXs in use in

Ontario Hydro operating plants consist of a number of tubes, either straight or U-bent, attached to a common tubesheet, with support plates along their length, and contained in a shell of mild steel. Tube materials are mostly copper-nickel alloys and Fe-Ni-Cr austenitic alloys. Table 1/3,4/ provides a summary of available data and failure mechanisms to date for HXs in Ontario Hydro nuclear plants.

It is convenient to categorize HXs into two groups. Those operating at high temperatures, generally above 100°C, which include steam generators, feed-water heaters, reheaters, and bleed condensers and coolers, and those operating predominantly at temperatures below 100°C. In this first group, untreated lake water does not interface with the HX tubes. The environment consists of recirculating demineralized water, heat transport heavy water or steam/feed-water. As shown in Table 1, tube corrosion mechanisms have been mainly of the type of environmental cracking occurring at high temperatures such as stress corrosion cracking (SCC) and corrosion fatigue(CF).

In the latter group are included the moderator HXs, shutdown coolers, condensers, recirculating cooling water HXs, end shield coolers and various other small HXs which serve to cool a variety of system components such as pumps, compressors and lubricating oil systems. The majority of these HXs interface with lake water. Heavy water is usually routed through the tube inside surface (ID), with the lake water flowing on the shell-side. With this mode of operation, lake water deposits tend to form on the tube outside surface (OD). These deposits, shown on a tube bundles removed from a Moderator HX at Pickering A in Figure 1, can then act as sites for underdeposit crevice/pitting corrosion. This report deals exclusively with the corrosion testing of tube materials for this second group of HXs which interface directly with lake water.

Underdeposit pitting corrosion has resulted in tube failures in a number of lake water cooled HXs in operating nuclear plants as shown in Table 1. Recently, tube leaks in two critical HXs at Pickering, the Moderator HXs and the Shutdown Coolers, have resulted in significant economic losses. Tube failures have been associated with underdeposit pitting corrosion based on examination of tubes removed from these HXs. The exact mechanism(s) responsible for the underdeposit pitting attack in both HXs is presently unknown. To date, total economic losses arising from HX tube corrosion, including replacement energy costs, and the costs arising from bundle replacement, amount to 100 M$/5/.

Moderator HXs at Douglas Point and later Pickering A were tubed with 70-30 Cu-Ni (70/30). This material was found to perform

adequately with no significant underdeposit corrosion damage reported following metallurgical examination of tubes removed from Pickering A/6,7/. Fretting failures did occur, however, at Pickering A resulting in the eventual replacement of a failed tube bundle with another tubed with Incoloy 800 (I800). This replacement material subsequently failed after approximately two years service as a result ot underdeposit pitting corrosion initiating and propagating under lake water deposits on the tube OD/8,9/. Subsequent replacement bundles for Pickering A were tubed with 70/30. The premature failure of I800 was particularly significant since all post-Pickering A Moderator HXs were tubed with this material. More recently, I800 has failed within one year in Pickering B Moderator HXs. Incoloy 825 (I825) and Sanicro-28 (S28) have been specified and used as the tube materials tor Moderator HX tube replacement bundles in Pickering Units 5 and 6, and for Darlington Units 3 and 4 respectively. At Bruce A after 8 years operation, a single tube leak in the Moderator HXs has been caused by underdeposit pitting corrosion/8/.

Shutdown Coolers in all operating Ontario Hydro nuclear plants have been tubed with Monel 400 (M400). This alloy has performed adequately in Douglas Point (although leaks occurred 3 months prior to shutdown), Pickering A and Bruce A, with no reported tube failures or significant corrosion damage on removed tubes. M400, however, has failed rapidly as a result of pitting corrosion, following approximately 30 months exposure to stagnant conditions in Pickering B/10/, and I825 has been specified as the material for replacement bundles.

1.3 Pitting Corrosion

Pitting corrosion is one ot the commonest forms of localized corrosion and a source of a large number of failures in industrial plant equipment. In HX components exposed to an external untreated form of cooling water, it is one of the most difficult types of corrosion to predict and guard against. Pitting susceptibility depends on the alloy composition, fabrication, thermo-mechanical treatment, and environmental conditions. Small changes in material and environment can have a large influence on the incidence and severity ot pitting attack. The apparently large influence of such minor changes was well demonstrated in the recent failures ot M400 in the Pickering Shutdown Coolers cited above, where small differences in the tube thermo-mechanical treatment and trace element impurity distributions may have resulted in greatly increased corrosion susceptibility, and hence premature failure.

It is widely accepted that pitting under deposits can occur as a result of differential aeration which can lead to breakdown of a

passive surface film or disruption of a corrosion product film. This results in the establishment of a local corrosion cell where the corroding area is the anode and the region with good oxygen supply and a protective film is the cathode. Oxidation and/or anodic dissolution of the base material occurs at the anode, whilst oxygen is reduced at the cathode. As the corrosion process proceeds, pH is reduced within the pit by the production of hydrogen ions, thus increasing the rate of dissolution. The breakdown and repassivation kinetics of passive film formation may be altered by the presence of certain ions, particularly chloride and sulphate ions. Even in the presence of aggressive anionic species, the presence/absence of oxygen in the form of bridging hydroxyl groups can determine whether the film repairs or pitting corrosion ensues. Figure 2 schematically depicts the various stages of crevice corrosion. Deposits play a further role in the corrosion process, that of reducing heat transfer at the tube OD surface, thus increasing temperature and hence corrosion rates and/or modifying mechanisms at this surface.

Pitting is a two stage process. The first stage, that of pit initiation, involves breakdown of the material's protective film and limited dissolution of the metal ions from the base material. This is essentially a nucleation process characterized by a probability, or frequency of nucleation/11,12/. For a given environment, this probability is strongly dependent on the integrity of the protective film, through both substrate and film dependent parameters. Inhomogeneities in the base material such as grain boundary precipitates, segregation of alloying elements, inclusions, and slip/dislocation networks, all influence the integrity of the film and hence its susceptibility to breakdown. Similarly, inhomogeneities in the electrolyte composition under deposits, variations in elemental distributions and binding state within the oxide film, and mechanical stresses can influence the probability of local film breakdown.

The role of molybdenum (Mo) additions in the initial breakdown of passive films leading to pit initiation in Fe-Ni-Cr-Mo alloys remains in dispute. Mo has been proposed/13/to:

(i) increase the repassivation rate of the alloy and since pitting is initiated at potentials where the breakdown rate exceeds the repassivation rate, the net effect of Mo is to shift the pitting potential to more noble values,

(ii) stabilize a salt film on the surface of the alloy which impedes anodic dissolution,

(iii) lead to a thickening of the passive film

(iv) impede the adsorption of Cl^- onto the surface of the alloy by increasing the oxygen affinity of the alloy, and

(v) lead to the formation of an amorphous oxide film with a glassy structure.

The second stage is the propagation or growth phase. When the passive film breaks down, it is generally accepted that corrosion pits, once formed, will propagate as a result of the development and maintenance of elevated local acidity in the pit. Still unresolved is the role of Mo in the pit growth phase in stainless steels. Various theoretical explanations have been developed to explain its role. Moriya and Ives/14/ have found that Mo concentrations inside pits grown on a Ni-Mo alloy, are higher than those found on the unpitted surface. Their results support other work on Fe-Mo alloys/15,16/, and suggest that Mo inhibits further propagation of corrosion pits, but is not involved in the initiation phase. Should the role of Mo be associated with stifling of pit growth, then it is important to determine when this occurs in relation to the tube wall thickness.

Thus, in order to assess the performance of materials in lake water, it is necessary to address both the initiation and propagation stages of pitting corrosion. Ideally, a material should demonstrate a low probability both for pit initiation and significant pit growth. Given the presence of thin-walled tubes ($\leq$1.2 mm) in operating HXs, and the consequences of isolated tube leaks, a high propensity for pit initiation, would tend to exclude a material for subsequent selection unless it could be demonstrated that pit propagation would cease prior to growth through-wall.

1.4 Interpretation of Potential-Current Relationships

Electrochemical testing has played a large role in investigations of the pitting susceptibility of materials, particularly stainless steels/17,18/. These tests when carried out in acidic media, provide characteristic potential (E) versus current (I) responses and recognized critical potentials such as the breakdown potential (E_b), the protection potential (E_{prot}), the primary passivation potential (E_{pp}), and the corrosion potential (E_{corr}). Figure 3 shows a typical cyclic potentiodynamic polarization plot for stainless steels in acidic media. Corrosion response can be separated into three regions; active below E_{pp}, passive between E_{pp} and E_b, and transpassive above E_b. In relation to pitting corrosion, three regimes can be defined as:

(i) $E > E_b$ pit nucleation and growth

(ii) $E_b > E > E_{prot}$ pit growth but no nucleation

(iii) $E_{prot} > E$ immunity to pitting

The degree of hysteresis or charge difference between forward and reverse scans (ΔQ in Figure 3) is a measure of the sum of all irreversible processes such as pitting, film dissolution, film formation, non-uniform general corrosion and de-alloying occurring during the forward scan.

Potential-current relationships also exist when the material of interest is held at a fixed potential and the current decay transient is recorded. Three regimes can be defined depending on the potential regime in which the specimen is held. If a continuously decaying current is observed, the specimen is at a potential below that of the breakdown potential, E_b, and continued passivity ensues. If the current is observed to initially decay (passivation) followed by an increase after a finite time, then the potential of the specimen lies above the breakdown potential and the minimum in the curve is termed the incubation time, t_{inc} and is shown schematically in Figure 4. The breakdown potential, E_b, can thus be defined as the lowest potential in which an increasing current decay response is obtained.

Various definitions of the incubation time, t_{inc}, have been advanced/19/ as follows:

(i) t_{inc} may be the time required for the pit which has been developing from the start of the test to enlarge to a size where the pitting current exceeds the passivation current on the rest of the sample surface and hence can be detected,

(ii) t_{inc} is the time for the local action in flaw bases to decrease the pH to a low level where metal dissolution can be sustained and pitting can develop,

(iii) t_{inc} is the time required for the development of a two dimensional film which replaces the passive film locally, and/or

(iv) t_{inc} is the time required for aggressive anions to penetrate the passive film and to produce localized dissolution.

1.5 Materials

Titanium (Ti) and the stainless steels rely on passive film formation for their pitting resistance. In stainless steels, the Cr content is the major factor in promoting corrosion resistance, but other elements including Ni, and notably Mo in the case of conveying resistance to pitting corrosion, can play supporting roles/20,21/.

Copper alloys, which do not form passive films, rely on the formation of protective corrosion product films for their corrosion resistance. Alloying elements such as Ni result in the production of a more coherent film with a lower defect density thus inhibiting ion transport through the film and reducing the corrosion rate. The performance of these copper alloys in Ontario Hydro nuclear plant HXs has, however, been unpredictable/22/ (see Table 1).

A large body of literature is available on the performance and laboratory-assessed pitting resistance of the materials. For the austenitic Fe-Ni-Cr-Mo alloys, an empirical ranking in this test program has been developed based on pitting indices and pitting temperature, as shown in Table 2/8/, although this is based on seawater exposures. It has been proposed that materials with a pitting index of $\geq$ 36 should be specified for Ontario Hydro HX tube applications/23/. With reference to Table 2, this implies that of the austenitic Fe-Ni-Cr-Mo alloys chosen for the present study, only I625, AL6X, 904L and S28 would be suitable.

2.0 EXPERIMENTAL PROCEDURE

Various methods are available to evaluate the pitting susceptibility of materials in lake water. Client needs for early results, required that the initial experimental program be laboratory-based. Two types of tests were employed, namely electrochemical and immersion tests. Electrochemical tests can simulate a wide range of oxidizing conditions by changing the sample potential relative to a reference electrode. This is important in view of the extent of differential aeration that can occur under deposits. Immersion testing, both under heat flux and isothermal conditions partly simulates conditions in operating HXs. Crevices were created by packing silt collected from the Pickering site around portions of tube, and with grooved teflon discs. Lake water from the Pickering site was used as the aqueous medium both in the electrochemical and immersion tests.

This program was performed jointly with AECL-CRNL. Electrochemical testing was largely undertaken at OHRD, while the immersion tests were performed at both locations.

2.1 Materials

Three groups ot materials known to resist pitting attack were chosen for the present study, namely: Ti, austenitic Fe-Ni-Cr-Mo alloys and Cu-Ni alloys. Ti has demonstrated outstanding resistance to corrosion in a wide variety of corrosive media. Ti tubing has been selected for particularly harsh power plant HX marine environments including condensers and recirculating cooling water HXs for AECL-designed CANDU 600s, and CEGB plant condensers cooled by marine and polluted waters/24,25/. It is however, expensive, and as a result ot its relatively low elastic modulus, requires a larger number of support plates than other materials in order to avoid fretting wear and possible associated fatigue at supports.

The austenitic alloys Inconel 625 (I625), Allegheny Ludlum's AL6X, Uddeholm's 904L, Sanicro 28 (S-28) manufactured by Sandvik, and Incoloy 825 (I825) were chosen on account of their resistance to pitting corrosion in chloride-containing media/26/. Incoloy 800 (I800) was chosen because of its known susceptibility to pitting attack in Lake Ontario water. Two Cu-Ni alloys, M400 and 70/30 were selected primarily on account of their good corrosion performance in the Pickering A Shutdown Coolers and Moderator HXs, respectively.

Test materials, with the exception of Ti supplied by Kobe Steel, were obtained trom Metal Samples Co., Alabama, US, who in turn had procured them from primary manufacturers. Two types of samples were obtained: flat rolled samples ot dimensions 25.4 mm x 51 mm x 3.2 mm, and tube samples which were largely 19 mm OD with a 1.65 mm wall thickness. Material designations, major constituent elements, and other information on thermo-mechanical treatment, etc, are given in Table 3. Microstructures and surface conditions of all materials were examined by optical microscopy. Grain sizes and hardness determinations were performed.

Materials were tested in both the as-received condition (120 grit was specified) or in the polished (600 grit paper and 3 μm diamond paste) condition. Samples were examined following test exposures using optical and electron microscopy, followed by Energy Dispersive X-ray (EDX) analysis where required.

2.2 Electrochemical Testing

Electrochemical test equipment shown in Figure 5 consisted of a saturated calomel reference electrode (SCE), with a platinum wire counter electrode immersed with the sample and holder in Lake Ontario water. Potential/current data was controlled and monitored using an HP 85 computer and 3497 data acquisition and

control unit, and an AIS Model PEC-1 Potentiostat. Compensation for the high electrolyte resistance of lake water was not employed due to equipment limitations.

Samples were mounted between teflon plugs with viton seals to prevent leakage as shown in Figure 5. Cylindrical sections of tubing were prepared and the ends ground to 120 grit (silicon carbide). Samples were degreased in trichloroethane, rinsed in distilled water and alcohol, and air dried. The test solution consisted of Lake Ontario water taken from the Pickering A low pressure service water system. The solution was maintained at 40°C $\pm$ 2°C by means of an immersion heater in a water bath. Some limited testing was performed at other temperatures between 20°C and 60°C. This temperature range is believed to simulate temperatures existing at the tube outside surface under deposits in operating HXs. De-aeration was achieved by bubbling Nitrogen through the test solution at a flow rate of 150 cc/min for 1 h prior to the test.

Two types of electrochemical tests were performed: cyclic potentiodynamic polarization (CPP) and potentiostatic polarization (PP) tests. In CPP testing, the corrosion potential E_{corr} was monitored for 1 h prior to the test commencement to ensure electrode equilibrium and stability. The potential scan was initiated at -0.400 V SCE (cathodic) and taken through (E_{corr}) to 1.600 V SCE. This was followed by a reverse scan. Two scan rates of 0.25 V/h and 1.2 V/h were used. Potentiostatic steps 2.5 mV in magnitude were employed with current measured after a 15 s decay. Upon completion of a forward and reverse scan, the breakdown potential, E_b, the protection potential, E_{Prot}, and the difference in the integrated charge transferred between the forward and reverse scans, ΔQ, were recorded. The definition of these electrochemical parameters are shown schematically in Figure 3. The effect of surface finish was also assessed by testing the as-received surface condition and that produced by polishing to 600 grit with SiC. In some cases repeat tests were performed to establish reproducibility and confidence limits of the results.

In the PP tests, a limited number of samples in the as-received condition were pulse-polarized immediately upon immersion to potentials in the range 0.4 V SCE to 1.2 V SCE. Samples were polarized for 24 h. This test method was used to evaluate pit incubation times (t_{inc}), where t_{inc} is defined as the global minimum in the current versus time curve as a function of applied potential as shown schematically in Figure 4.

2.3 Immersion Testing

2.3.1 Heat Flux Immersion Testing

Tubes sealed at one end using a welded plug, were surrounded along part of their length with packed silt contained within a wire mesh of stainless steel supported by teflon discs. The silt was obtained both from a Pickering A Moderator HX, and more recently from the Pickering intake. Samples were immersed in a beaker containing Lake Ontario water from the Pickering site, and maintained at a temperature of 25°C $\pm$ 1°C by means of an external bath of tap water. Tubes were heated with internal resistance heaters immersed in oil to 65°C $\pm$ 4°C. Outside tube wall temperatures under silt were monitored during the test with thermocouples attached by spot welding to the wall. Measured tube outside wall temperatures increased as the test progressed from 25°C to 52°C $\pm$ 4°C. Apparatus for heat flux immersion testing is shown in Figure 6. Tests were conducted at AECL-CRNL and OHRD. Materials tested and exposure times are shown in Figure 7.

2.3.2 Isothermal Immersion Testing

Six racks of plate samples were assembled, separated by teflon-creviced spacers. Five racks contained materials in the as-received condition of 120 grit, and another rack contained samples polished with three micron diamond paste. The samples were placed partially submerged in a bed of silt and immersed in Lake Ontario water maintained at a constant temperature of 40°C $\pm$ 2°C. Both the silt and water were taken from the Pickering site. Figures 8 and 9 show the test arrangement and program schedule, respectively. At AECL-CRNL, tube samples surrounded by silt held in place by a stainless steel mesh were immersed in Lake Ontario water at various temperatures and exposure times as shown in Figure 10.

3.0 RESULTS

3.1 Materials Tested

Materials data supplied by the vendor, and the results of grain size and hardness determinations are included in Table 3. Only minor compositional variations existed between plate and tube material. Small differences were observed in grain size and hardness values between plate and tube samples within an alloy type. Larger variations in mechanical properties and grain size were observed between the various materials.

Composite through-wall tube microstructures for all materials are shown in Figures 11, 12 and 13. Microstructures and surface

conditions of all tube and plate samples are given in Appendix 1. All of these figures are included primarily for future reference to allow for comparison of microstructures of possible future HX materials with those tested in the present study. Further work to classify these materials on the basis of specific microstructural features would provide additional reference documentation. Basically, all the materials show characteristic annealed microstructures as would be expected for these fully solid solution alloys.

3.2 Electrochemical Tests

3.2.1 Cyclic Potentiodynamic Polarization (CPP)

Forward scans of CPP plots obtained with a solution temperature of 40°C are presented for all materials in Figures 14 and 15 for the four combinations of scan rate and surface condition. The plots for the Ti and austenitic alloys are presented unconventionally by including only data above O V SCE and 0.1 A/cm^2, thus eliminating large scatter in data below this point. The plots shown in Figure 14 are difficult to follow, although they are included in this form so that differences (between Ti and I625), and similarities (between the Fe-Ni-Cr alloys) can be seen. Further analysis is provided in the Discussion Section (4.0).

Four tests were run for I825 at a scan rate of 0.25 V/h and 600 grit surface condition in order to determine the repeatability and scatter for a given test condition. 95% (2σ) confidence intervals for the forward scans of these tests are shown in Figure 16. I825 tube material procured as a replacement material for the Pickering B shutdown coolers, showed similar results, in the forward plots during CPP testing, to I825 material obtained from Metal Samples Co.

Figure 17 illustrates the effect of scan rate on forward plots for 600 grit prepared I825. A reduction in scan rate from 1.2 V/h to 0.25 V/h produced a slight leftwise, and downward shift of the polarization curve to lower current densities. Generally at the lower scan rates, a more pronounced activation peak was observed, with slightly higher current densities at potentials above 0.8 V SCE.

Forward plots of I825 at a scan rate of 0.25 V/h in both the as-received and 600 grit condition are shown in Figure 18. As was generally the case with other materials tested, higher current densities were observed with material in the as-received condition when compared to the 600 grit condition.

Complete CPP plots showing forward and reverse scans for all test materials with a surface condition of 600 grit and scan rate of 0.25 V/h are shown in Figure 19. Similar trends were observed in other plots not shown, taken for the remaining three combinations of scan rate and surface condition. The differences between these plots and the ideal plot shown in Figure 3 demonstrate the variability of CPP plots between different materials, and the difficulty in their interpretation. This is discussed further in section 4.2.1.

The degree of hysteresis between the forward and reverse scans is an indication of the extent of non-reversible processes occurring during the forward scan. This may be defined by a parameter, ΔQ, which is the difference in integrated charge transferred between the forward and reverse scans (see Section 1.4). Table 4 shows calculated values of ΔQ for all materials and combinations of scan rates and surface conditions. 95% (2σ) confidence limits of ΔQ for four CPP tests for I825 are also shown in this Table for a scan rate of 0.25 V/h and surface condition of 600 grit. For a surface finish of 600 grit and a scan rate of 0.25 V/h, ΔQ was 0 for Ti, I625, and 70/30. ΔQ increased for the remaining alloys in the order AL6X, 904L, S28, I825, I800 and M400. Analysis of ΔQ values is given in Section 4.2.1.

Test data from the present series of experiments has been combined with some earlier work at Ontario Hydro Research Division to provide a preliminary indication of the temperature dependence of ΔQ for the materials I625, 904L, S28, I825 and I800 in the as-received condition for a scan rate of 1.2 V/h, as shown in Figure 20. Also shown in this Figure is approximate curve fitting to the limited data. Further data is required to confirm and improve confidence in these curves. Over the temperature range explored, I800 shows the largest values of ΔQ whereas I625 showed the lowest values of ΔQ. Examination of Figure 20 shows that all of the alloys show a strong sensitivity of ΔQ with temperature. Insufficient data near threshold ΔQ levels is available for 904L, S28, I825 and I800 within the temperature range 25-40°C to allow adequate discrimination between these materials.

Values of E_b and E_{prot} determined for all materials for scan rates of 1.2 V/h and 600 grit surface conditions are given in Table 5. Eb was determined from the activation peaks occurring between 0.7 - 0.9V SCE. E_{prot} was determined as shown in Figure 3. In regard to the austenitic Fe-Ni-Cr-Mo alloys, no consistent trend of E_b or E_{prot} is evident with variations in Mo content. Values determined for breakdown potentials and protection potentials did not correlate with optical microscopy since pitting was observed to occur at potentials well below the

reported breakdown potentials determined by analogy to stainless steels in acidic media. The extension of these parameters to materials such as M400 or 70/30 does not appear warranted in view of the difference in film characteristics and depassivation mechanism.

Surface conditions of all samples following CPP testing at a scan rate of 0.25 V/h and initial surface condition of 600 grit are shown in Figures 21-29. These Figures show an overall representative view of the sample surface and a view of 100X showing unusual features such as defects or pits observed. Samples tested in other surface condition/scan rate combinations displayed similar relative behaviour in terms of extent of pitting attack, and are not included. However, a summary of observations of surface appearance i.e. of all samples tested is shown in Table 6.

In addition to optical microscopy of the overall surface condition shown in the latter Figures, a limited further detailed examination of observed pits in I825 and I800 was performed, the results of which are shown in Figure 30. These are included primarily for future reference purposes.

3.2.2 Potentiostatic Polarization

As stated in Section 2.2, pit incubation times (t_{inc}) can be derived from the global minimum in the current decay versus time curves in potentiostatic polarization testing. In Figure 31, t_{inc} is plotted versus applied potential for I800, I825 and AL6X. Over the potential range, E = 0.4 - 1.0 V SCE, t_{inc} for I800 was observed to vary between 10 min to 4 h with a logarithmic dependence of t_{inc} within the potential range. Note that the line shown for I800 represents the best fit of all data from Reference 29 -all data points are not included. Both AL6X and I825 display a strong potential dependence of t_{inc} above 0.85 V SCE, and in the range 0.85 - 0.9 V SCE, pitting is apparently more readily initiated in I825 compared to I800. Curves shown for I825 and AL6X are based on similar behaviour of Metglass 2826A and discussed in Section 4.2.2. The curves do not represent best statistical fit to the data, and further data is required for increased confidence.

3.3 Immersion Tests

Table 7 summarizes results to date from isothermal and heat flux tests performed at both Ontario Hydro Research Division and AECL-CRNL. Where available, average pit growth rates are shown, based on maximum pit depth observed following the test period, and without accounting for incubation times or variations in pit propagation rates as a function of time. From Table 7, Ti, I625

and AL6X did not pit at any test exposure/time combination during isothermal testing. Pitting was observed to occur on the remaining alloys. In addition, crevice corrosion of I800 was noted along with de-alloying of both M400 and 70/30.

In regard to heat flux testing, no pitting was observed in either Ti or I625. A single pit was observed to occur in AL6X. A greater frequency of pitting was observed in 904L compared to AL6X; all heat flux exposures to date have resulted in pitting of 904L. Pitting was also observed to occur in S28, I825, I800 and M400. No pitting was observed in heat flux testing of 70/30, although extensive non-uniform general corrosion and de-alloying of the alloy was noted.

Optical and electron microscopy results of examinations of pits resulting from immersion testing are shown in Figure 32 primarily for reference purposes. Samples selected for this detailed examination are shown in Table 7. Results of limited analysis of materials within pits following testing are given in Table 8. No orientation effects of isothermal or heat flux test coupons were noted in this study.

4.0 DISCUSSION

As discussed previously, the major objective of this work is to help provide a basis for HX materials selection for lake water service in Ontario Hydro operating plants. Thus, materials for the test program have been chosen based on their current usage, or their resistance to pitting corrosion in seawater (see Table 2).

4.1 Materials

Constituent phases in the materials tested can best be described by classifying the materials into three major groups referred to in Section 2. The largest group of materials tested in the program fall into the classification of austenitic Fe-Ni-Cr-Mo alloys; all contain Mo with the exception of I800. These materials are predominantly austenitic, although AL6X contains a small amount of ferrite. Constituent phases are shown as a function of Ni and Cr equivalents in Figure 33/27/. Alloy performance deduced from both electrochemical and immersion testing would indicate that Cr equivalence dominates over nickel equivalence in the resistance to localized corrosion. Alloy ranking correlates well with Cr equivalent with the exception of S-28. This type of diagram may be a useful criteria for defining regimes for pit initiation, pit growth and pit immunity based on Ni and Cr equivalents. Forward Looking Research work is presently being undertaken in this area by S. Thorpe at the Massachusetts Institute of Technology (MIT).

The alloys M400 and 70/30 fall into the Cu-Ni alloy group which form a continuous series of solid solutions over the alloy range as shown in Figure 34/28/. Hence microstructures of these materials contain a single phase constituent. Ti also falls into the category of single phase materials.

In terms of their microstructural constituents, ie, the presence of phases, and the nature and distribution of inclusions and intermetallics, these test materials are generally similar to those expected to be obtained commercially for Ontario Hydro nuclear HX applications. It should, however, be clearly noted that differences in thermo-mechanical treatments in a given material can profoundly influence material condition. Thermo-mechanical treatment can influence material grain size and distribution, the size and distribution of inclusions, textural relationships, residual stresses, and the nature of any surface film/oxide. This in turn can influence the materials's corrosion susceptibility. Thus any material chosen for field application as a result of the work described within should be compared closely to the specific test material used in this program.

4.2 Electrochemical Testing

4.2.1 Cyclic Potentiodynamic Polarization

Forward plots of CPP tests for all materials shown in Figure 14 do not include portions of the curves at negative potentials and at current densities below 0.1 A/cm^2. Although, this is an unconventional way of displaying the data, it allows for better discrimination between materials, and eliminates inaccurate current responses below 0.3 - 0.4 V (see Figure 19), arising from equipment limitations. This has not enabled us to study the initial film formation in the materials in the potential region below which pitting occurs.

Forward plots for AL6X, 904L, S28, I825 and I800 shown in Figure 14 are quite similar. All display spontaneously passive behaviour, and what appears to be an activation peak (towards lower current densities) at approximately 0.6 - 0.8 V SCE, and a reduction in current density for a given potential step at around 0.8 - 1.0 V SCE. There is some evidence of lower current densities and enhanced activation peaks (between 0.6 - 0.8 V SCE) for those materials with higher Mo levels, this effect being most pronounced at the lower scan rate of 0.25 V/h, with AL6X showing consistently lower current densities in this potential region. I825 appears to have a similar response to I800.

The lack of discrimination between these plots, however, is particularly apparent in relation to the degree of scatter

obtained for four forward CPP tests on I825, shown in Figure 16 as 95% confidence limits. On this basis, it is not possible to adequately discriminate between these Fe-Cr-Ni materials based on comparison of their forward plots.

Ti shows consistently lower current densities over the entire potential range. I625, on the other hand, displays anomalous behaviour not consistent with its expected corrosion performance. Examination of I625 tube surfaces following testing, however, showed no evidence of pitting attack (see Figure 22 - note that a defect caused by mechanical damage is shown in this Figure). Ni-based alloys typically display a greater degree of nobility in lake water than Fe-based alloys. In a nominally low aggressive environment such as lake water, insufficient initial dissolution of I625 occurs to allow incorporation of beneficial species such as Cr into the passivating film. Hence it is likely that these high current densities are as a result of the formation of a less protective passive film. Confirmation of this could be achieved by further work to measure the thickness and composition of the film as a function of charge transfer.

70/30 was not spontaneously passive compared to the austenitic alloys as seen by the presence of an initial anodic peak in Figure 15. For all scan/rate and surface finish combinations, 70/30 displays only a very narrow range of passivity about -0.025 V SCE due to the formation of a protective corrosion product film. Above this potential, 70/30 displayed transpassive behaviour and underwent accelerated non-uniform general corrosion and pitting.

The stability of the passive film on M400 is sensitive to both surface finish and scan rate. By comparison of Figure 15a and 15b, the as-received air-formed film on M400 has different characteristics than the film formed in situ in lake water reflected in the higher critical current density, higher passive current and reduced potential range over which passivity ensued. This effect is enhanced by perturbation of the M400 electrode by increasing the scan rate as seen by a comparison of Figures 15c and 15d. This provides supporting evidence that the nature of the film formed on M400 as a result of previous processing is critical to the electrochemical performance of this alloy in lake water as reflected in the differing performance of M400 in Pickering A and B.

Lowering the scan rate generally resulted in decreased current densities at the anodic peak occurring between 0.6 - 0.8 V SCE and increased current densities occurring above this potential range, as shown in Figure 17. As a result of the greater degree of electrochemical equilibria expected during testing at lower scan rates, improved in-service laboratory correlation is

expected. Slow scan rates are desired for the determination of breakdown potentials because with increasing scan rate insufficient induction time for pit initiation is allowed at less noble potentials. Lowering the scan rate from 1.2 V/hr to 0.25 V/hr provided for improved discrimination between materials in CPP testing and in ΔQ determinations.

Material surface condition is an important parameter, and was found to vary greatly between samples in the as-received condition as shown in Appendix 1. It is expected that, as surface condition worsens, the probability of pit initiation increases as a result of greater surface activity and an associated larger number of potential pit initiation sites. Generally, this was verified in the CPP forward plots where current densities were higher for material in the as-received condition when compared to materials in the 600 grit condition, as shown in Figure 18. Thus to minimize the potential for pit initiation in a given alloy, it is highly desirable that specifications include a requirement for optimum surface condition. This conclusion is based on limited data from the present study. Further work would increase confidence in these results.

CPP plots showing forward and reverse scans and the charge difference (ΔQ) between these scans shown in Figure 19 and Table 4 appear to demonstrate a trend toward increasing ΔQ with decreasing Mo content in the austenitic stainless steels, although the large degree of experimental scatter in these measurements does not allow substantive conclusions to be drawn. For Ti and I625, $\Delta Q = 0$ for all tests. AL6X also shows low ΔQ values both in the as-received and 600 grit conditions. Although ΔQ is not directly related to the amount of pitting, when combined with metallographic analysis of sample surfaces following CPP testing (Figures 21 - 29), it may provide an indication of pitting susceptibility within one alloy classification with similar film characteristics. An exact measure of ΔQ for pitting is only separable after further testing involving (i) voltammetry for identification of the potential dependence of ionic species and (ii) impedance studies to characterize film properties of ionic transport, resistance, capacitance, and identification of the pre-passivation sequence.

Within a group of materials such as the austenitic Fe-Ni-Cr alloys, ΔQ increases with temperature over a specific temperature range. With reference to Figure 20, for temperatures in the range 40 - 60°C, I625 is seen to have consistently lower ΔQ values (for a given temperature), whilst I800 has consistently higher values of ΔQ. However, below 40°C, there is insufficient test data to allow for comparison of threshold temperatures between the materials. Interpretation of this Figure is further complicated since data were obtained during two separate series

of tests with different test techniques, and at only 1.2 V/h scan rate with an as-received surface condition; the relative position of the curves can change with scan rate and surface condition. Also as previously discussed, since pitting corrosion is only one of several contributors to ΔQ, it is not possible to directly compare pitting susceptibility based on ΔQ alone without knowledge of the role played by the other contributors.

Pseudo-pitting breakdown potentials (E_b) shown in Table 5, determined from the activation peak occurring between 0.7 and 0.9 V SCE show similar values for all the austenitic stainless steel materials, and hence do not allow for discrimination between these materials; in fact I625 displays anomalous behaviour with the lowest value in this group. Similarly, values for E_{prot} shown for the remaining materials in Table 5 do not show any reasonable trend. It is not possible to extend the value of these parameters determined by CPP testing to determine pitting resistance of materials in lake water by analogy to stainless steels in acidic media. The practice of using such criteria for our future candidate materials selection appears to be unwarranted.

4.2.2 Pit Induction Testing

Pit incubation times (t_{inc}) shown for I800, AL6X and I825 as a function of potential are given in Figure 31. Based upon only two data points an apparent logarithimic dependence of the induction time of I800 was found in this study in excellent agreement with the work of Palumbo/29/. The incubation times for I825 and AL6X displayed a marked potential dependence similar to that observed by Thorpe/30/ in the breakdown of passive films on Metglass 2826A. Below approximately 0.85 V SCE, passivity in these alloys is conveyed by the formation of a protective chromium (Cr^{+3}) oxyhydroxide film and the overall protective nature of the film is governed by the interaction of the remaining alloying elements with the distribution of Cr. In Metglass 2826A, a small potential regime lying just above the $Cr^{+3} \rightarrow Cr^{+6}$ transition (where passivity is lost) is observed where the current contribution arising only from the active pits (not the general passive surface current) approaches zero. Over this small potential range, the formation of an iron hydroxide film permits a temporary suppression of pit nucleation and growth at the expense of a higher general surface current. The large incubation times at approximately 1.1 V could be explained by the presence of a similar regime in AL6X and I825. Above these potentials, the Fe hydroxide film is unstable and pitting resumes with a large reduction in the incubation time for pit nucleation.

An increase in the Mo content in Fe-Cr-Ni-Mo alloys leads to an increase in the threshold pit incubation potential and leads to longer times for pit nucleation for all potentials as seen by a comparison of the curves for I825 and AL6X in Figure 31. By comparison to the Mo free alloy I800, both I825 and AL6X show longer incubation times with the exception of the potential regime near 0.85 V SCE. The reason for this behaviour is unknown at present. This may account for the increased nucleation frequency observed in I825 compared to I800 after scanning through this potential regime during CPP testing.

The time taken for pits to nucleate is a function of material condition. The influences of flaws in the base material on film breakdown, or of environment in creating the necessary local conditions for breakdown, are poorly understood. Since t_{inc} is an indication of the materials' susceptibility to pitting corrosion, then any assessment of the relative susceptibility of these materials to pitting is dependent on the potentials existing in the service environment. Based on Figure 31, it appears that pitting occurs more readily and at shorter incubation times over a broad range of potentials for I800, and over progressively narrower potential ranges for I825 and AL6X respectively. This could be interpreted to imply that, assuming a full range of potentials exists in the service environment, the probability of pitting corrosion decreases in the order I800, I825 and AL6X. The range of potentials existing in service is presently unknown.

4.2.3 Metallographic Analysis of Samples Following Electrochemical Testing

The above discussion has been limited to interpretation of potential-current relationships occurring during potentiodynamic and potentiostatic electrochemical testing. Further information can be gained from examination of the surface condition of samples following potentiodynamic testing. Photomicrographs of these surfaces are given in Figures 21 - 29 for a scan rate of 0.25 V/h and a standardized initial surface condition of 600 grit.

Figures 21 and 22 show the absence of pits in either Ti or I625, and support the high ranking for these materials developed above with respect to their ΔQ value. As shown in Table 6, the good performance of these materials in potentiodynamic testing was maintained for other scan rate/surface condition combinations, with no pits observed. This provides reassurance that the anomalous behaviour of I625 during CPP testing, with respect to its high current densities relative to the austenitic stainless steels, is not due to pitting corrosion.

In contrast to the results for Ti and I625, isolated shallow pits and/or 'micropitting' were present on samples of AL6X and 904L following testing, as shown in Table 6. ΔQ values for these materials were also low relative to the other materials tested.

Detailed examination of pits formed during these tests, shown in Table 6 and Figure 30 indicate differences in pit morphology between these Fe-Ni-Cr-Mo alloys. In particular, I800 appears to have considerable undercutting within pitted areas as shown in Figures 30c and d which makes detection of this type of pitting and an assessment of true propagation rates difficult. I825 shows generally shallower pits compared with I800 with intergranular attack in the base of pits formed during CPP testing (see Figures 30a and b). The significance of this type of attack is that it can lead to accelerated metal wastage by grain dropping resulting in premature failure and is the only type of attack which appears to be substrate dependent. Analysis of material within the bases of pits in this material show increased levels of Mo compared to unpitted sample surfaces (Table 8) which should lead to the suppression of pit growth by the formation of MoO_2^{2-}. Values for concentrations of other elements have also been included in Table 8 for reference purposes only.

I825 and S28 displayed a higher population of pits than I800 following CPP testing, indicating an increased tendency for pit initiation in these materials. Given I800's known susceptibility to pitting corrosion in service applications, the relatively poor performance of I825 and S28 in CPP testing does not provide assurance that these materials will perform better than I800 in similar environments. The significance of the relatively low threshold temperature for pit nucleation in I825 shown in Figure 20 is difficult to assess as a result of lack of detailed knowledge with respect to:

(i) pit propagation rates in I800 and I825,

(ii) the population distribution of actively growing pits relative to the total pit distribution, and

(iii) the repassivation and reactivation characteristics of pits in I800 and I825.

In the absence of this information, and, on the basis of the data reported here, I825 and S28 are not suitable future candidate materials for lake water-cooled HXs.

The copper alloys M400 and 70/30 showed evidence of pitting attack, non-uniform general corrosion, and de-alloying, which

corresponds to the high current densities observed during CPP testing. Similar results were found in immersion tested samples (see Table 7). The mechanism of corrosion protection is different in these materials when compared to the other materials tested which rely on the formation of passive films. Copper alloys tend to rely on corrosion products for their corrosion protection; thus, direct comparison is not possible. However, the good service performance of these materials in some applications has already been noted. From CPP testing, it follows that relatively low (<0 V SCE) electrochemical potentials must be present in service for adequate performance.

4.3 Immersion Tests

Results of limited isothermal and heat flux immersion testing shown in Table 7 support the good performance of Ti and I625 observed during electrochemical testing. A pit of approximately 50% wall thickness has been observed, however, in AL6X following only 24 weeks of heat flux testing. In the remaining austenitic stainless steels, 904L, S28, I825 and I800, pits have been observed following short duration exposures to both isothermal and heat flux conditions.

The poor resistance of these materials to pitting corrosion during immersion testing is surprising given the relatively low aggressivity of the test environment compared to service conditions where biological involvement is probably greater, and continuous flow of lake water can provide higher concentrations of aggressive species in the silt and locally under deposits.

The noted presence of pits in this small population of samples tested, further serves to illustrate the poor performance of these materials with respect to pit initiation under deposits in lake water.

As stated previously in this discussion, pit initiation is one stage of the pitting process. In order to provide an adequate data base for material selection, it is necessary to evaluate the growth rate of pits and more importantly whether the pits will continue to grow through-wall, or will repassivate and cease to grow. This is particularly important when evaluating the performance of Mo-containing alloys in which pits may cease to propagate once the concentration of molybdate compounds reaches a critical value within the pit/16/. In the absence of this contribution from alloying elements such as Mo within the base material, the environment within the pit will become more aggressive as corrosion proceeds, and pits will continue to grow following initiation. Calculated growth rates (0.3 - 1.84 mm/annum shown in Table 7) of pits formed during immersion testing at AECL-CRNL, indicate that if this initial pit growth rate

is sustained, pits will progress through wall (1.2 mm) well within the service life.

4.4 Limitations

Although electrochemical tests can provide an indication of susceptibility to pitting corrosion in a short time, and should enable a ranking of materials to be developed, extension of the results to the field can be difficult. Lack of detailed analysis of potential/current relationships over specific regimes during CPP testing has contributed to the difficulty in interpreting electrochemical results. Laboratory immersion tests cannot simulate the effects of continuous lake water flow with the biological and chemical differences associated with such an environment. A further limitation of our immersion test involved the statistically random nature of pitting. Although each specimen exposed contained multiple crevice sites, it was not possible to test a sufficiently large population of samples to be statistically significant. In addition, at present it has not been possible to perform adequate quantitative metallography to support both the electrochemical and immersion testing programs due to equipment limitations without an excessive commitment of manpower, although it is hoped further work will be performed in the future program. Despite these limitations inherent in laboratory based assessments of pitting susceptibility, in the absence of suitable performance data from actual operating equipment, such tests are useful in providing a relative ranking of pitting resistance.

5.0 CONCLUSIONS

5.1 Titanium showed the greatest resistance to pitting corrosion of all the materials tested. Based on the present result, external literature, and excellent service experience with this material, it is expected to be immune to pitting corrosion in lake water-cooled HXs.

5.2 Inconel 625 also exhibited high resistance to pitting attack in our tests. It's anomalous behaviour in cyclic potentiodynamic polarization testing with relatively high current densities, is attributed to film formation, since no pitting was observed. Although service experience with this material is limited, based on the present results, it is highly likely that I625 will perform adequately in lake water service.

5.3 AL6X and 904L were somewhat superior to the remaining austenitic Fe-Ni-Cr-Mo alloys tested, although pits were observed in these materials following both immersion and electrochemical testing. Based on immersion testing AL6X displays a lower propensity for pit initiation. Further work is required to assess the suitability of these materials with respect to pit propagation and to quantify performance differences.

5.4 The materials S28, I825 and I800 displayed high susceptibility to pitting corrosion, and large numbers of pits were observed in S28 and I825 following cyclic potentiodynamic polarization testing. In view of the poor service performance of I800 at Pickering A, and based on the present results, S28 and I825 are not recommended for HX service applications.

5.5 M400 and 70/30 showed poor resistance to both general corrosion and pitting attack in the present tests. The corrosion behaviour of M400 showed a marked dependence of film stability in CPP testing on both film formation kinetics (scan rate) and film composition (surface finish). The criteria are important in assessing the difference between the in service behaviour of M400 at Pickering A and B. Until the difference has been rationalized and controlled, this material is not recommended as a future HX material.

6.0 RECOMMENDATIONS

Based on the above study, the following recommendations for future work are advanced:

6.1 Electrochemical equipment capable of performing dynamic IR compensation is essential and should be obtained for studying the electrochemistry of film formation and the true polarization behaviour of these materials in a poorly conductive electrolyte such as lake water. Furthermore, future acquisitions should include AC equipment to study the impedance characteristics of these films and to identify potential/ionic specie relationships which will be critical to understanding the passivation phenomena of Fe-Ni-Cr-Mo alloys in lake water.

6.2 To date this study does not address the role of biology in the electrochemical process and this should be forthcoming in both laboratory and in situ studies within the heat exchanger test rig.

6.3 The heat exchanger test rig should be utilized to obtain in situ electrochemical potentials in tubes and the nature of changes in potential by deposit formation to allow a linking between laboratory and in service performance.

6.4 To date, this study shows that no substrate dependent, crystallographic defect is associated with the pitting response of Fe-Ni-Cr-Mo alloys in lake water, and that their corrosion properties are governed by film characteristics. A specific study is required to assess the composition and passivation characteristics of films formed on austenitic Fe-Ni-Cr-Mo alloys and their relation to film breakdown and pit initiation and propagation.

6.5 A specific study is required on the propagation rates in Fe-Ni-Cr-Mo alloys and the repassivation/reactivation of pits produced on these alloys. To this end, equipment for quantitative metallography is required to prevent a large commitment of manpower to this task.

6.6 In regard to the copper-nickel alloys, M400 and 70/30 further work is required to determine the significance of $\Delta Q = 0$ for 70/30 in light of good ranking of localized corrosion resistance of austenitic alloys by this parameter. Furthermore, the exact nature of the oxide film formed on M400 and the characteristics which convey passivity to this alloy require further work.

ACKNOWLEDGEMENTS

Part of the test program was conducted at Atomic Energy of Canada Ltd., Research Company, Fuel and Materials Division, under Mr. R.L. Tapping. The Ontario Hydro Research Division laboratory test program was performed by Mr. S.W. Borda and Ms. B. Guest. An appreciation is extended to Messrs. P.J. King, R.G. Barton and Dr. K. Lam for their assistance.

Approved by:

J. Brown
Manager
Metallurgical Research Dept

Submitted by:

B. Warr
Engineer
Corrosion and Tritium Technology

S. Thorpe
NATO Science Fellow
Massachusetts Institute of Technology
Department of Materials Science and Engineering

Reviewed by:

P.C. Lichtenberger
Supervising Engineer
Corrosion and Tritium Technology

BW:ljh:lAg

TABLE I

ONTARIO HYDRO NUCLEAR PLANT HEAT EXCHANGER DATA (1)

HX/Cooler Name	Type (2)	Douglas Point NGS							Pickering NGS A B (7)							Bruce NGS A B							Darlington NGS A						
		Tube	Tube			Shell			Tube	Tube			Shell			Tube	Tube			Shell			Tube	Tube			Shell		
		Mat (3)	Env (4)	T°C(5)	Foll (6)	Env	T°C	Foll	Mat	Env	T°C	Foll	Env	T°C	Foll	Mat	Env	T°C	Foll	Env	T°C	Foll	Mat	Env	T°C	Foll	Env	T°C	Foll
LAKEWATER COOLERS																													
1. Moderator	HW	70/30	D_2O	55	- (8)	LW	26	-	70/30(10) 1800	D_2O	66	-	LW	20 35	UDP (10)	1600	D_2O	70 88	-	LW	35 20	UDP	1800	D_2O	65	-	LW	32	-
2. Mod Pump Stator	SP (11)	CU	LW	20	-	Air	-	-	N/A (9)	-	-	-	-	-	-	90-10	LW	20	-	Air	40	-	90/10	LW	24	-	Air	48	-
3. Mod Pump Mtr Brg	PC	CU	LW	20	-	OIL	-	-	CU	SM	20	-	OIL	40	-	N/A	-	-	-	-	-	-	-	-	-	-	-	-	-
4. HT Mtr Stator	SP (12)	N/A	-	-	-	-	-	-	90/10	LW	20	-	Air	40	-	90/10	LW	20	-	Air	40	-	90/10	LW	24	-	Air	48	-
5. HT Mtr Brg	PC (13)	CU	LW	-	-	OIL	60	-	CU	SM	20	-	OIL	60	-	CU 90/10	LW	20 27	-	OIL	60	-	90/10	LW	24	-	OIL	70	-
6. HT Press Pup Oil	C	-	-	-	-	-	-	-	CU	SM	20	-	OIL	30	-	CU	LW	20	-	OIL	-	UDP	-	-	-	-	-	-	-
7. HT Pup Gland Seal	HW (14)	M400	D_2O	38	-	LW	20	-	1600	D_2O	265 42	-	LW SM	20 66	-	1600	D_2O	265	-	SM	83 45	-	1800	D_2O	267	-	LW	53	-
8. Shutdown	HW	M400	D_2O	55	-	LW	28	UDP	M400	D_2O	54 177	-	LW	26 23	-	M400	SM	163 177	-	LW SW	65 67	-	1800	D_2O	54	-	LW	31	-
9. End Shield	S/P (15)	70/30	LW	20	-	SM	40	UDP	90/10	LW	34	-	SM	59	-	90/10	LW	20	-	SM	70/ 61	-	TI	SM	69	-	LW	33	-
10. Thermal/Bioshield	HW	70/30(16)	LW SM	22 33	-	Air LW	45 27	-	90/10	SM	32	-	LW	24	-	N/A	-	-	-	-	-	-	-	-	-	-	-	-	-
11. Emerg Core	P/S	TI	D_2O	54	-	LW	38	-	TI (17)	LW	40	-	SM	71	-	TI	D_2O	100	-	LW	53	-	TI	-	-	-	-	-	-
12. Irrad Fuel Bay	HW	70/30	SM	32	-	LW	27	-	304L 316	SM	37 32	-	LW	29	-	304L	SM	35 -	-	LW -	29 -	-	TI	SM	29	-	LW	23	-
13. Maintenance	HW	N/A	-	-	-	-	-	-	N/A	-	-	-	-	-	-	1600 1800	D_2O	54 58	-	LW	38 62	-	-	-	-	-	-	-	-
14. Liq Zone Control	S	N/A	-	-	-	-	-	-	304	LW	26	-	SM	66	-	304L	LW	33 38	-	SM	58 93	-	-	-	-	-	-	-	-
15. Turb Lub Oil	S	304	LW	24	-	OIL	60	UDP	CU	LW	24	-	OIL	60	UDP	CU 90/10	LW	24 27	-	OIL	60	-	- A86R	LW	-	-	OIL	70	-
16. Gen Hydrogen	SP (18)	CU	LW	37	-	H	53	-	CU	LW	37	-	H	53	-	CU	LW	30	-	H	53		90/10	LW	-	-	H	-	-
17. Gen Stator	P (19)	A86R	SM	46	-	LW	29	-	ALBR (20)	SM LW	62 23	-	LW SM	35 -	-	ALBR(20)	SM LW	60 27	-	LW/SM	35	CC	18/8 A86R	LW	-	-	SM	-	-
18. Gen Seal Oil	SM (21)	ALBR	LW	-	-	OIL	-	-	CU	LW	-	-	OIL	-	-	CU	LW	-	-	OIL	-	-	-	-	-	-	-	-	-
19. Condenser	SM	A86R	LW	22	-	STM	-	-	A86R (22)	LW	22 24	-	STM	- 32	-	A86R 304L	LW	22	-	STM	- 32	-	304L	LW	23	-	STM	32	-
20. Cond Air Ex Pump	S	A86R	SM	-	-	STM	-	-	-	LW	70	-	STM	-	-	304	STM	-	-	STM	193	-	304L	SM	32	-	STM/Air	250	-
21. Boil Feed Pup Oil	PC	-	-	-	-	-	-	-	A86R	LW	30	-	OIL	50	-	N/A	-	-	-	-	-	-	-	-	-	-	-	-	-
22. Boil Feed Pup Air	P	-	-	-	-	Air	-	-	A86R 90/10	LW	30 23	-	Air	-	-	CU	LW	24 27	-	Air	- 40	-	90/10	SM	24	-	Air	48	-
23. Main Transf Oil	P	-	LW	38	-	OIL	55	-	A86R	LW	38	-	OIL	-	-	90/10 904(23) ALAX	LW	20	-	OIL	-	UDP(23) SCC	-	-	-	-	-	-	-
24. Spot Transf Oil	P	-	-	-	-	-	-	-	90/10	LW	38	-	OIL	-	-	CU	LW	38	-	OIL	-	-	-	-	-	-	-	-	-
25. Gen Transf Oil	P	-	-	-	-	-	-	-	A86R	LW	30	-	OIL	-	-	CU	LW	30	-	OIL	-	-	-	-	-	-	-	-	-
26. CCW Pup Oil	PC	N/A	-	-	-	-	-	-	CU	LW	30	-	OIL	-	-	N/A	-	-	-	-	-	-	-	-	-	-	-	-	-
27. Main Enter Air	P	-	LW	38	-	Air	-	-	CU	LW	20	-	Air	-	-	CS	ASK	-	-	Air	-	-	-	-	-	-	-	-	-
28. MCP	P (24)	TI	SM	77	-	LW	54	-	90/10	LW	29	-	SM	57	UDP	TI	SM	83	-	LW	52	-	TI	LW	50	-	SM	38	-
29. Booster Bldg Acc	P	CU/AL	LW	38	-	Air	-	-	-	LW	30	-	Air	-	-	90/10	LW	30	-	Air	-	-	-	-	-	-	-	-	-
30. Service Air Comp	PSM	-	LW	38	-	Air	-	-	A86R	Air	30	-	LW	30	-	CU	Air	30	-	LW	30	-	-	-	-	-	-	-	-
31. LP Inst Air Comp	PSM	-	LW	38	-	Air	-	-	A86R	Air	30	-	LW	30	-	CU	Air	30	-	LW	30	-	-	-	-	-	-	-	-
32. HP Inst Air Comp	PSM	-	LW	38	-	Air	-	-	A86R	Air	30	-	LW	30	-	CU	Air	30	-	LW	30	-	-	-	-	-	-	-	-
D_2O BOILR																													
33. Steam Generator	HW	M400	D_2O	290	-	SM	250	-	M400	D_2O	290	-	SM	266	-	1600	D_2O	290 318	SCC	SM	260 268	CF	1800	D_2O	-	-	SM	-	-
34. Blood Condenser	HW	N/A	-	-	-	-	-	-	M400	D_2O	140 117	-	D_2O	150	-	1600	D_2O	133	-	D_2O	250 204	-	1800	D_2O	167		D_2O	205	-
35. Blood Cooler	HW (25)	M400	D_2O	140	-	SM	80	-	M400	D_2O	140 214	-	SM	70 56	-	1800	D_2O	300 220	-	SM	74 85	-	1800	D_2O	204	-	SM	56	-
36. Fuel Mech D_2O	HW (26)	1600	D_2O	232	-	STM	150	-	1600	D_2O	-	-	SM	-	-	304L	D_2O	82	-	Air	49	-	304L	D_2O	38	-	SM	25	-
37. Reheater	HW VS	90/10	STM	250	-	STM	221	CE	CS	STM	250	-	STM	230 226	-	CS 410	STM	253	-	STM	237	-	321	STM	261	-	STM	247	-
38. LP Feed Htr	HW	A86R	FW	112	-	STM	150	-	A86R	FW	107	-	STM	150	-	90/10 304	FW STM	118 182	-	STM	148	-	304	STM	123	-	STM	174	-
39. HP Feed Htr	HW	90/10	FW	175	-	STM	200	-	90/10	FW	171	-	STM	200	-	90/10 304	FW STM	171 204	-	STM	200	-	304	STM	160	-	STM	183	-

NOTES:

(1) Includes data available as of 85-6-21

(2) Type of HX
- T = T
- S = Straight
- U = U-tube
- V = Vertical
- H = Horizontal
- F = Finned
- C = Coil
- P = Plate

(3) Tube Material
- 70/30 = 70 Cu-30Ni
- CU = Copper
- M400 = Monel 400
- TI = Titanium
- 304 = 304 stainless steel
- 304L = 304 stainless low C grade
- A86R = Admiralty Brass
- CU/AL = Copper with Al fins
- 90/10 = 90Cu-10Ni
- I400 = Inconel 600
- ALBR = Aluminum Brass
- I600 = Incoloy 800
- 904 = 904L stainless steel
- ALAX = Allegeny Ludlum Type 6x stainless
- 321 = 321 stainless steel
- CS = carbon steel
- 18/8 = 18/8 stainless steel

(4) Environment
- LW = Lakewater
- SM = Demineralized Water
- H = Hydrogen
- STM = Steam/Condensate
- FW = Feedwater
- AIR = Ambient

(5) Maximum Design Temperature (°C)

(6) Failure
- UDP = Under Deposit Pitting
- SCC = Stress Corrosion Cracking
- CC = Crevice Corrosion
- EE = Exfoliation
- CF = Corrosion Fatigue/ or Fatigue

(7) Where available different, data for Pickering "B" & Bruce "B" inserted below data for "A" units.

(8) Data not available

(9) N/A - Not Applicable

(10) 1800 replacement bundle in P-A U-3, 1800 in P-B. Both failed by UDP.

(11) Darlington is HS

(12) Darlington is HS

(13) P-B is HC, Darlington is HC

(14) Coil in Shell for P-B

(15) Darlington is plate, B-B horizontal U tube, B-A is HU

(16) Thermal & Biological shield cooler are separate at DPNCS. Biological shield coolers are tubed with Cu.

(17) P-B, P-A Bruce Mod HE

(18) Darlington is VS, P-B and B-B is HE

(19) DPNCS-SH

(20) 1 HE at P-A & B-A - TI

(21) DPNCS II V

(22) 304 ss is ASE & peripheral regions

(23) Both Materials at B-A. Original Material, A86R failed by UDP & SCC

(24) P-A is HU

(25) P-A is VU

(26) Darlington is HC

TABLE 2

RANKING OF AUSTENITIC STAINLESS STEELS IN SEAWATER
BY PITTING TEMPERATURE (°C) AND PITTING INDEX
(wt % Cr + 3.3 wt % Mo)

Alloy	Pitting Temperature (°C)	Pitting Index
304	-7	19
800	2	21
316	10	25
825	35	31
904L	44	37
S28	63	39
AL6X	60	40
625	97	51

TABLE 3a
MATERIALS FOR TEST PROGRAM

Material	Alloy Designation	% Major Constituents					Primary Source	Mechanical Props Tube / Plate			Average Grain Size (ASTM)		Hardness (Vickers)		(CR = Cold Rolled)
		Fe	Ni	Cr	Mo	Other		YS	UTS	% e	Tube OD Center	Plate Surface Center	Tube OD Center	Plate Surface Center	Heat Treatment Tube / Plate
Ti	R50400	-	-	-	-	-	Kobe Steel	366 318	432 451	30 30	8 8	2 1	144 156	148 152	Annealed CR + Annealed
I625	N06625	4.5	60	22	8.5	3.5 Cb +Ta	Huntington	-	-	-	11 11	10 10	234 227	207 206	Annealed CR + Annealed
AL6X	N08366	bal	25	20	6.3	-	Allegheny Ludlum	-	-	-	5 5	5 6	155 143	135 136	Annealed CR + Annealed
904L	N08904	bal	25	20	4.6	1.5 Cu	Uddeholm	- 290	- 608	- 52	9 7	9 8	155 155	147 145	Annealed CR + Annealed
S28	N08028	bal	31	27	3.4	1.0 Cu	Sandvik	273 -	615 -	44 -	7 6	8 5	144 139	150 148	Cold Finish Annealed CR + Annealed
I825	N08825	bal	43	23	2.7	1.7 Cu	Huntington				12 12	11 11	204 197	214 212	Annealed CR + Annealed
I800	N08800	bal	32	20	-	-	Huntington	- 307	- 621	- 40	12 10	10 10	169 161	152 147	Annealed CR + Annealed
M400	N04400	1.9	66	-	-	31 Cu	Huntington	- 239	- 548	- 42	7 7	7 8	146 137	124 126	Annealed CR + Annealed
70/30	C71500	0.6	30	-	-	68 Cu	Anaconda (tube) & Revere (plate)	173 194	420 404	- 44	10 9	9 9	94 93	98 100	N/A N/A

TABLE 3b

DETAILED ANALYSES OF MATERIALS TESTED

Tubing

Material	C	Mn	P	S	Si	Cr	Ni	Al	Mo	Cu	Ti	N	Co	Zn	Other
Ti	0.005														H - 0.0016 Fe - 0.06 N - 0.0048 O - 0.074
I625	0.03	0.20	0.010	0.001	0.29	21.77	60.69	0.12	8.62		0.21				Cb+Ta- 3.58 Fe - 4.48
AL6X	0.018	1.52	0.030	0.002	0.40	20.47	24.65		6.35						N/A
904L	0.015	1.42	0.023	0.002	0.41	20.10	24.90		4.55	1.54		0.043			N/A
S28	0.013	1.75	0.15	0.003	0.04	26.87	30.97		3.41	0.96					N/A
I825	0.02	0.38		0.003	0.01	22.37	44.29	0.03	2.72	1.74	0.76				Fe - 27.70
I800	0.08	0.99		0.001	0.30	20.25	32.52	0.53		0.48	0.41				Fe - 44.4
M400	0.11	1.07		0.002	0.30		65.51	0.033		31.12					Fe - 1.85
70/30 Cu-Ni		0.73					30.40			67.96				0.32	Pb - 0.01 Fe - 0.58

Flat Coupons

Material	C	Mn	P	S	Si	Cr	Ni	Al	Mo	Cu	Ti	N	Co	Zn	Other
Ti	0.02											0.012			O - 0.129 Fe - 0.03
I625	0.04	0.16	0.010	0.001	0.34	22.34	60.20	0.14	8.48		0.25				Cb+Ta -3.51 Fe - 4.53
AL6X	0.020	1.47	0.030	0.002	0.50	20.45	24.65	0.006	6.30	0.19	0.005	0.042	0.19		B - 0.0008
904L	0.014	1.66	0.027	0.006	0.60	19.50	24.2		4.60	1.39					N/A
S28	0.015	1.73	0.015	0.003	0.03	26.7	30.9		3.37	0.96					N/A
I825	0.02	0.37		0.004	0.25	22.68	42.17	0.05	2.72	1.75	0.91				N/A
I800	0.07	0.90		0.002	0.19	20.36	31.15	0.40		0.47	0.37				Fe - 46.09
M400	0.10	1.02		0.001	0.21		65.82	0.053		30.92					Fe - 1.88
70/30 Cu-Ni	<0.03	0.79	0.003	0.005			30.50			67.87				0.2	Pb - 0.007 Fe - 0.65

TABLE 4

CHARGE DIFFERENCE - ΔQ (mC/cm^2) IN LAKE WATER AT 40°C FOR VARIOUS COMBINATIONS OF SCAN RATE AND MATERIAL SURFACE CONDITION

Material	1.2 V/h				0.25 V/h			
	As Received		600 Grit		As Received		600 Grit	
	Test	ΔQ	Test	ΔQ	Test	ΔQ	Test	ΔQ
Ti	214	0	215	0	238	0	239	0
I625	197	0	196	0	280	0	237	0
AL6X	213	10	212	10	(1)	0	235	117
904L	217	84	216	21	232	550	248	268
S28	199	35	198	115	230	281	231	906
I825	245	380	210	116	(2)	1 083	(3)	1 617 (±959)(5)
I800	244	4 122	194	297	222	2 349	223	2 230
M400	189	1 249	188	1 855	240	9 724	241	12 189
70/30	193	1 357	247	0	(4)	0	243	0

Notes: (1) Average of three tests (234, 250, 251)
(2) Average of three tests (224, 226, 228)
(3) Average of four tests (218, 225, 227, 229)
(4) Average of two tests (242, 249)
(5) 95% Confidence Limits

General Note: The method of determination of ΔQ is given in Section 1.4.

TABLE 5

PITTING POTENTIALS IN LAKE WATER AT 40°C FOR ALL MATERIALS USING A SCAN RATE OF 1.2 V/h AND INITIAL SURFACE CONDITION OF 600 GRIT

Material	E_b (V)	E_{prot} (V)	$E_b - E_{prot}$ (V)
Ti	-	-	-
I625	0.821	-	0
AL6X	0.870	1.097	0
904L	0.872	0.253	0.619
S28	0.844	0.317	0.527
I825	0.863	0.788	0.075
I800	0.865	0.261	0.640
M400	0.731	0.068	0.663
70/30	0.090	-	-

Note: E_b & E_{prot} are defined in Section 1.4

TABLE 6

OBSERVATIONS OF SURFACE APPEARANCE OF SAMPLES FOLLOWING CPP TESTING

Initial Surface Conditions - As Received/Scan Rate 0.25 V/h

Test #	Material	Observations
238	Ti	no pits
236	I625	no pits (poor initial surface condition)
234	AL6X	hemispherical pits stained, in line although no apparent reason
232	904L	isolated hemispherical pits, some undercutting evident
230	S28	more numerous pits than 904L, undercut, both crystallographic and not, stained
226	I825	numerous shallow pits associated with surface deformation, stained
222	I800	extensive general attack, fewer pits but greater development than I825
240	M400	very large isolated and numerous pits, crystallographic and hemispherical, dealloying
242	70/30	no pitting, but extensive accelerated non-uniform corrosion

Initial Surface Condition - 600 grit/Scan Rate 0.25 V/h

Test #	Material	Observations
239	Ti	no pits
237	I625	no pits
235	AL6X	isolated pits, shallow, lateral dissolution, crystallographic attack in base
233	904L	small isolated shallow pits
229	S28	numerous well developed hemispherical pits, random distribution, stained
227	I825	extensive pitting, >I800 and S28, stained, crystallographic
223	I800	few shallow hemispherical pits, no crystallographic attack
241	M400	areas of extensive dealloying and well developed hemispherical pits
243	70/30	extensive non-uniform general corrosion

Initial Surface Condition - As Received/Scan Rate 1.2 V/h

Test #	Material	Observations
214	Ti	no pits
197	I625	no pits (poor initial surface condition)
213	AL6X	pits with inner deposit, not crystallographic
217	904L	surface residue, surface finish insensitive, isolated and shallow pits
199	S28	few isolated pits, no crystallographic attack, stained
211	I825	more extensive pitting but shallower than I800, pitting associated with surface damage, staining
195	I800	some pitting
189	M400	extensive general corrosion and denickelification, lateral dissolution, broad open pits
193	70/30	extensive pitting with depth dissolution and dealloying

Initial Surface Condition - 600 Grit/Scan Rate 1.2 V/h

Test #	Material	Observations
215	Ti	no pits
196	I625	no pits
212	AL6X	very shallow "micropitting" associated with surface morphology
216	904L	few isolated pits, hemispherical with considerable depth
198	S28	extensive shallow pits, mixed crystallographic nature
210	I825	extensive shallow pits, stained, associated with surface morphology
194	I800	numerous isolated pits, hemispherical with undercutting
188	M400	hemispherical pits, isolated but numerous, denickelification
192	70/30	large hemispherical pits with considerable depth and dealloying

TABLE 7

SUMMARY OF RESULTS OF ISOTHERMAL AND HEAT FLUX IMMERSION TESTING

Isothermal	Ti	I625	AL6X	904L	S28	I825	I800	M400	70/30
T = 40°, 8 wk	-	-	-	-	-	-	-	-	-
T = 40°, 16 wk	-	-	-	X (a)	-	-	X (d)	X (e)	X (f)
T = 40°, 20 wk (600 grit)	-	CC	-	X	X	-	CC	X + DA	X + DA
T = 40°, 24 wk	-	-	-	X	X (b)	X (c)	CC	-	X
T = 40°, 32 wk	-	-	-	X	X	-	CC	DA	X + DA
T = 45°, 52 wk	NT	NT	-	-	NT	-	-	NT	X 0.03
T = 60°, 6 wk	-	NT	NT	-	-	NT	NT	NT	DA
T = 70°, 26 wk	NT	NT	NT	X 0.60	NT	X 0.30	NT	NT	NT
T = 70°, 52 wk	NT	NT	-	-	NT	-	-	NT	X

Heat Flux	Ti	I625	AL6X	904L	S28	I825	I800	M400	70/30
4 wk	-	-	-	X	-	-	X	X	DA
4 wk(600 grit)	NT	NT	NT	NT	X	NT	NT	NT	NT
6 wk	-	-	-	X 1.84	-	X 0.82	NT	NT	DA
8 wk	NT	NT	NT	NT	NT	NT	X 2.71	NT	NT
8 wk(600 grit)	NT	NT	-	NT	NT	X (h)	NT	NT	NT
12 wk	-	-	-	-	-	-	-	X	DA
24 wk	-	-	X 1.2	X (g) 0.3	-	X 0.3	X (i) 1.5	NT	DA
30 wk	NT	-	-	NT	NT	X	-	X	NT

Legend

-	tested, no pitting observed
X	tested, pitting observed and pitting rate in mm/a (if available)
NT	not tested
CC	crevice corrosion
DA	dealloying (and etching)
X(a-i)	Refers to Figures 32 a - i

= heat flux tests at OHRD. Others at CRNL.

TABLE 8

SUMMARY OF RESULTS OF EDX(1) ANALYSIS WITHIN PITS(2)

Material	Test	wt%												
		Al	Si	P	S	Cl	K	Ca	Cr	Fe	Ni	Cu	Zn	Mo
904 L	isothermal	13.2							1.3	8.3	2.0			8.8(3)
I825	CPP Fig 42 (b)							1.5	25.1	41.2	25.6			4.4(3)
I800	isothermal		19.2		6.8	5.0	4.7	48.3	3.7	8.3	4.0			
I800	CPP Fig 42 (c)				0.4			0.3	24.9	45.1	27.5			
70/30	isothermal		2.1					0.8		1.0	29.6	66.6		

Notes: (1) Normalized semi-quantitative (standardless) analysis.
(2) Not all elements analyzed
(3) High Mo level may be due to effects of S on analysis.

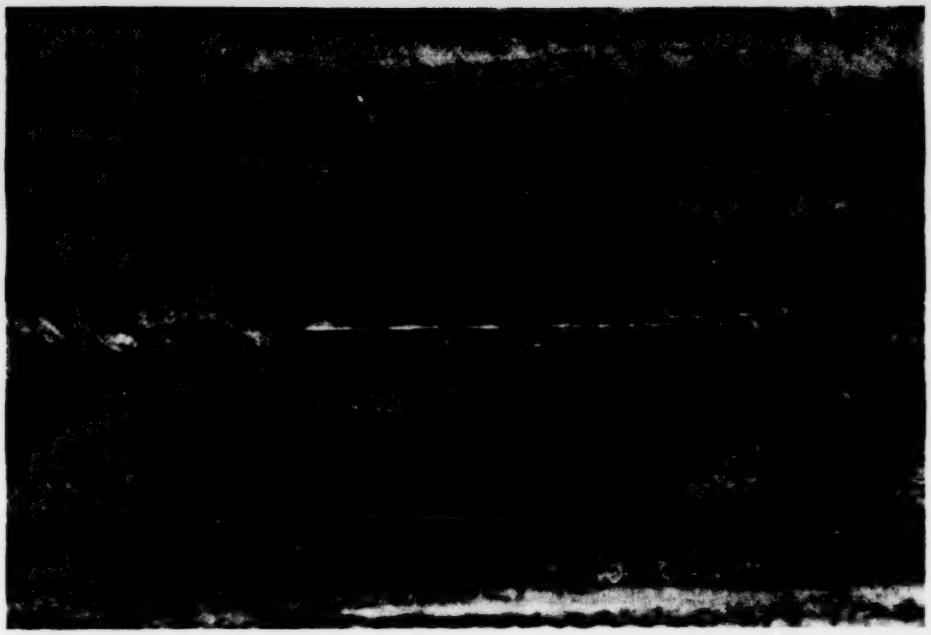

(a) 70/30 Cu-Ni

(b) Incoloy 800

FIGURE 1

TUBES, DEPOSITS, AND EVIDENCE OF UNDERDEPOSIT CORROSION IN TUBE BUNDLES REMOVED FROM PICKERING NGS-A UNIT 3 MODERATOR HEAT EXCHANGERS

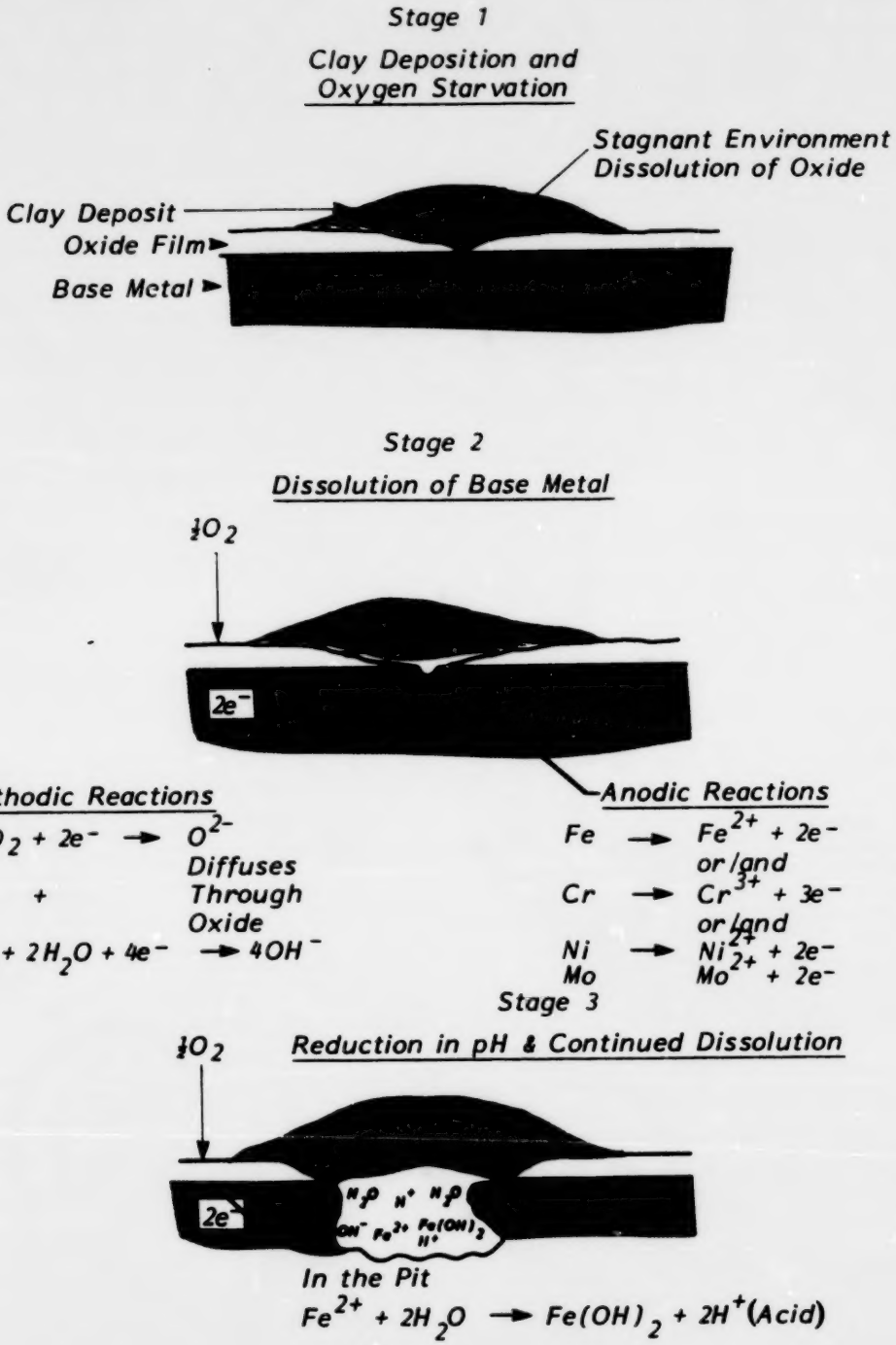

FIGURE 2

SIMPLIFIED DESCRIPTION OF STAGES IN CREVICE CORROSION (NOT ALL REACTIONS & PROCESSES ARE SHOWN)

E_b = Breakdown Potential
E_{prot} = Protection Potential
E_{pp} = Primary Passivation Potential
E_{corr} = Corrosion Potential

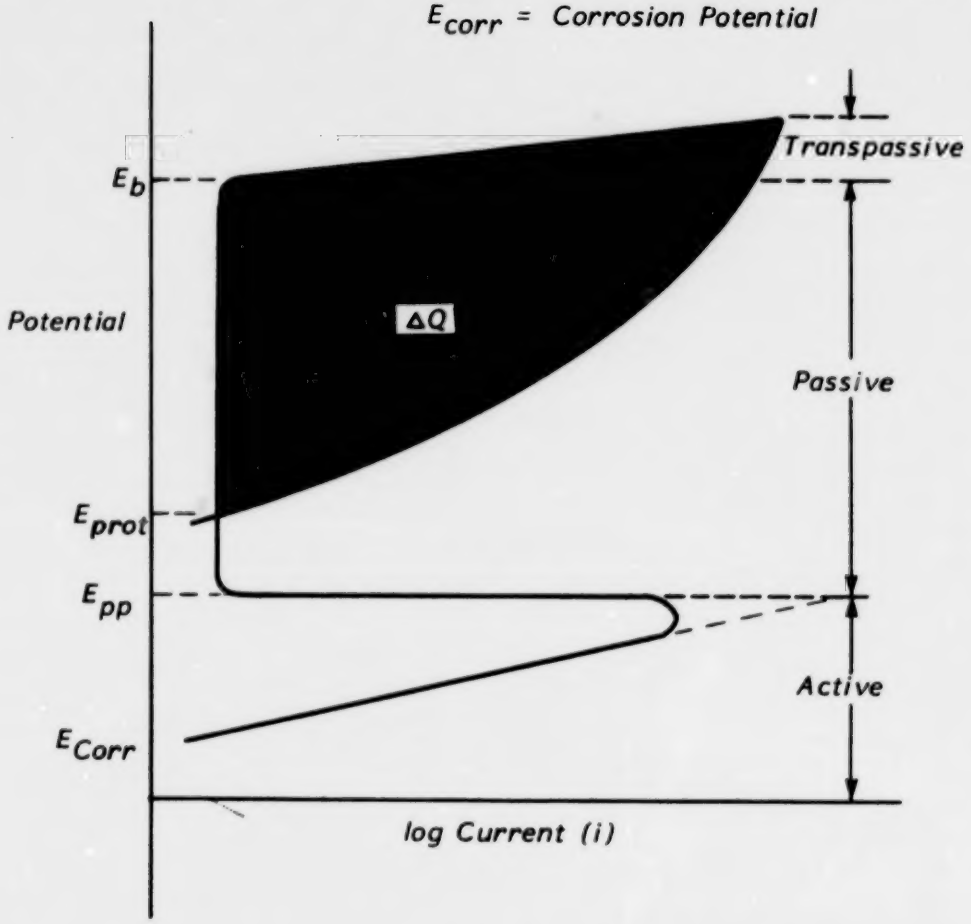

FIGURE 3

SCHEMATIC OF E vs LOG i RESPONSE FOR STAINLESS STEELS IN ACIDIC MEDIA

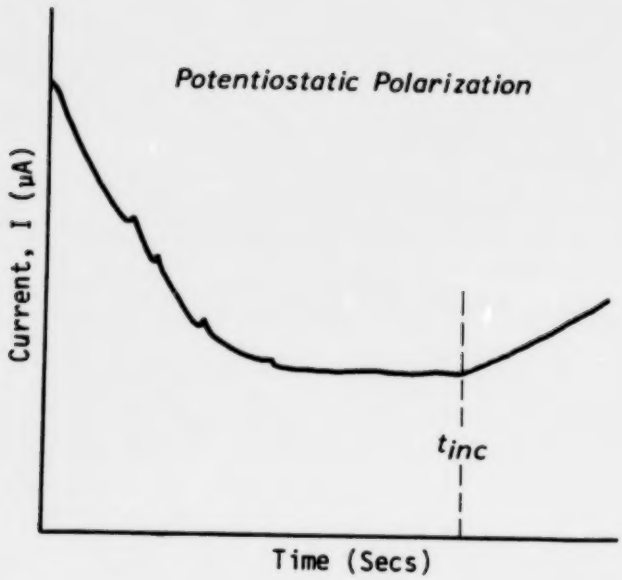

FIGURE 4

METHOD OF DETERMINATION OF PIT INCUBATION TIME (t_{inc}) WHERE t_{inc} ≡ GLOBAL MINIMA IN PLOT OF i VERSUS t AT CONSTANT POTENTIAL

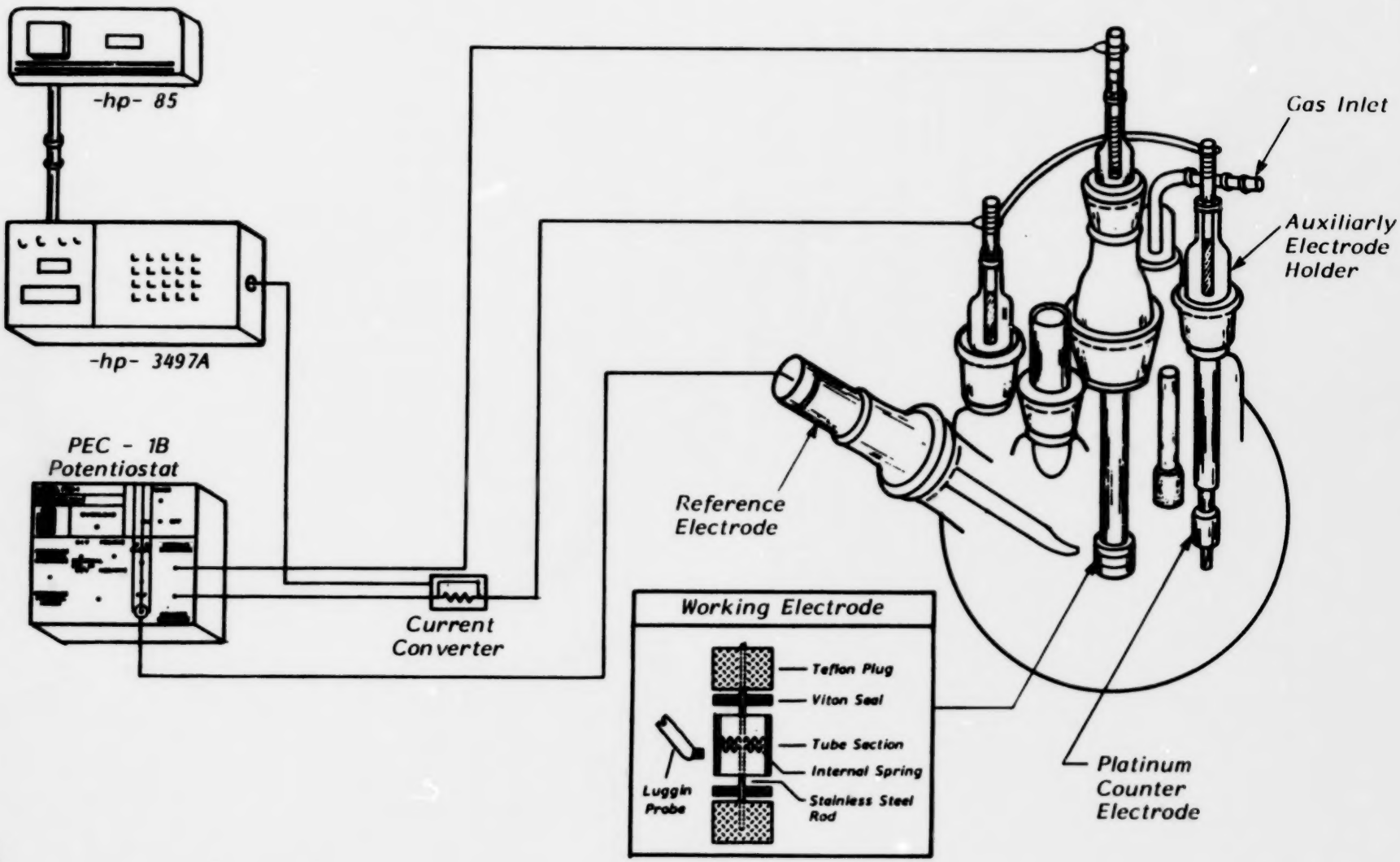

FIGURE 5

ELECTROCHEMICAL TEST APPARATUS SCHEMATIC

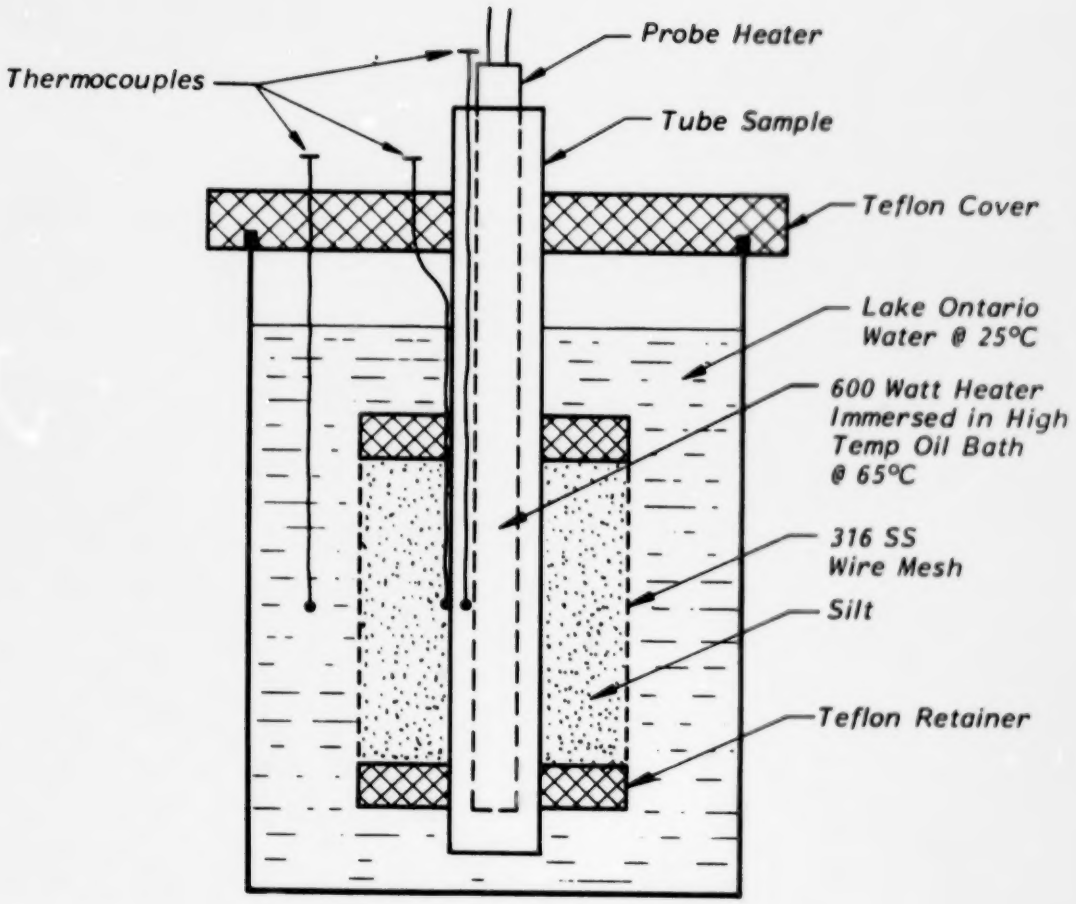

FIGURE 6

**HEAT FLUX IMMERSION TEST APPARATUS-
SCHEMATIC OF 1 TEST CELL**

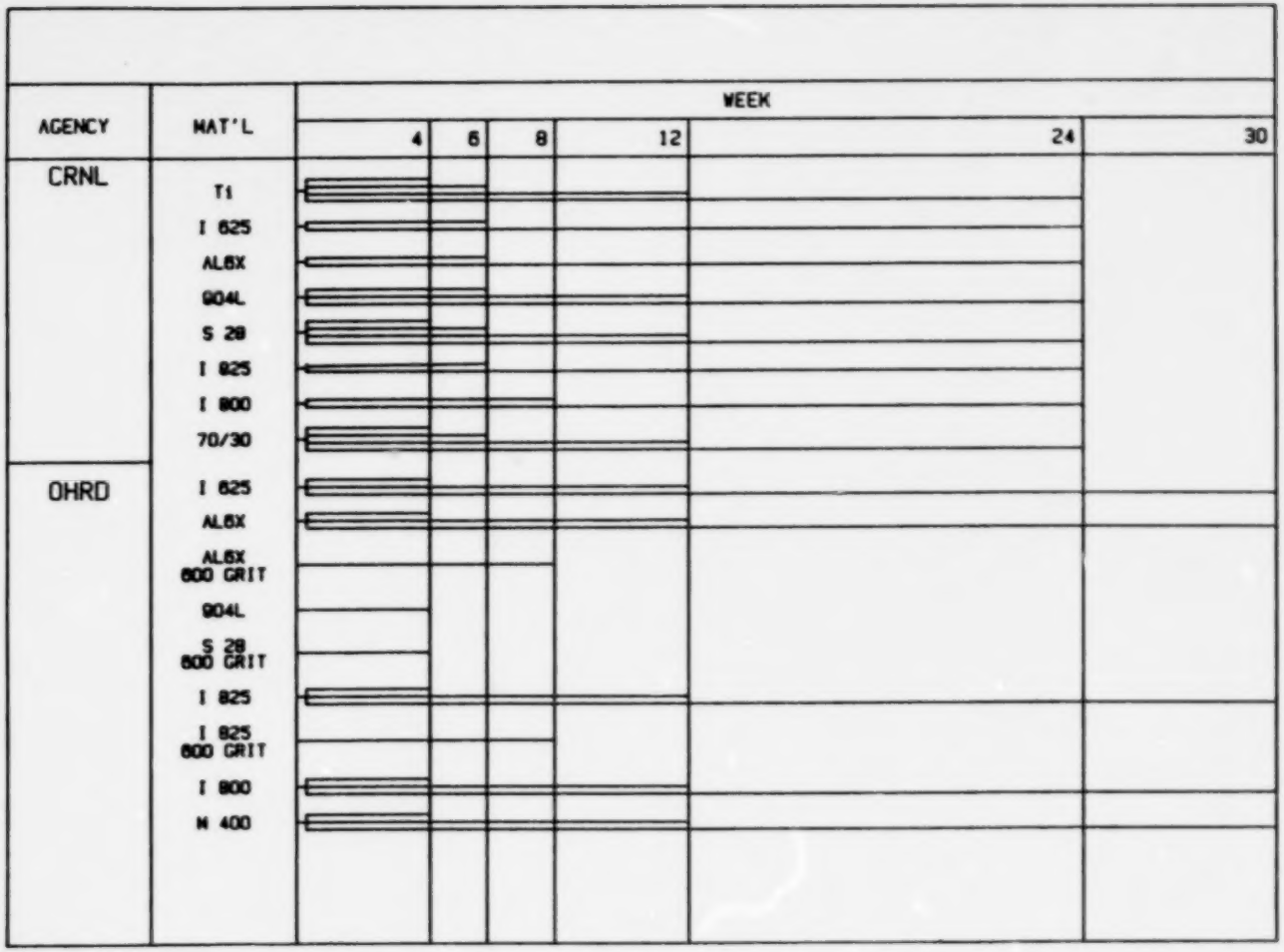

FIGURE 7

HEAT FLUX IMMERSION TEST PROGRAM SCHEDULE

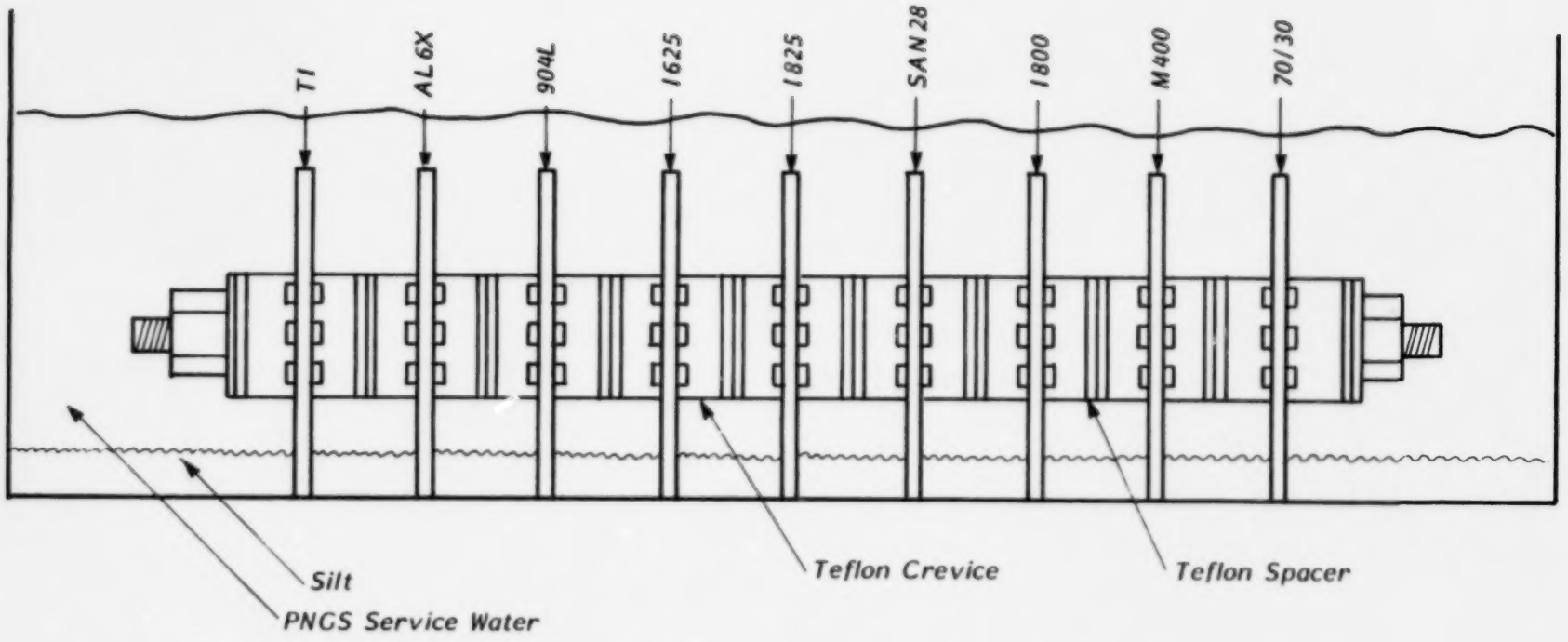

FIGURE 8
ISOTHERMAL IMMERSION TEST APPARATUS - SCHEMATIC

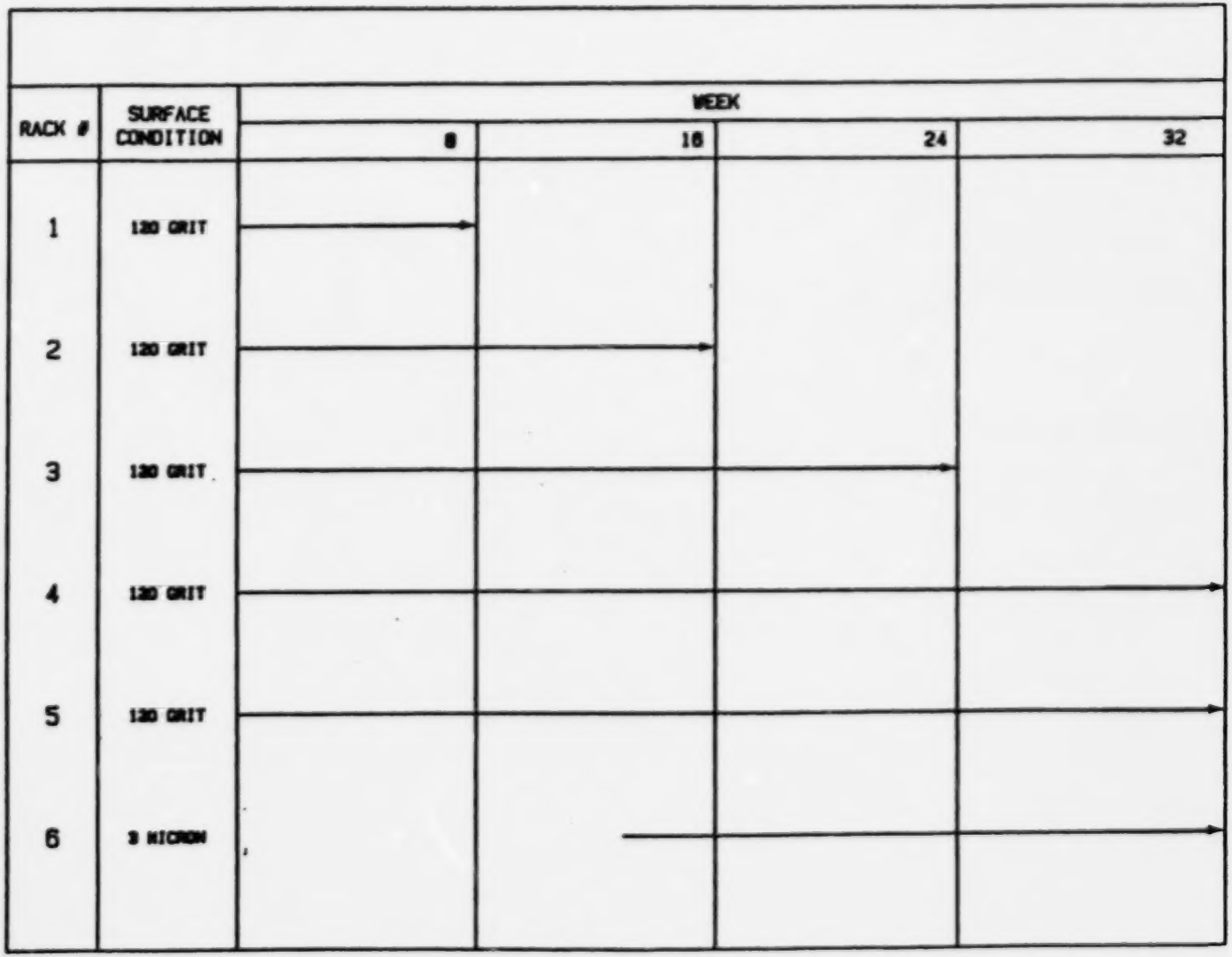

FIGURE 9

OHRD ISOTHERMAL (40°C) IMMERSION TEST SCHEDULE (ALL MATERIALS)

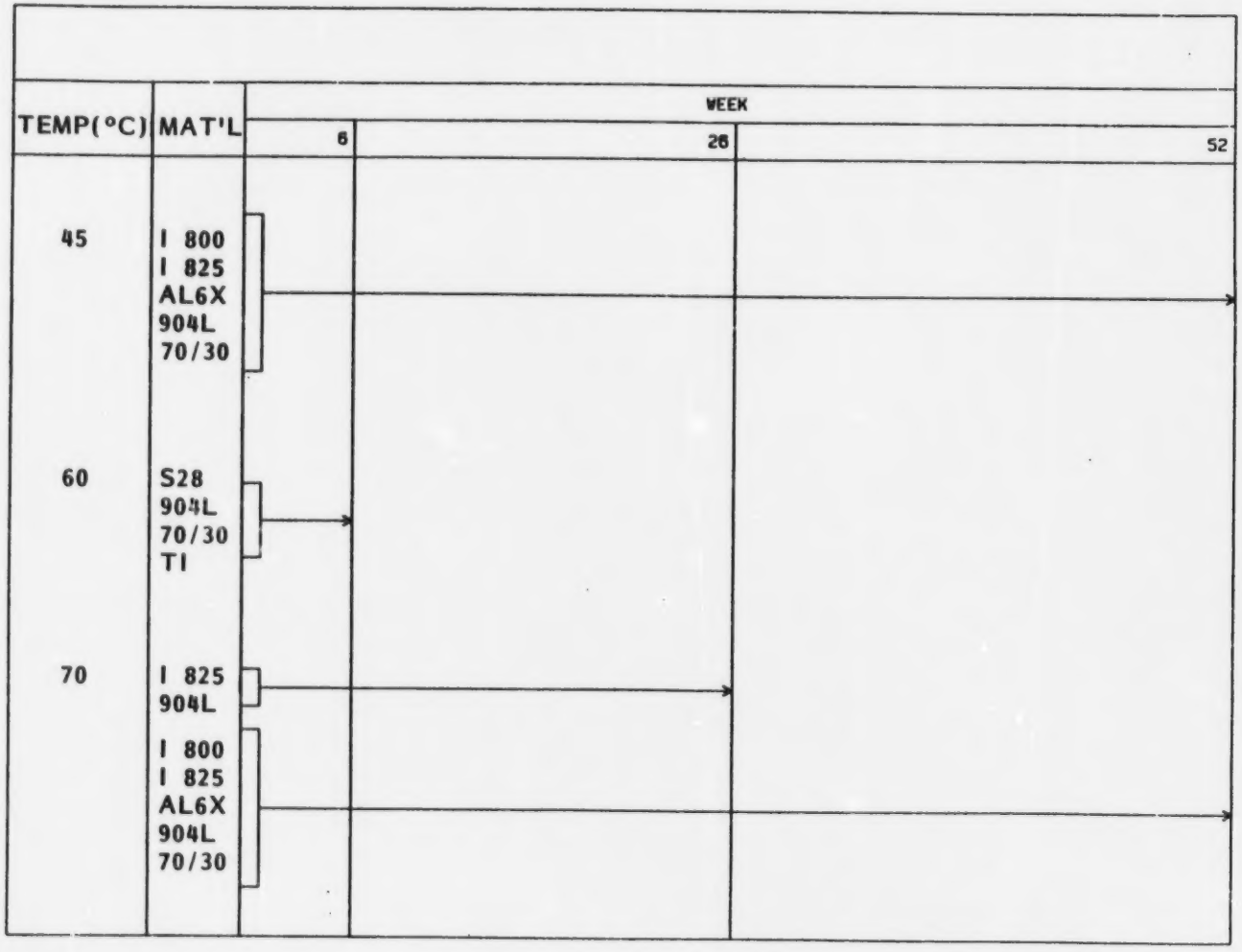

FIGURE 10

ISOTHERMAL IMMERSION TEST PROGRAM AT AECL-CRNL

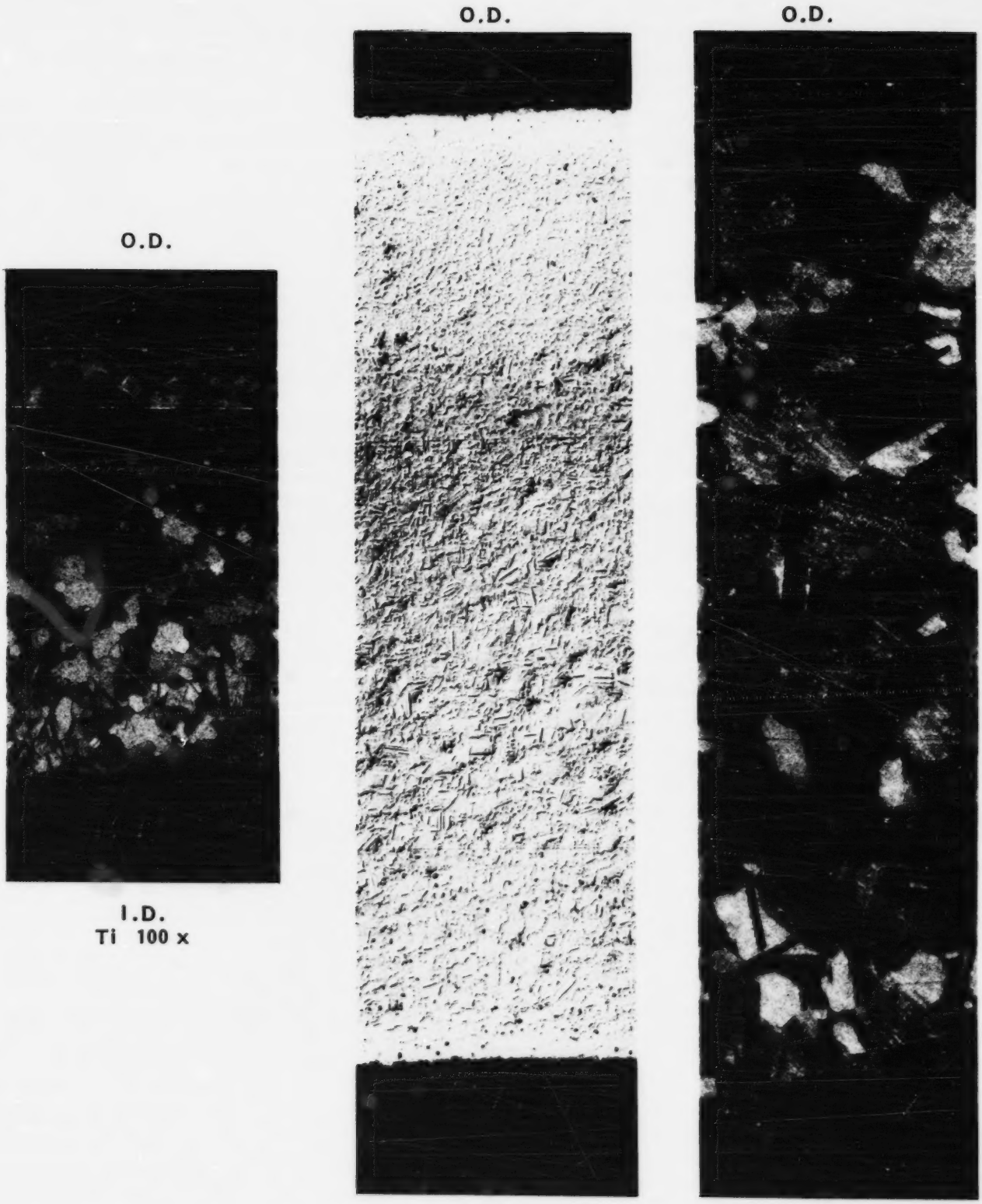

FIGURE 11

TUBE THROUGH-WALL COMPOSITE MICROSTRUCTURES

904L Tube 100 x

S28 Tube 100 x

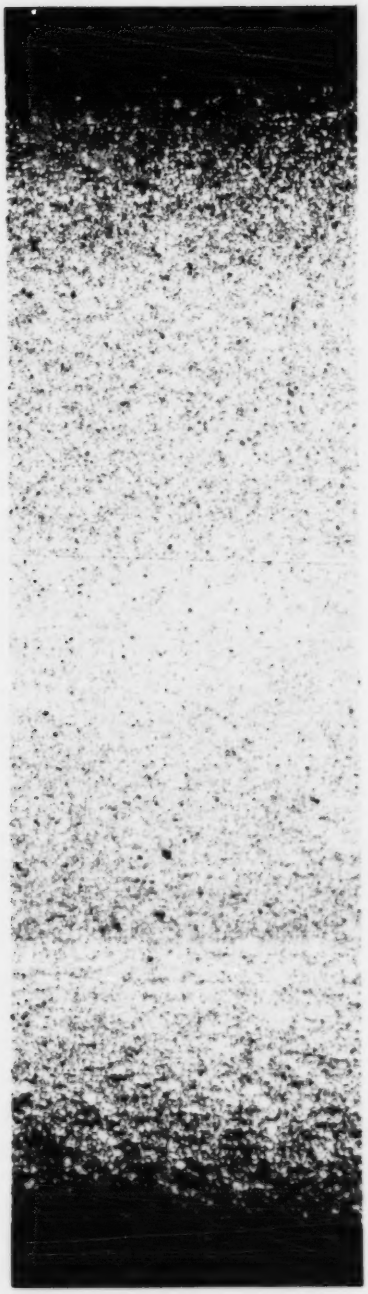

1825 Tube 100 x

FIGURE 12

TUBE THROUGH-WALL COMPOSITE MICROSTRUCTURES

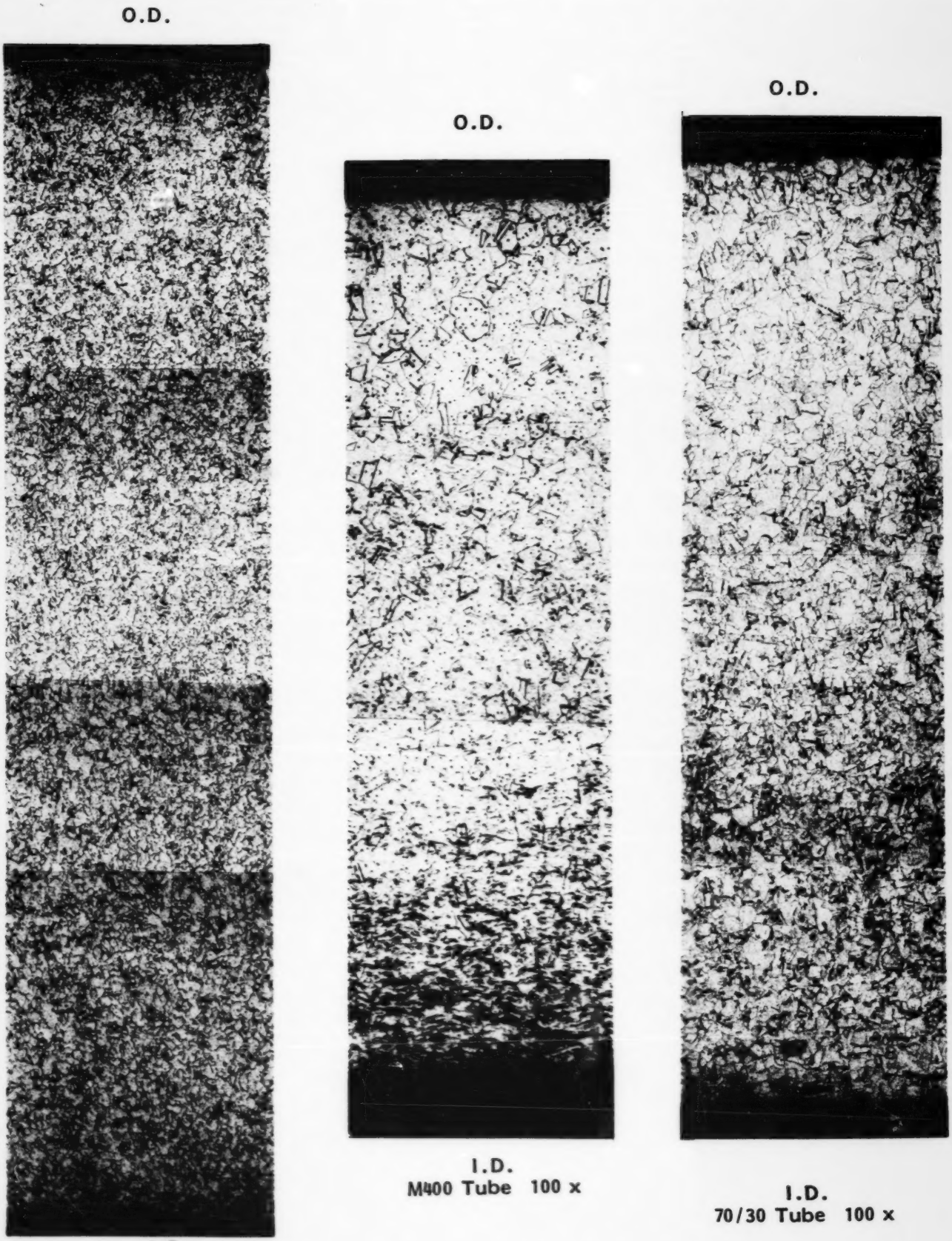

FIGURE 13

TUBE THROUGH-WALL COMPOSITE MICROSTRUCTURES

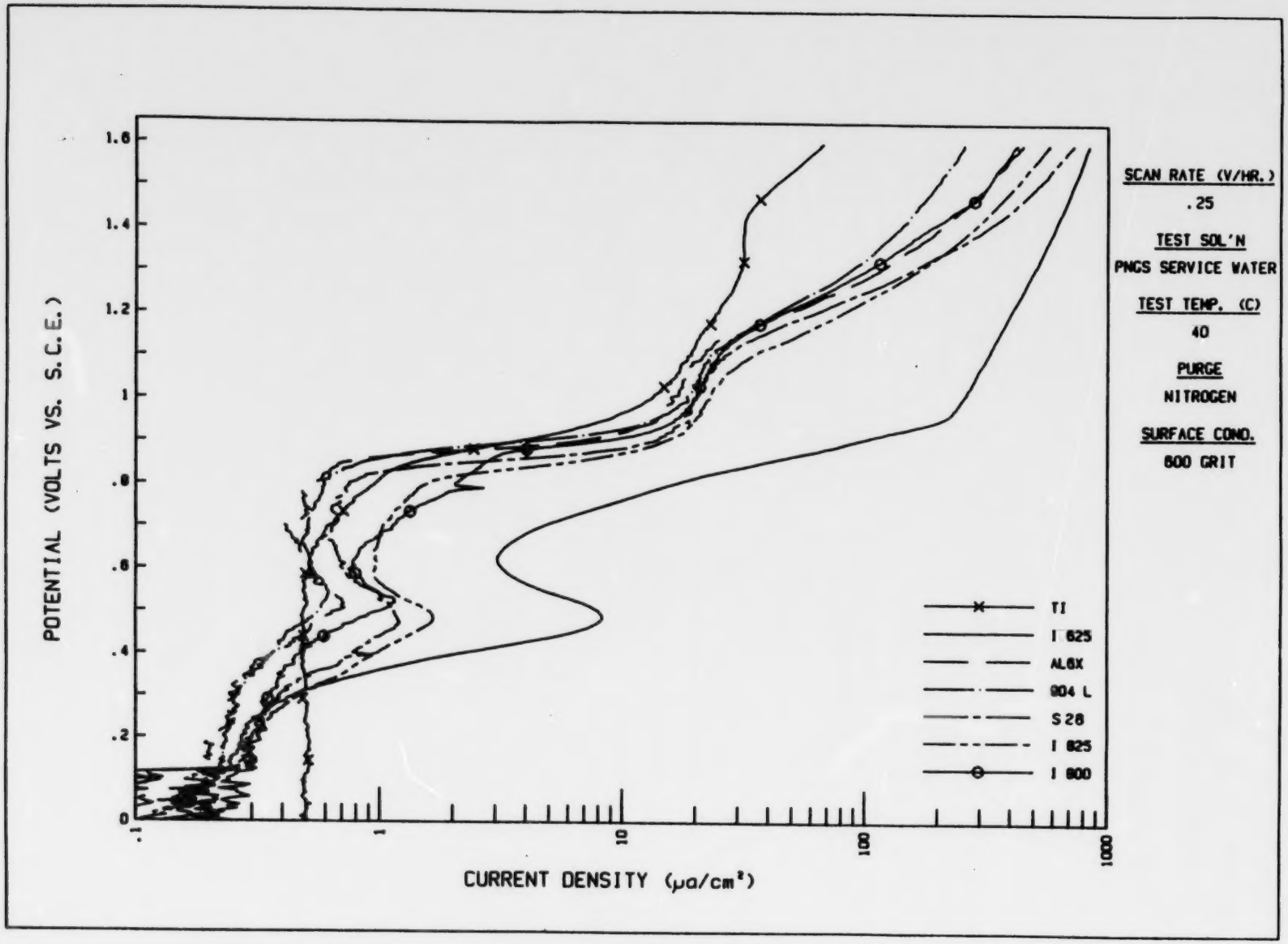

FIGURE 14a

CYCLIC POTENTIODYNAMIC POLARIZATION (CPP) FORWARD PLOTS FOR Ti, 1625, AL6X, 904L, S28, 1825, 1800 FOR A SCAN RATE OF 0.25 V/HR & INITIAL SURFACE CONDITION OF 600 GRIT

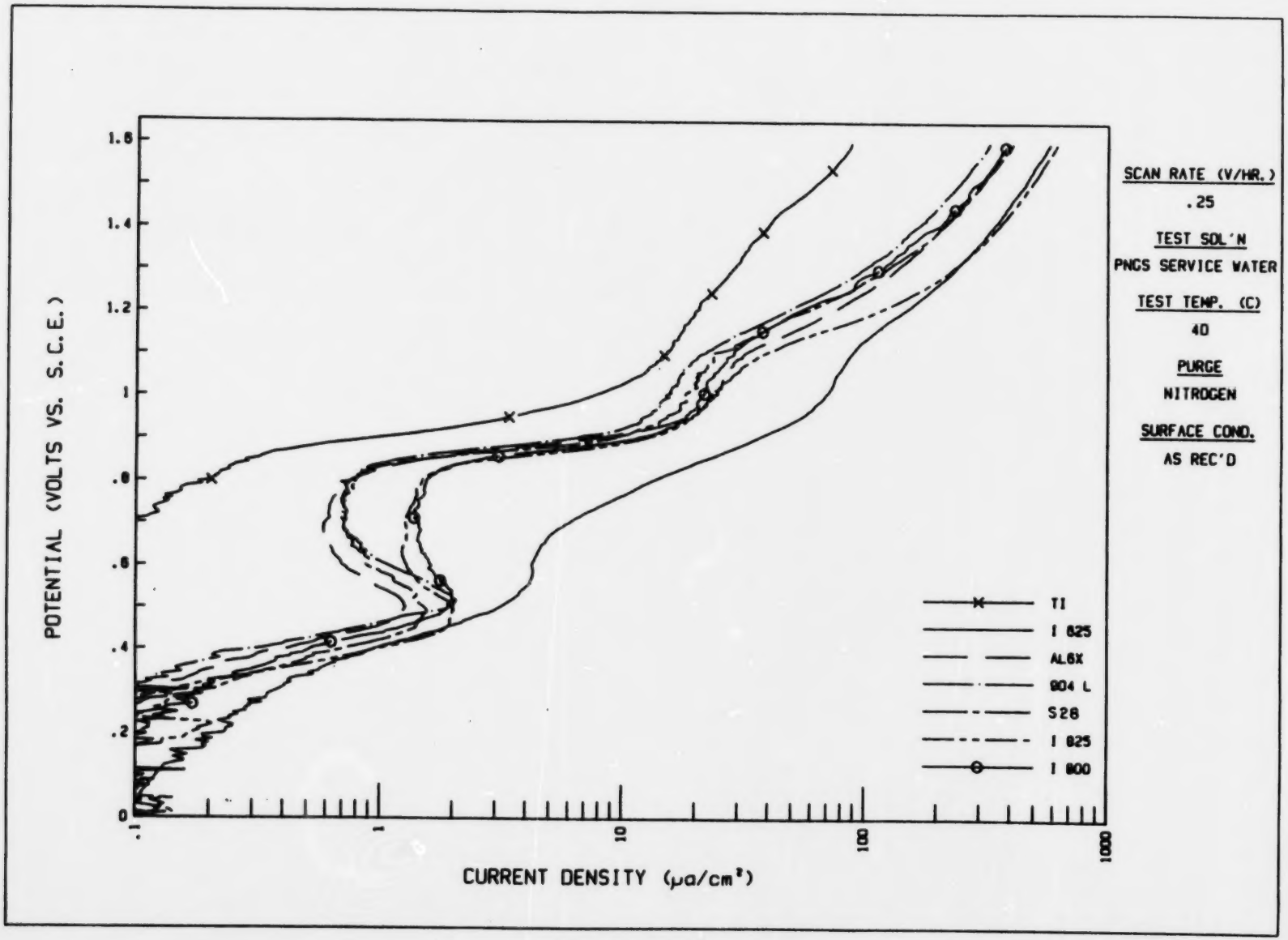

FIGURE 14b

CYCLIC POTENTIODYNAMIC POLARIZATION (CPP) FORWARD PLOTS FOR Ti, 1625, AL6X, 904L, S28, 1825, 1800 FOR A SCAN RATE OF 0.25 V/HR AND AS RECEIVED INITIAL SURFACE CONDITION

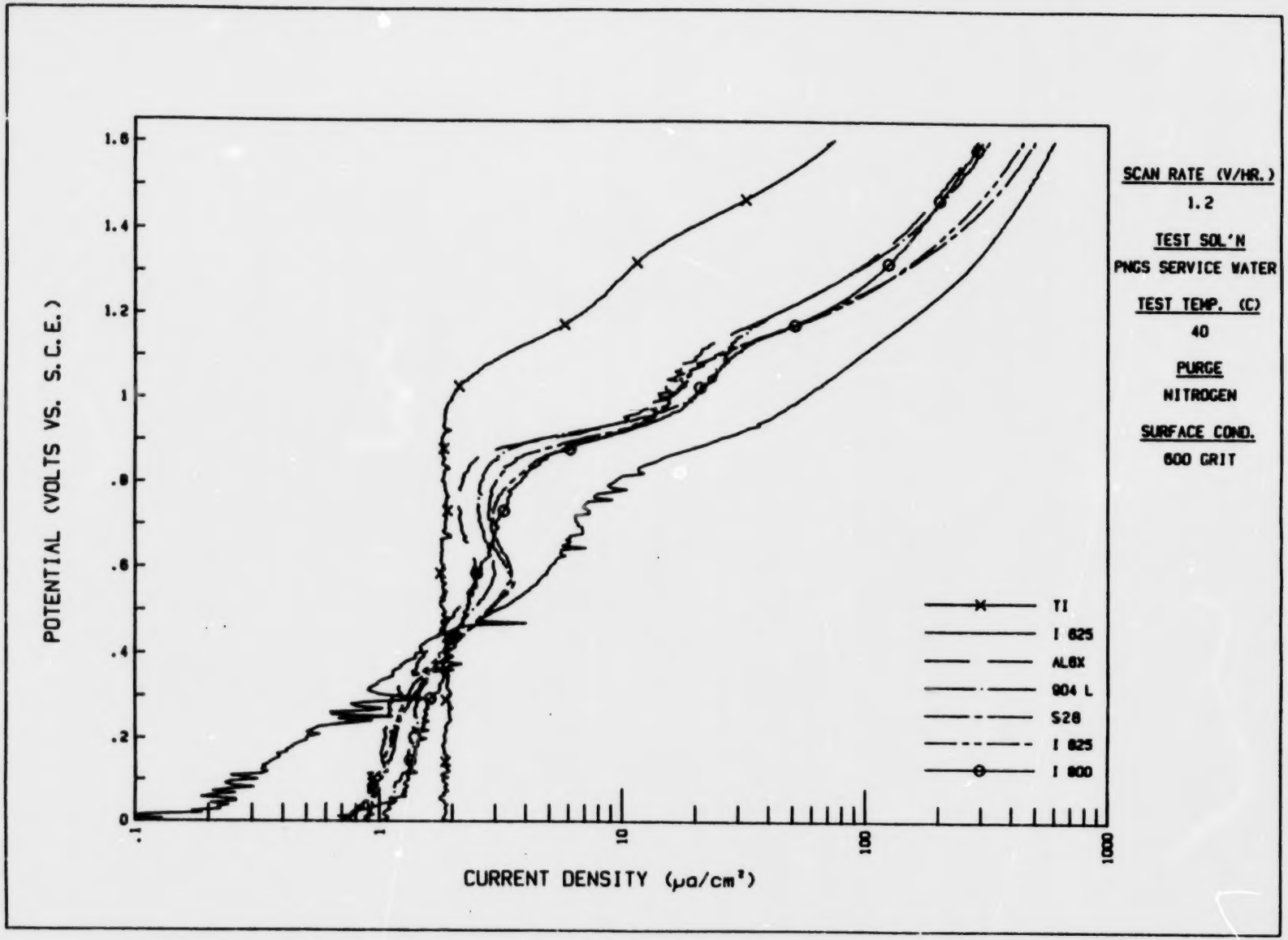

FIGURE 14c

CYCLIC POTENTIODYNAMIC POLARIZATION (CPP) FORWARD PLOTS FOR Ti, 1625, AL6X, 904L, S28, 1825, 1800 FOR A SCAN RATE OF 1.2 V/HR AND INITIAL SURFACE CONDITION OF 600 GRIT

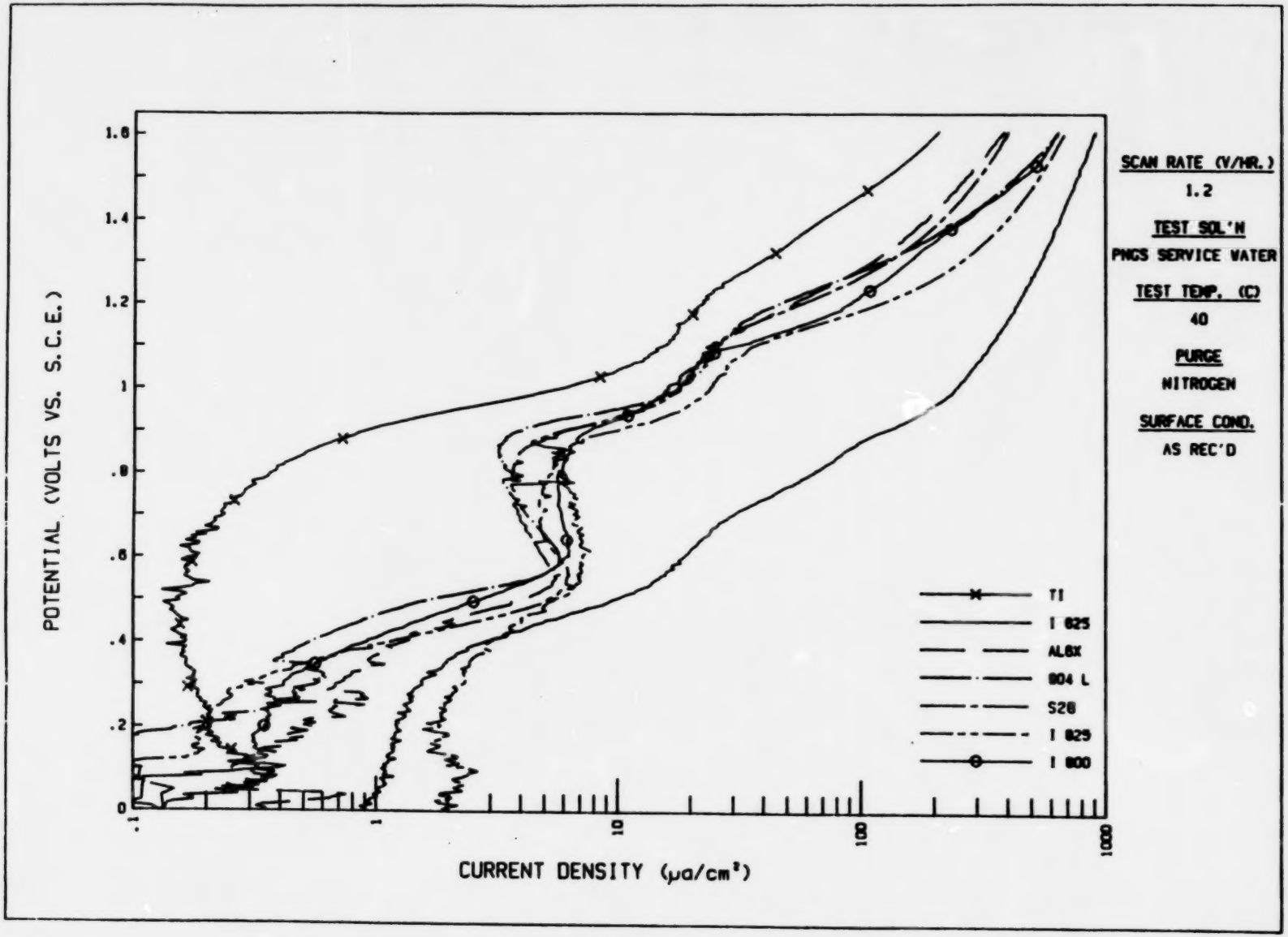

FIGURE 14d

CYCLIC POTENTIODYNAMIC POLARIZATION (CPP) FORWARD PLOTS FOR Ti, 1625, AL6X, 904L, S28, 1825, 1800 FOR A SCAN RATE OF 1.2 V/HR AND AS RECEIVED INITIAL SURFACE CONDITION

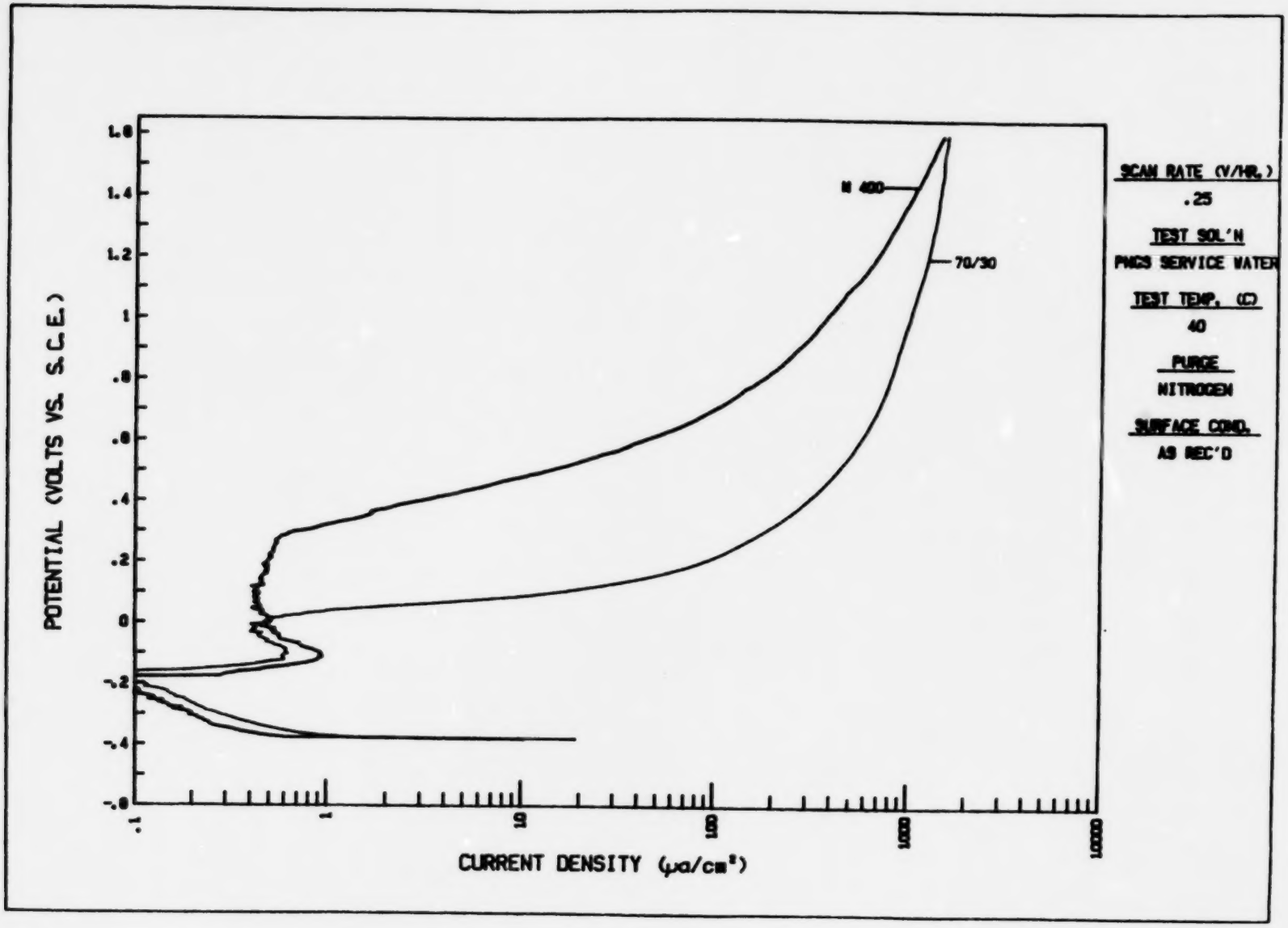

FIGURE 15a

CYCLIC POTENTIODYNAMIC POLARIZATION(CPP) FORWARD PLOTS FOR M400 & 70/30 FOR A SCAN RATE OF 0.25 V/HR AND AS RECEIVED INITIAL SURFACE CONDITION

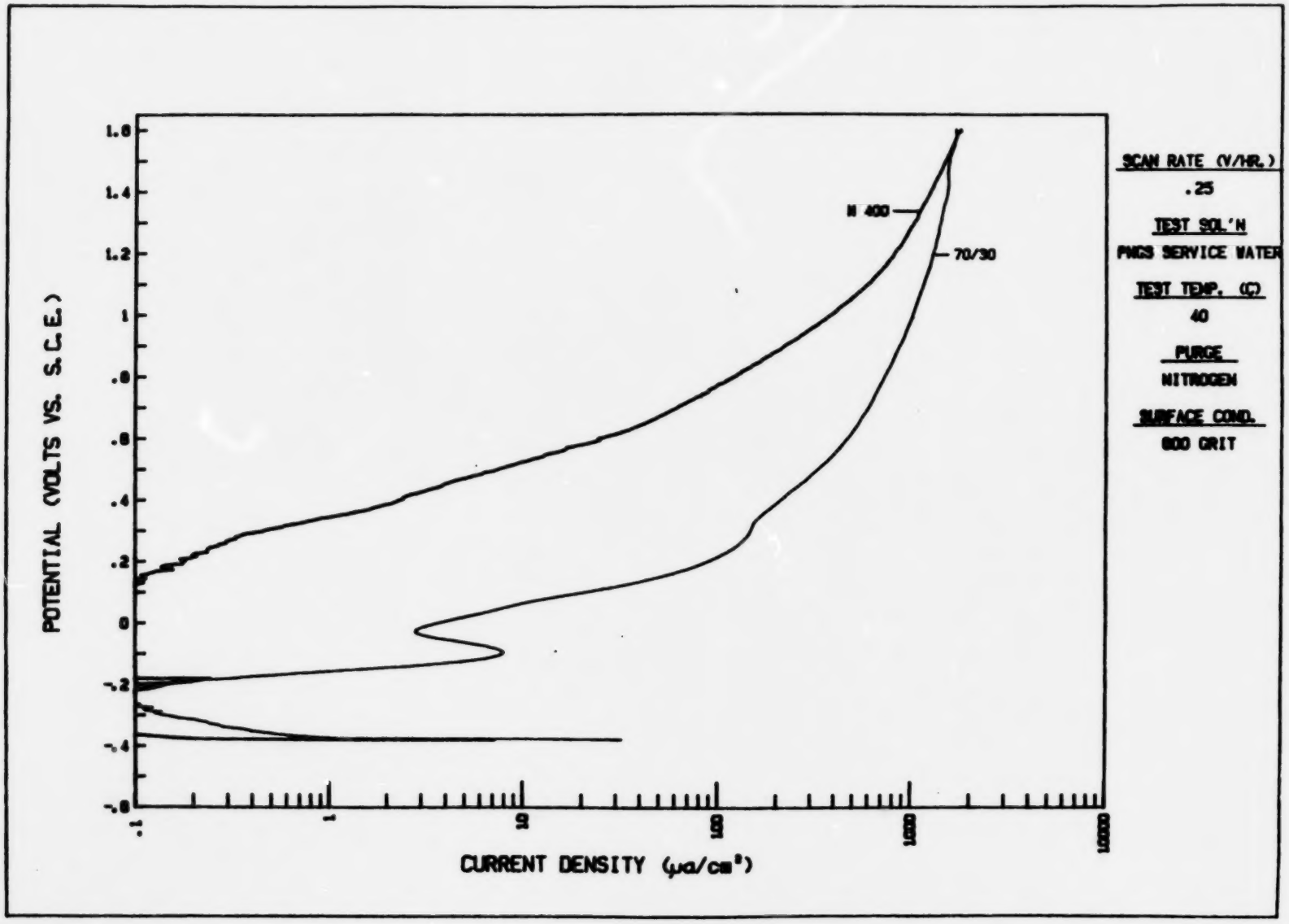

FIGURE 15b

CYLIC POTENTIODYNAMIC POLARIZATION(CPP) FORWARD PLOTS FOR M400 & 70/30
FOR A SCAN RATE OF 0.25 V/HR & INITIAL SURFACE CONDITION OF 600 GRIT

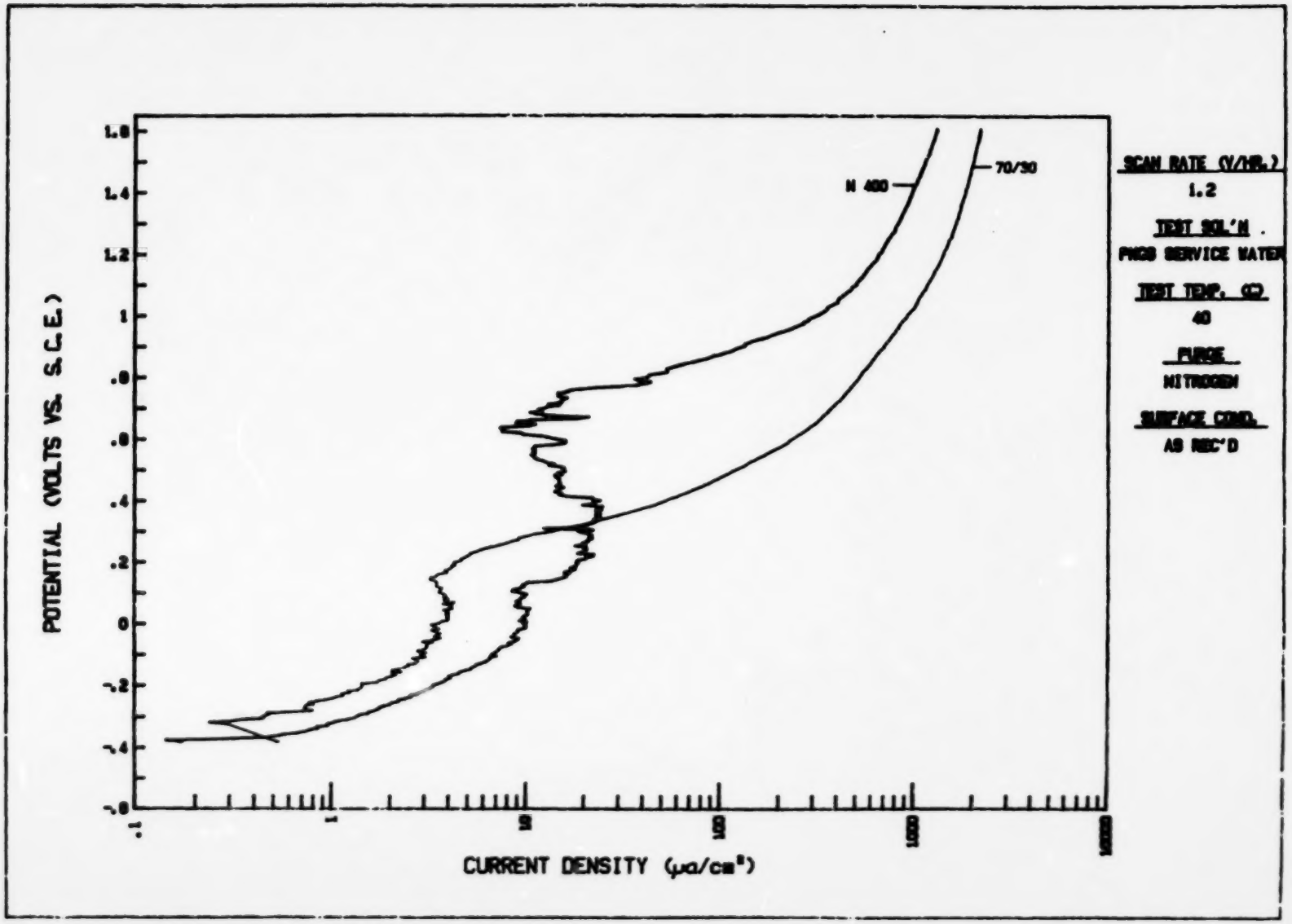

FIGURE 15c

CYCLIC POTENTIODYNAMIC POLARIZATION(CPP) FORWARD PLOTS FOR M400 AND 70/30 FOR A SCAN RATE OF 1.2 V/HR AND AS RECEIVED INITIAL SURFACE CONDITION

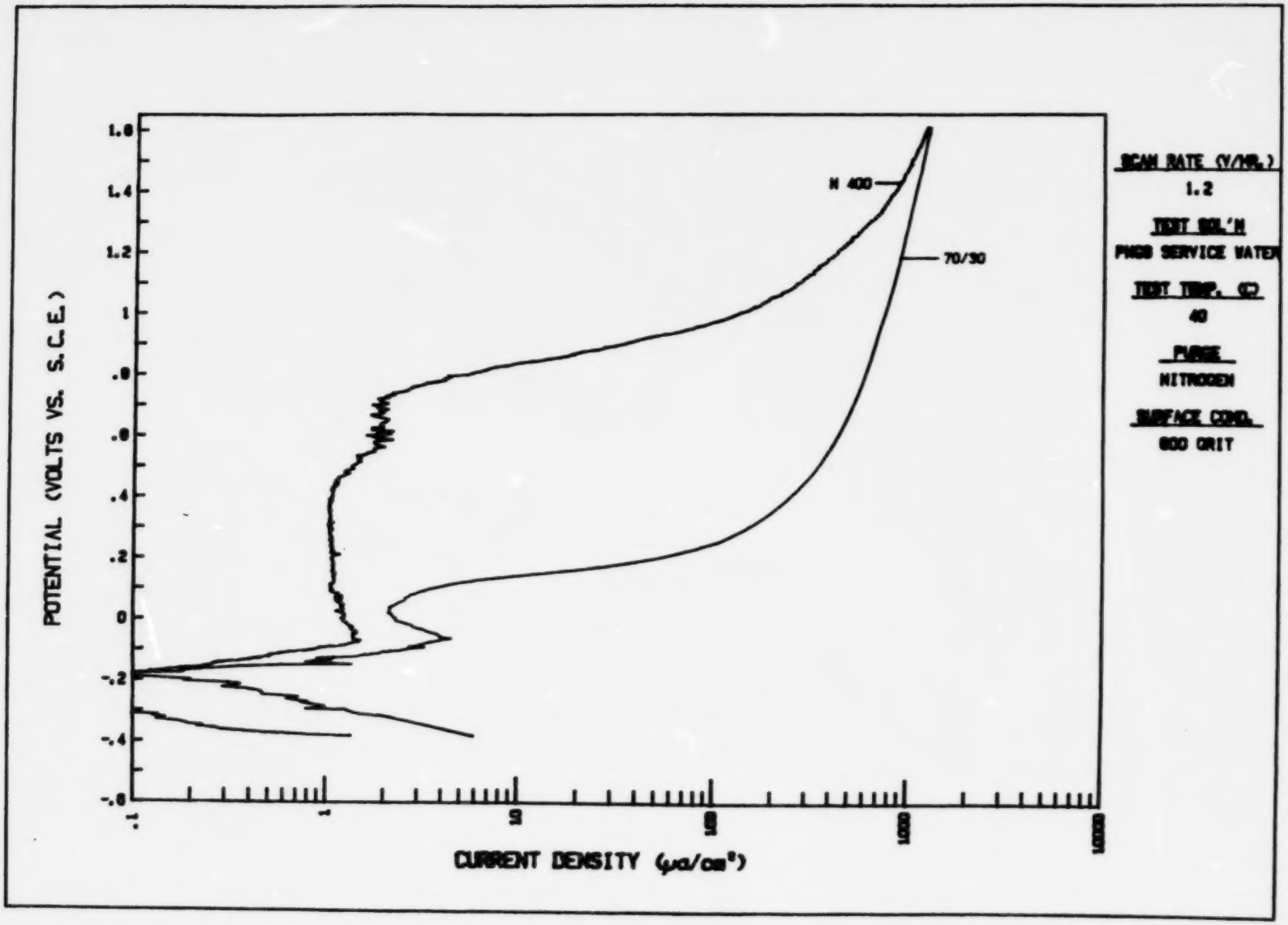

FIGURE 15d

CYCLIC POTENTIODYNAMIC POARIZATION(CPP) FORWARD PLOTS FOR M400 AND 70/30 FOR A SCAN RATE OF 1.2 V/HR & INITIAL SURFACE CONDITION OF 600 GRIT

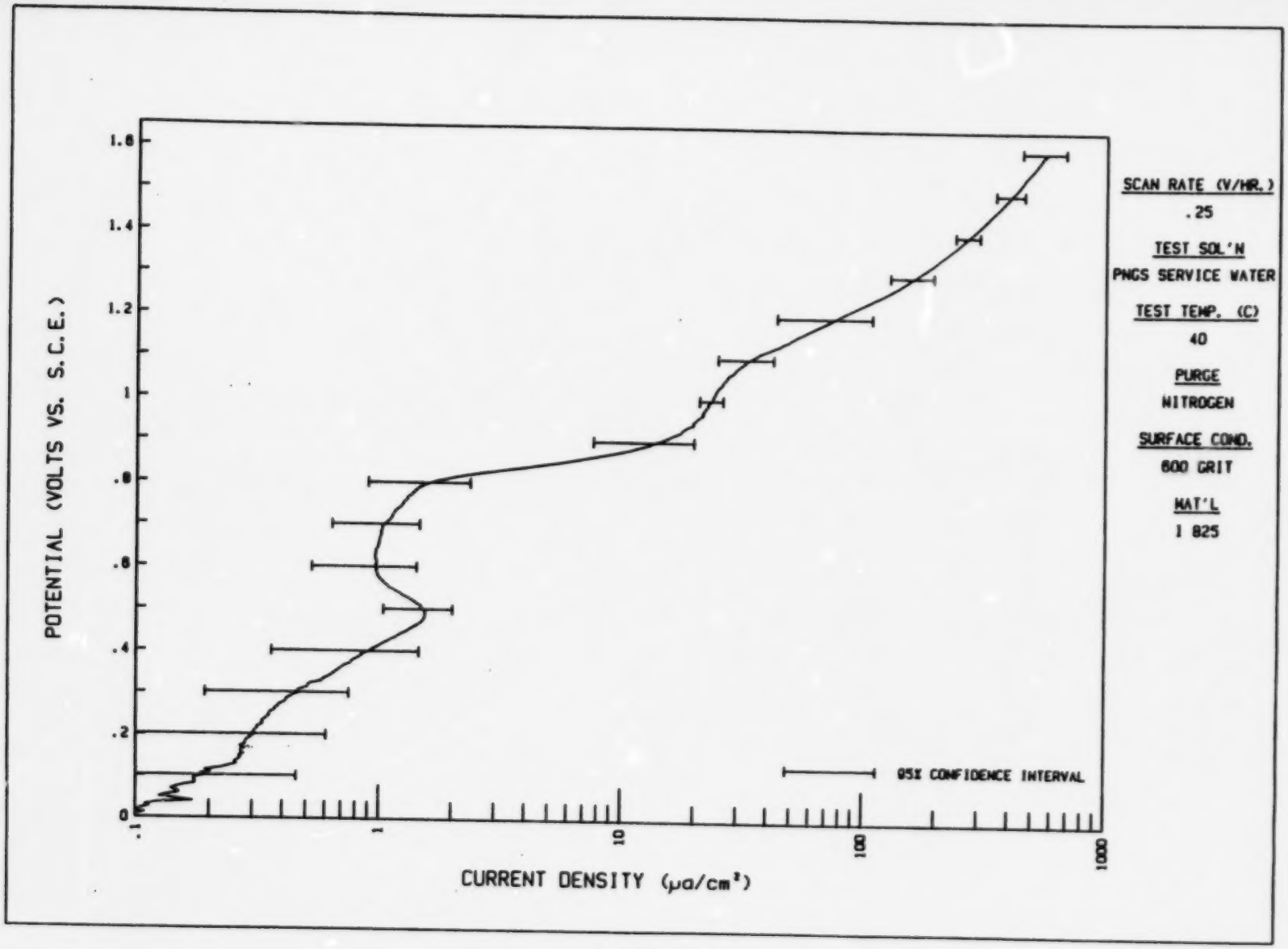

FIGURE 16

95% CONFIDENCE INTERVALS FOR 4 CPP TESTS OF 1825 FORWARD SCAN
(SCAN RATE 0.25 V/HR, 600 GRIT)

168845 RD

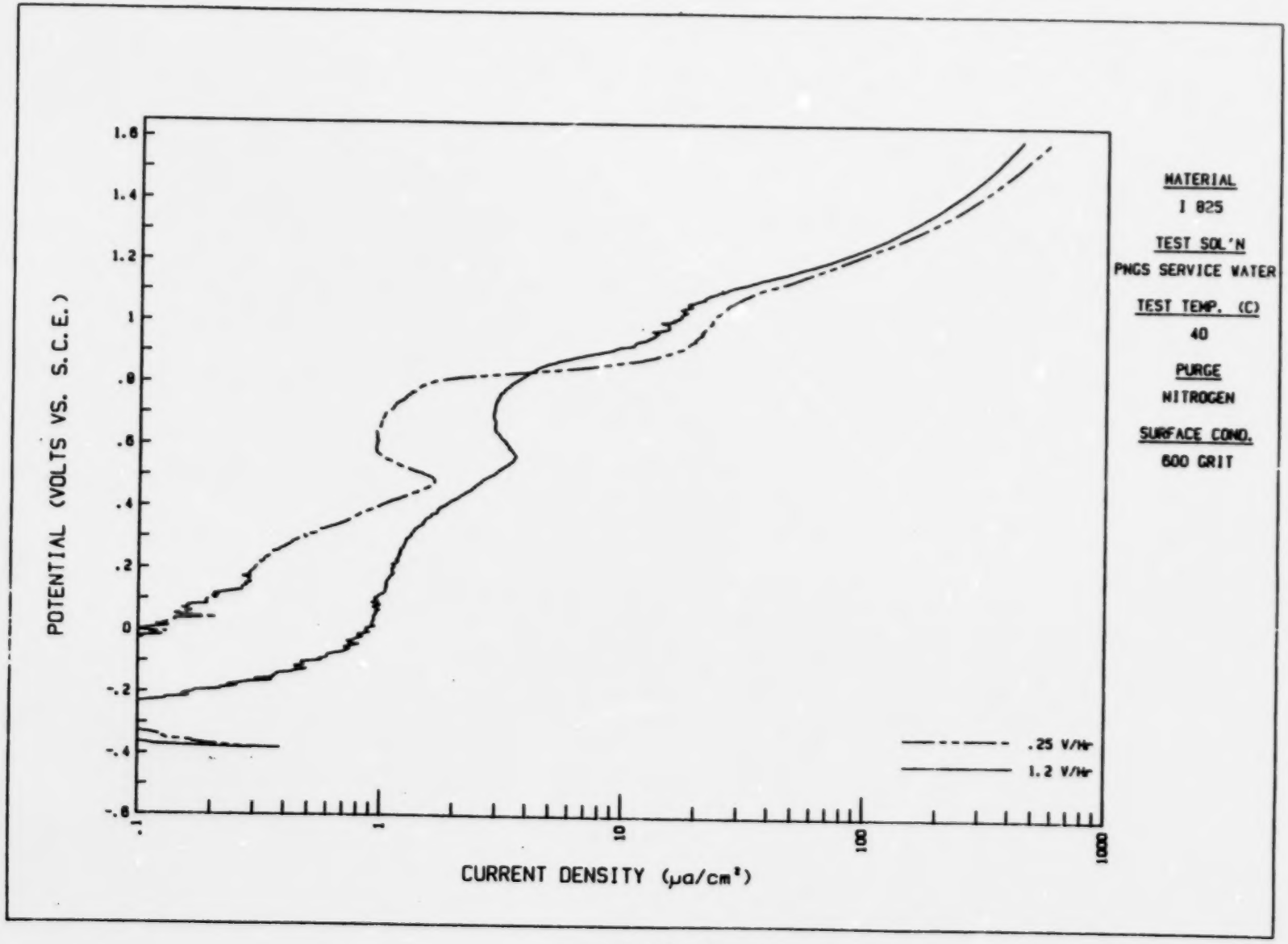

FIGURE 17

CYCLIC POTENTIODYNAMIC POLARIZATION (FORWARD SCAN) FOR I 825 AT AN INITIAL SURFACE CONDITION OF 600 GRIT SHOWING EFFECT OF SCAN RATE

168846 RD

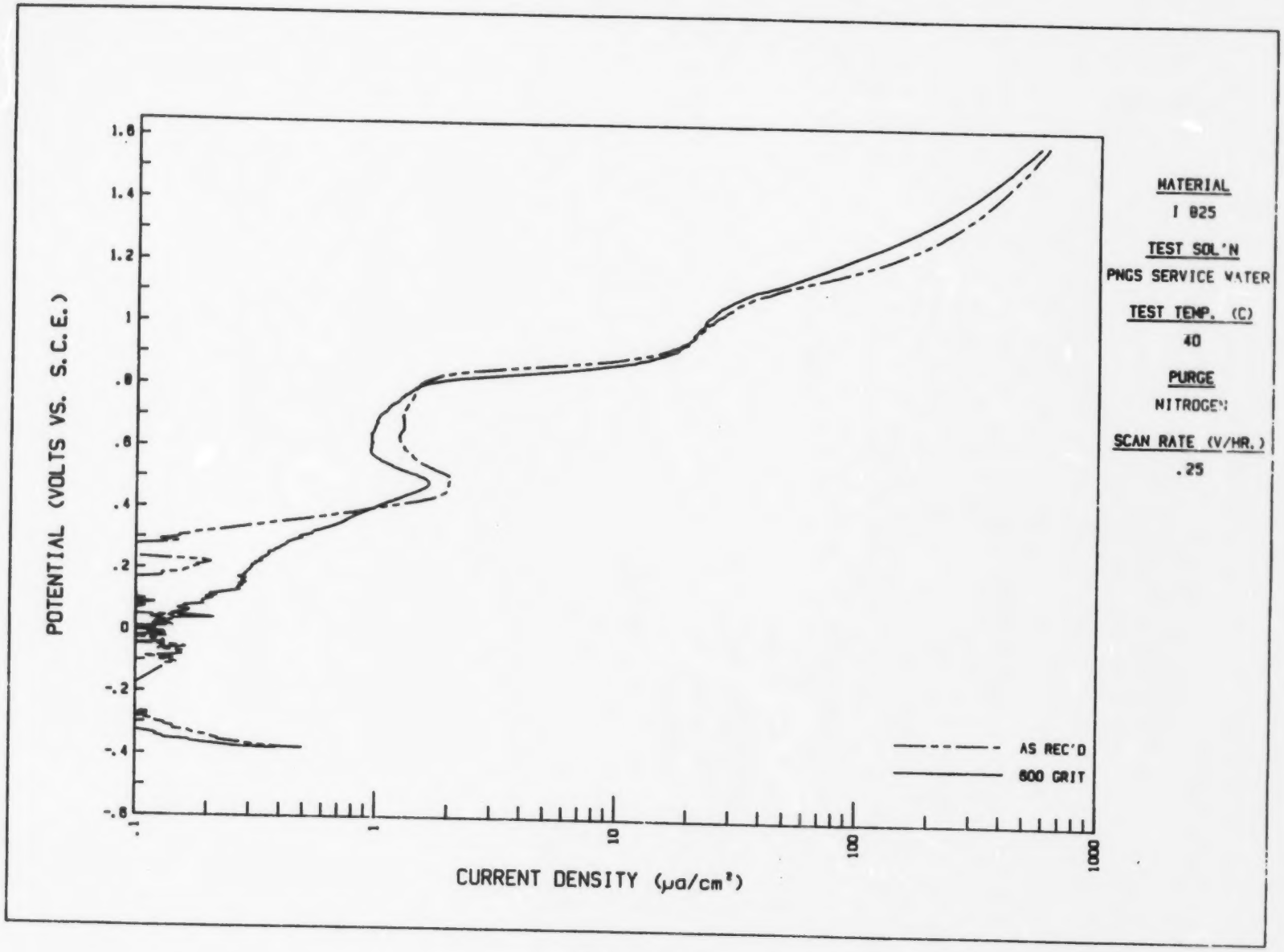

FIGURE 18

CYCLIC POTENTIODYNAMIC POLARIZATION (FORWARD SCAN) FOR I825 AT A SCAN RATE OF 0.25 V/HR SHOWING EFFECT OF INITIAL SURFACE CONDITION

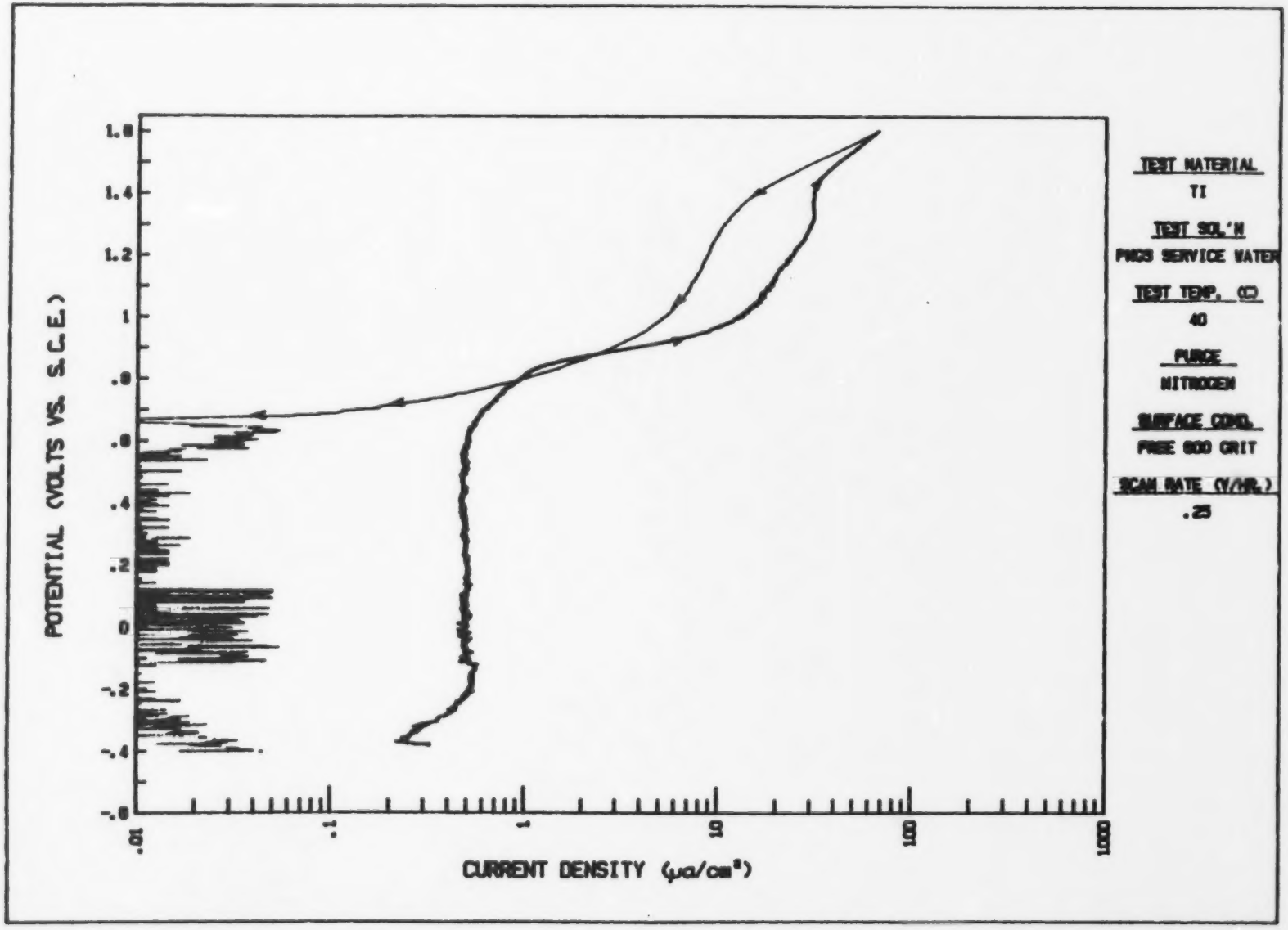

FIGURE 19a

CYCLIC POTENTIODYNAMIC POLARIZATION PLOT FOR TITANIUM WITH A SCAN RATE OF 0.25 V/HR AND INITIAL SURFACE CONDITION OF 600 GRIT

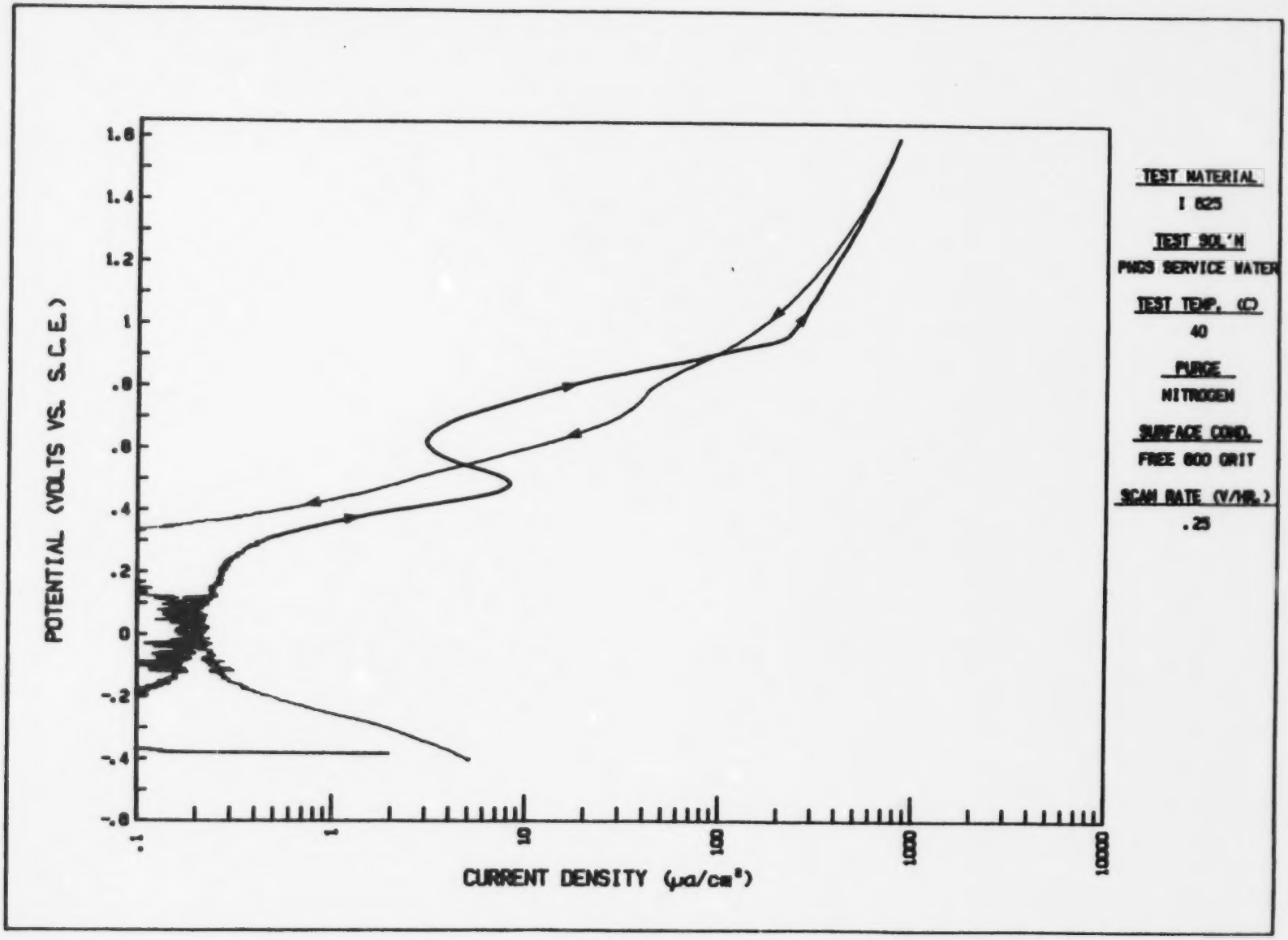

FIGURE 19b

CYCLIC POTENTIODYNAMIC POLARIZATION PLOT FOR 1625 WITH A SCAN RATE OF 0.25 V/HR AND INITIAL SURFACE CONDITION OF 600 GRIT

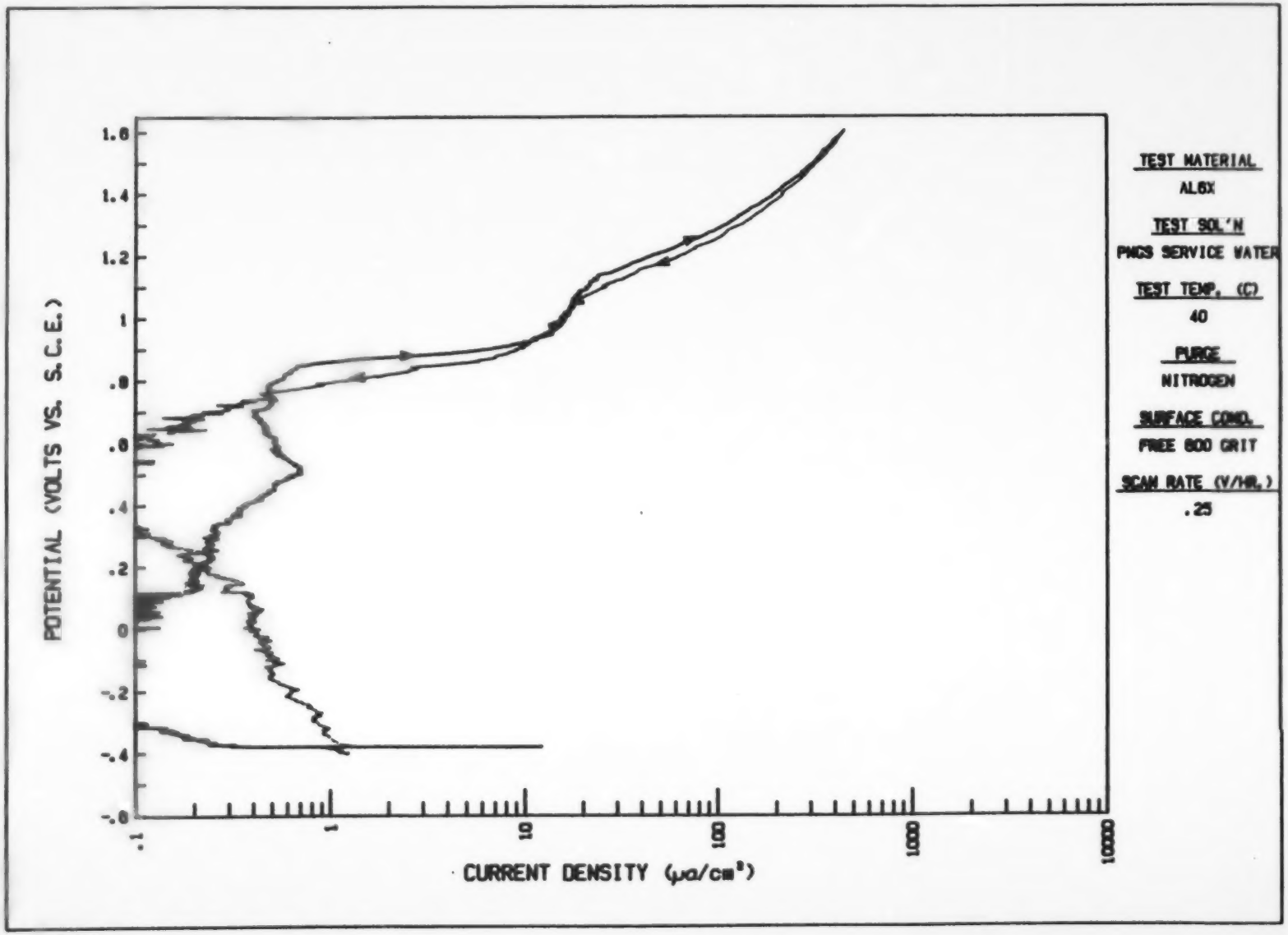

FIGURE 19c

CYCLIC POTENTIODYNAMIC POLARIZATION PLOT FOR AL6X WITH A SCAN RATE OF 0.25 V/HR AND INITIAL SURFACE CONDITION OF 600 GRIT

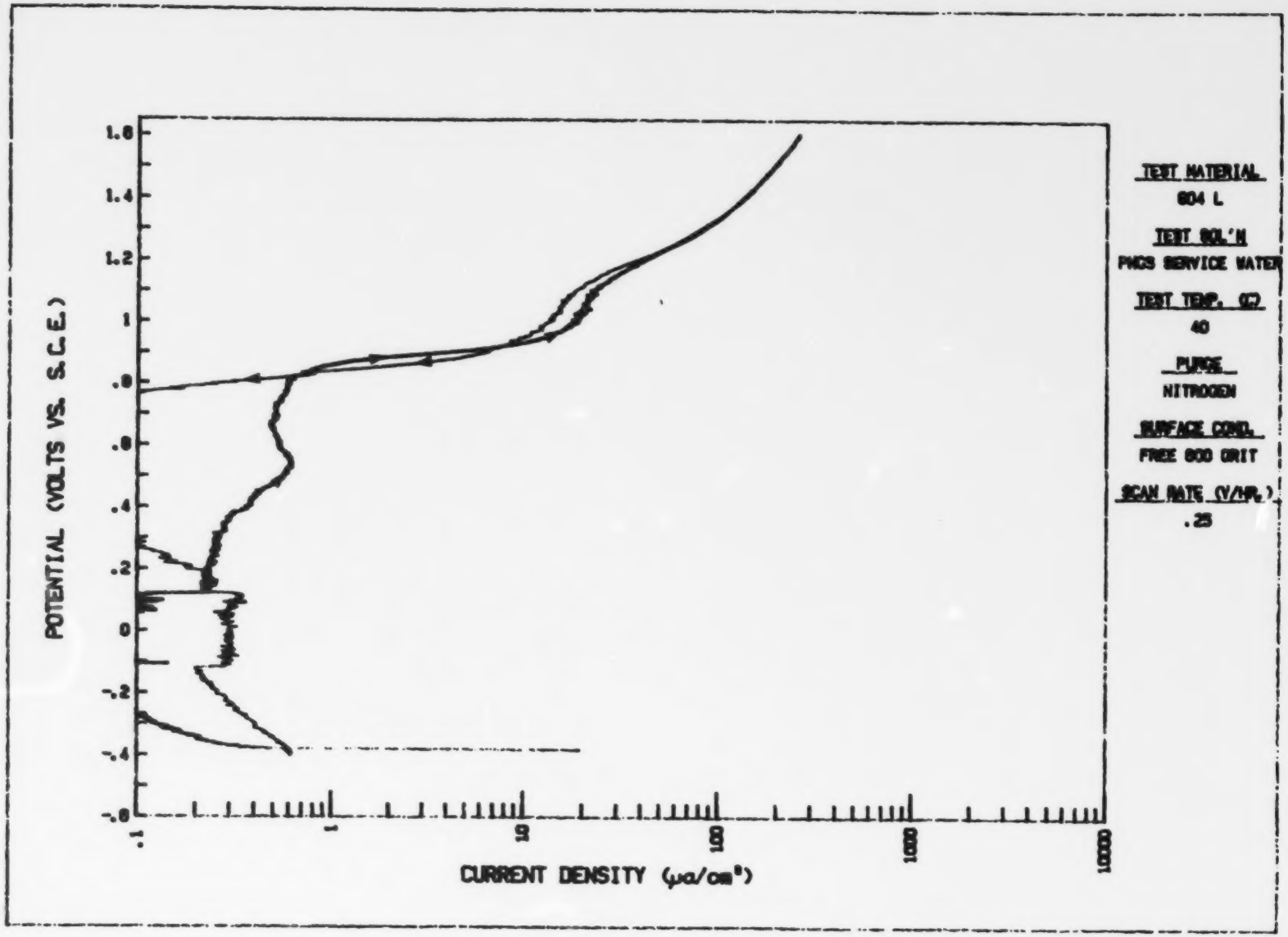

FIGURE 19d

CYCLIC POTENTIODYNAMIC POLARIZATION PLOT FOR 904L WITH A SCAN RATE OF 0.25 V/HR AND INITIAL SURFACE CONDITION OF 600 GRIT

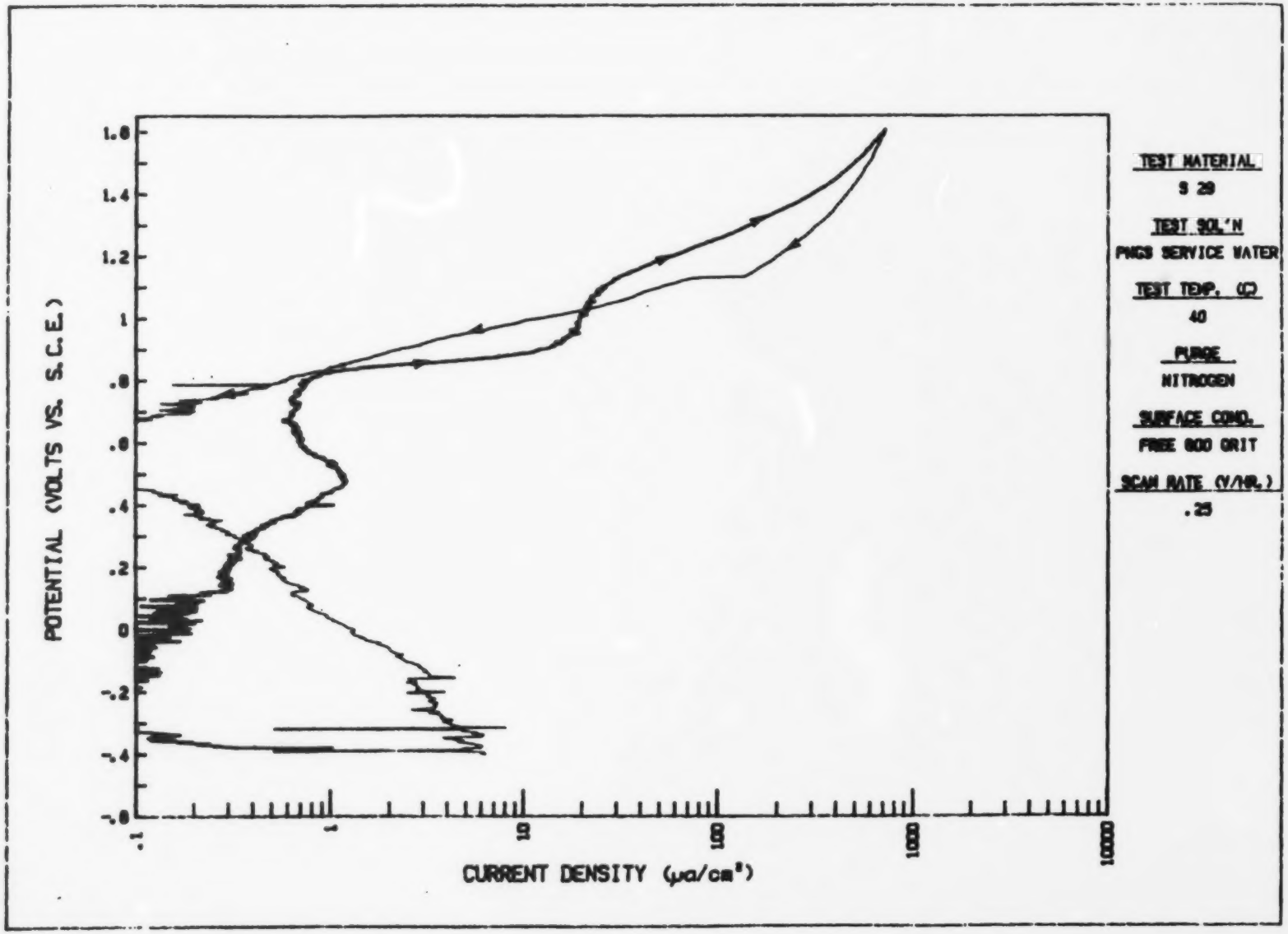

FIGURE 19e

CYCLIC POTENTIODYNAMIC POLARIZATION PLOT FOR S28 WITH A SCAN RATE OF 0.25 V/HR AND INITIAL SURFACE CONDITION OF 600 GRIT

1888D 8D

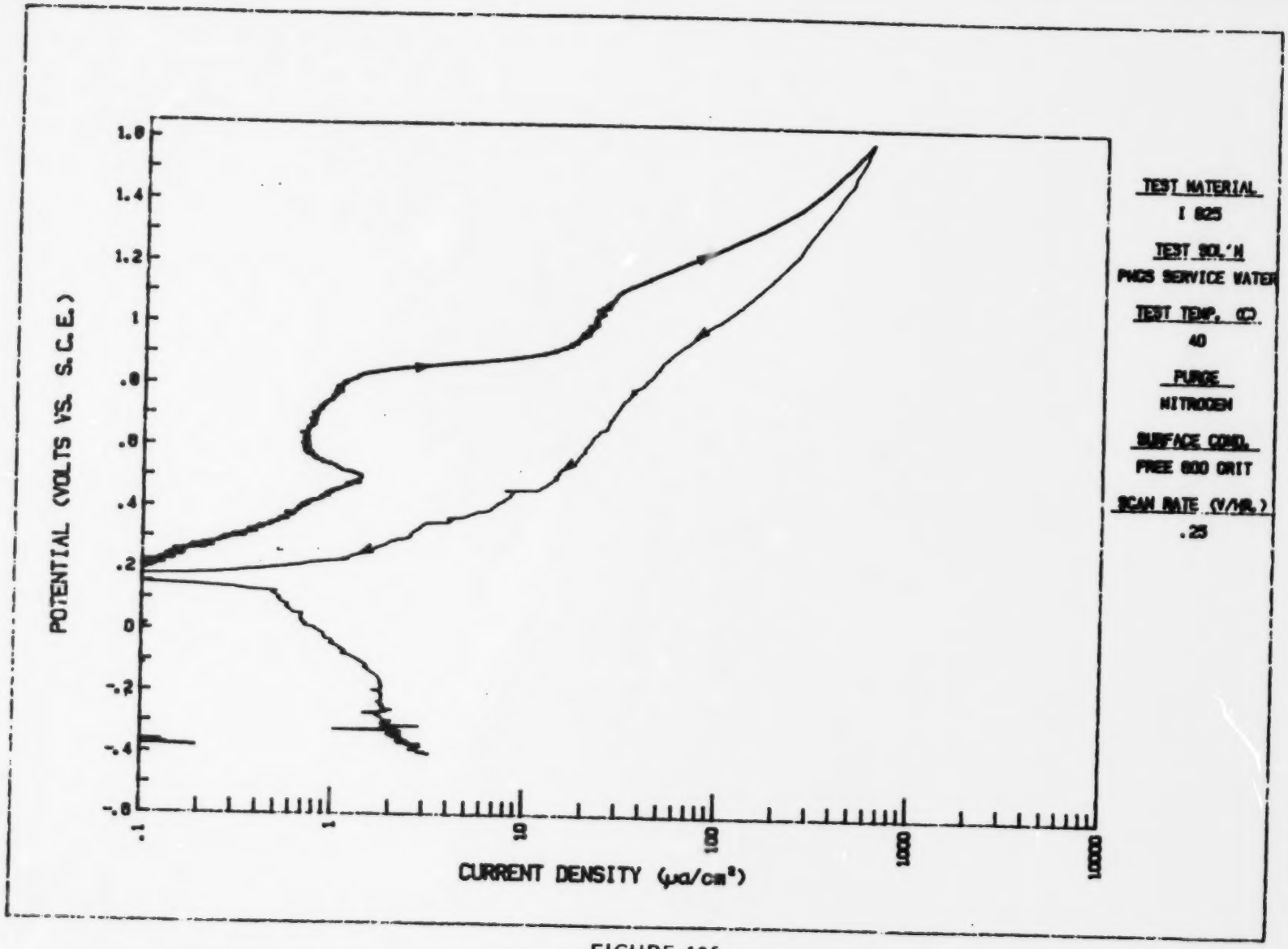

FIGURE 19f

CYCLIC POTENTIODYNAMIC POLARIZATION PLOT FOR 1825 WITH A SCAN RATE OF 0.25 V/HR AND INITIAL SURFACE CONDITION OF 600 GRIT

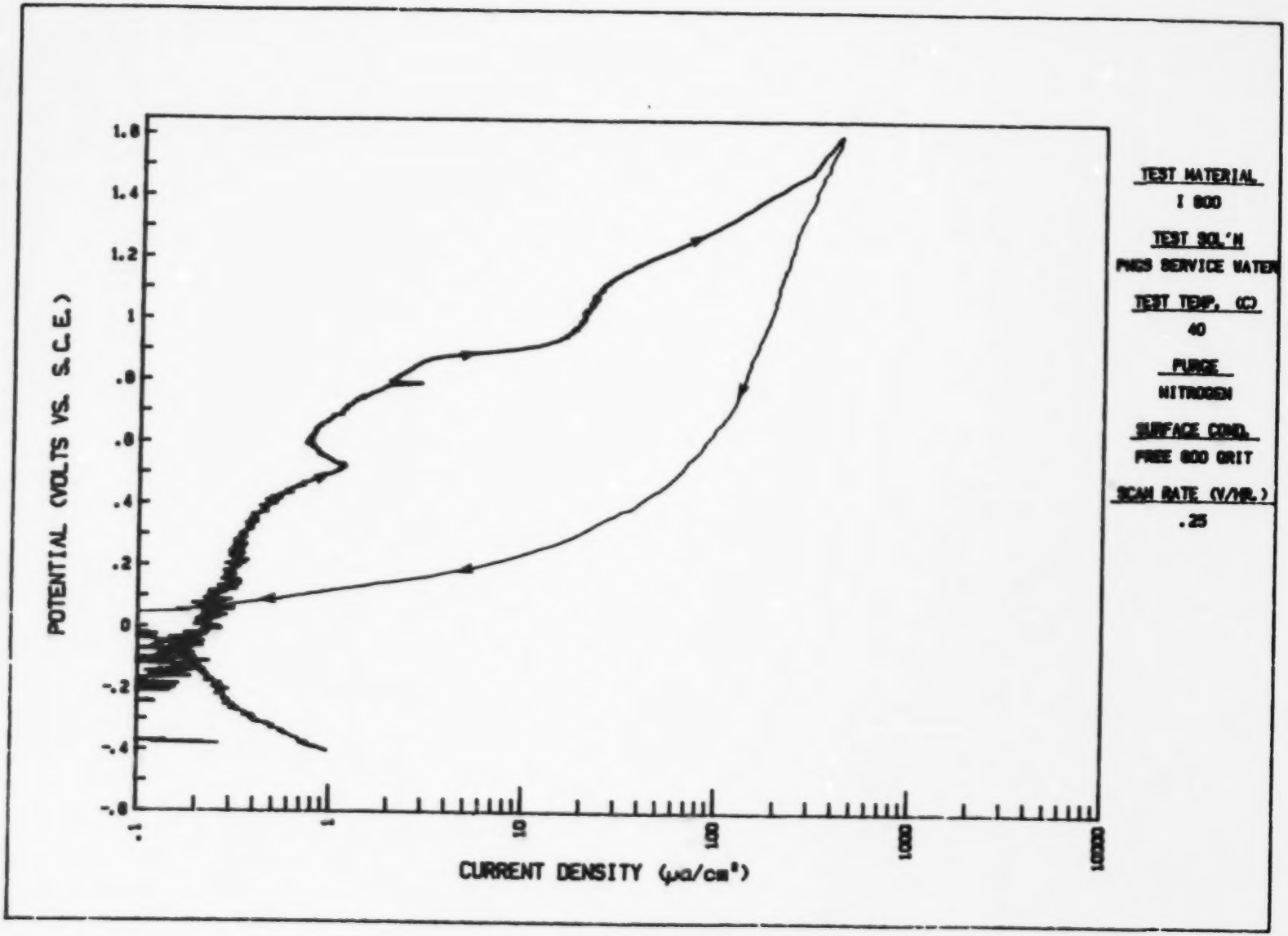

FIGURE 19g

CYCLIC POTENTIODYNAMIC POLARIZATION PLOT FOR I800 WITH A SCAN RATE OF 0.25 V/HR AND INITIAL SURFACE CONDITION OF 600 GRIT

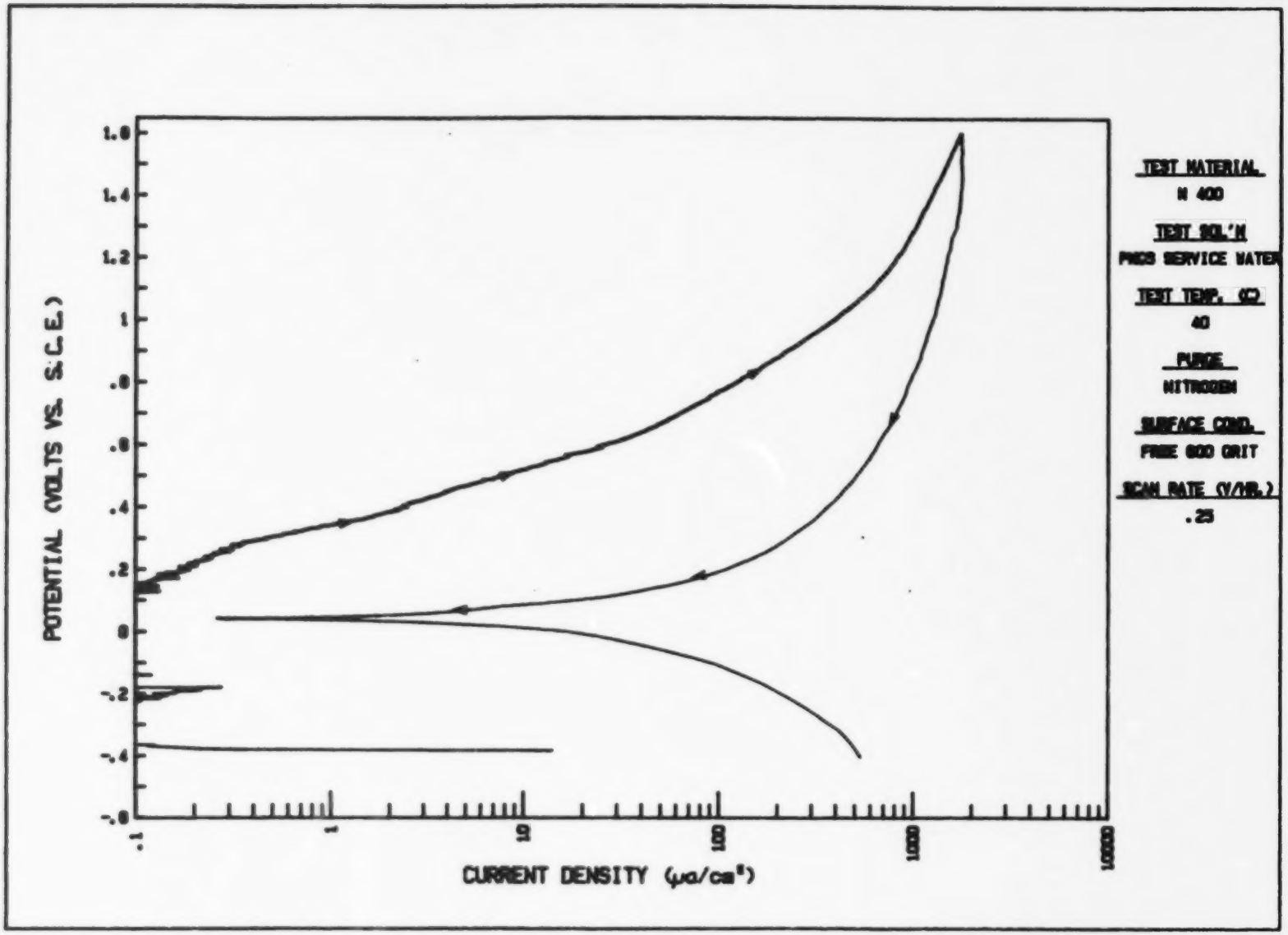

FIGURE 19h

CYCLIC POTENTIODYNAMIC POLARIZATION PLOT FOR M400 WITH A SCAN RATE OF 0.25 V/HR AND INITIAL SURFACE CONDITION OF 600 GRIT

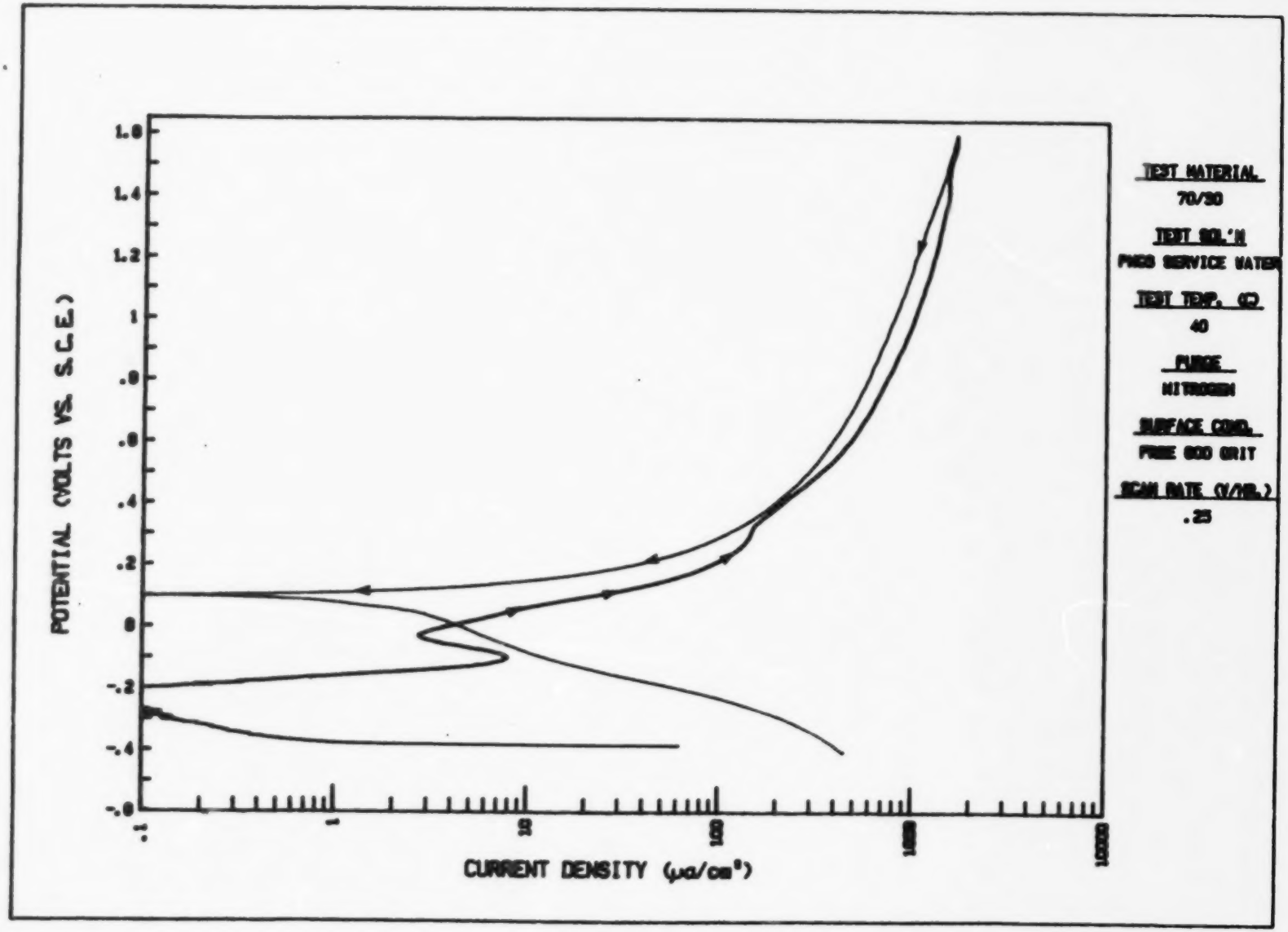

FIGURE 19i

CYCLIC POTENTIODYNAMIC POLARIZATION PLOT FOR 70/30 WITH A SCAN RATE OF 0.25 V/HR AND INITIAL SURFACE CONDITION OF 600 GRIT

1588B4 RD

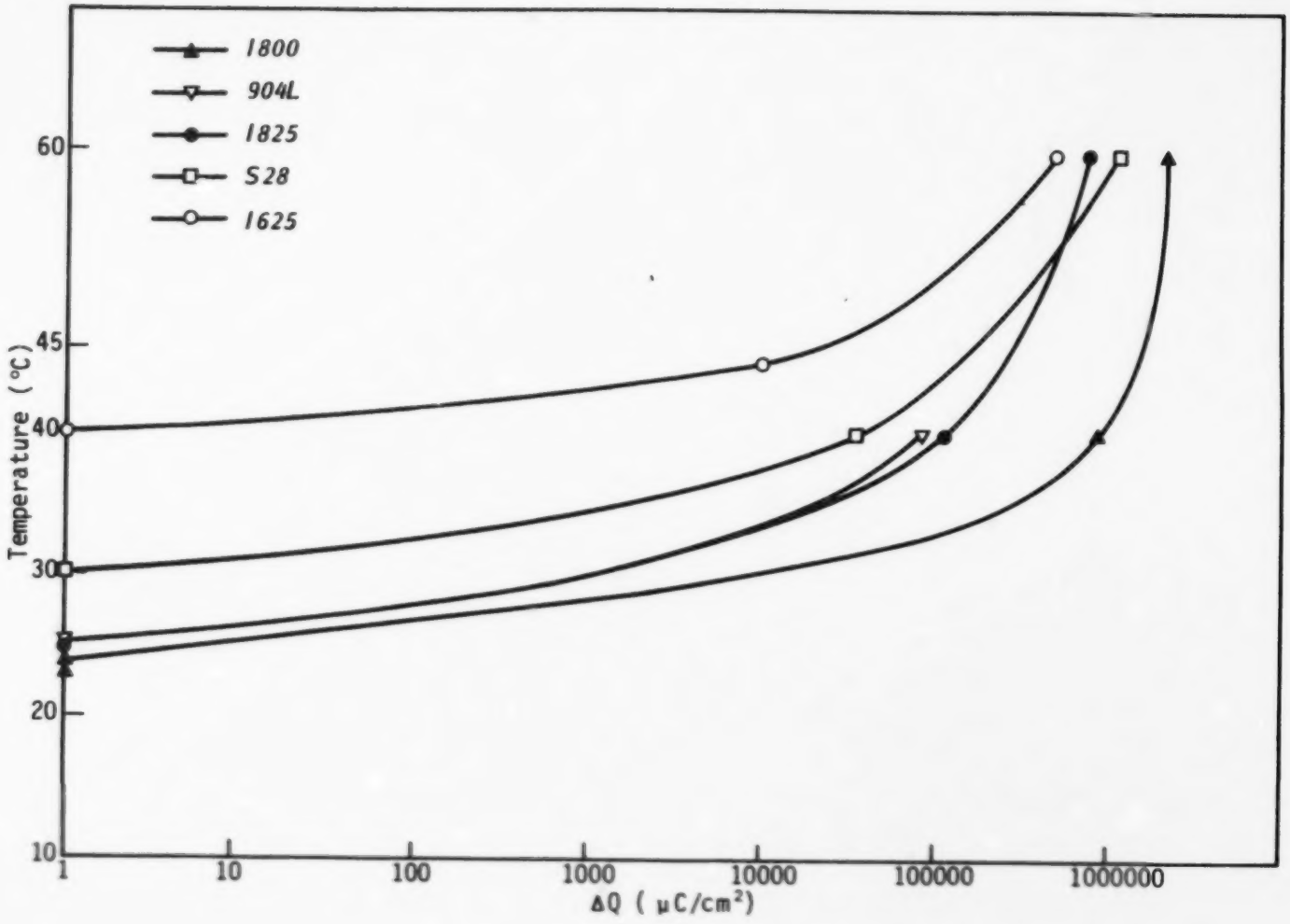

FIGURE 20

TEMPERATURE DEPENDENCE OF ΔQ FOR 1800, 904L, 1825, S28, 1625 (SCAN RATE 1.2V/h AS RECEIVED)
(NOTE CURVE FITTING NOT STATISTICALLY - BASED. MORE DATA NEEDED TO IMPROVE CONFIDENCE)

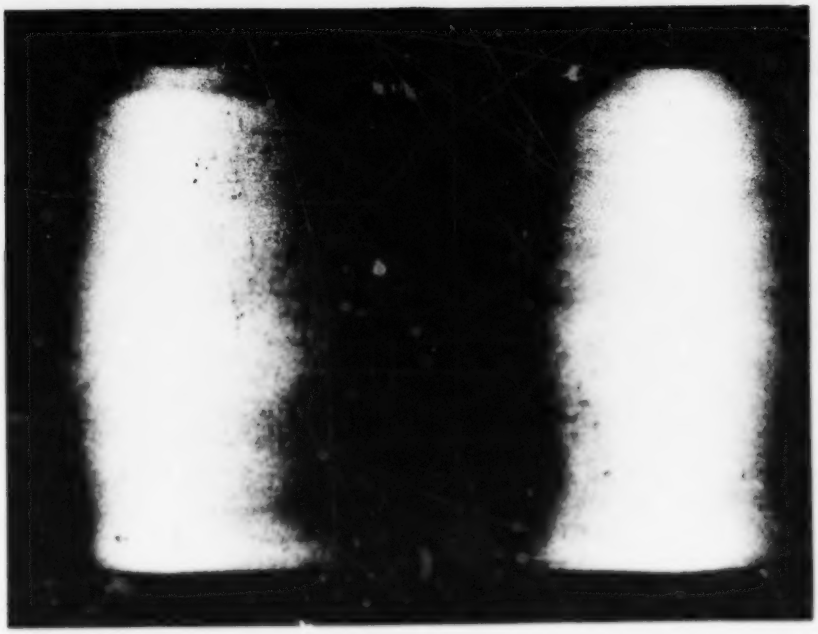

(a) Overall View 7.5x
(no pitting observed)

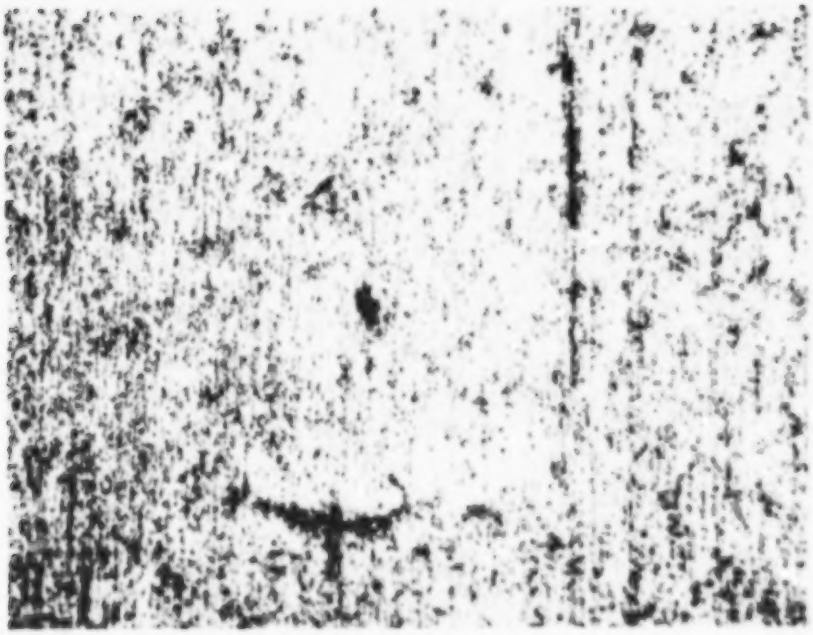

(b) Tube Surface 100x
(no pitting observed)

FIGURE 21

SURFACE APPEARANCE OF TITANIUM TUBE SAMPLE FOLLOWING CYCLIC POTENTIODYNAMIC POLARIZATION (CPP) TESTING AT SCAN RATE OF 0.25 V/HR AND INITIAL CONDITION OF 600 GRIT

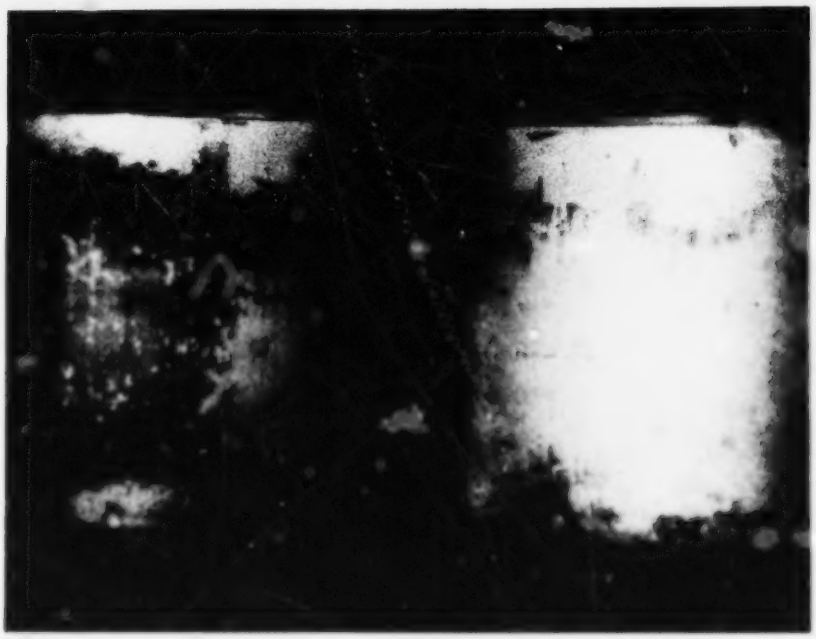

(a) Overall View 7.5x
(no pitting observed)

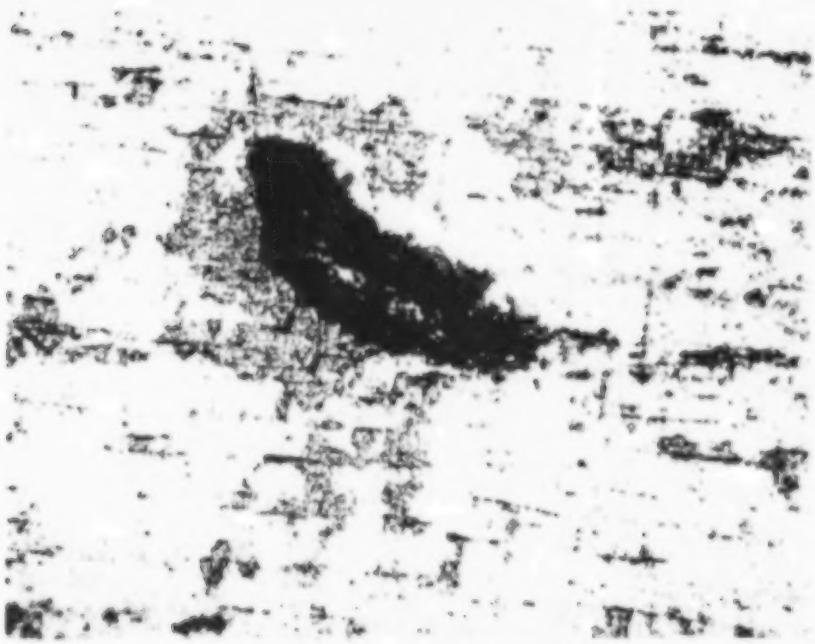

(b) Tube Surface 100x
(isolated mechanical damage)

FIGURE 22

SURFACE APPEARANCE OF 1625 TUBE SAMPLE FOLLOWING CYCLIC POTENTIODYNAMIC POLARIZATION (CPP) TESTING AT A SCAN RATE OF 0.25 V/HR AND INITIAL CONDITION OF 600 GRIT

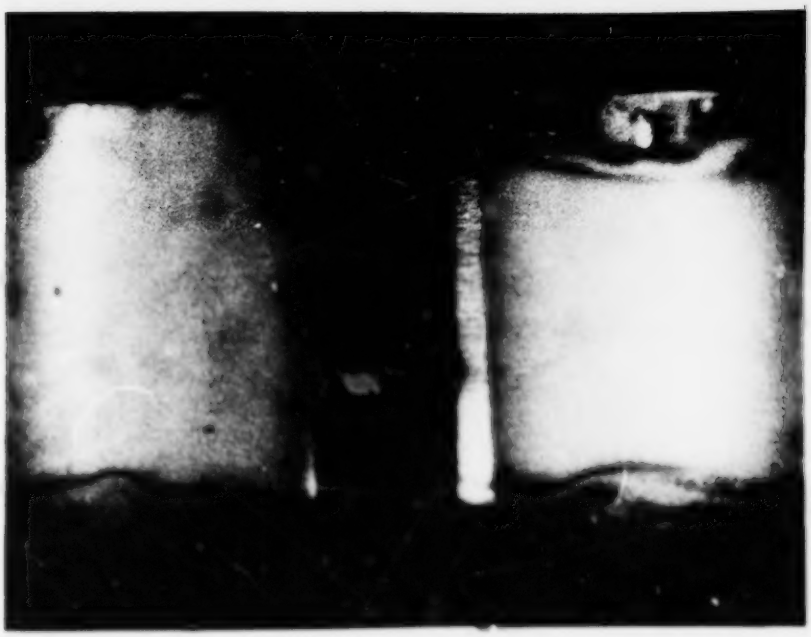

(a) Overall View 7.5x
(surface generally free of pitting)

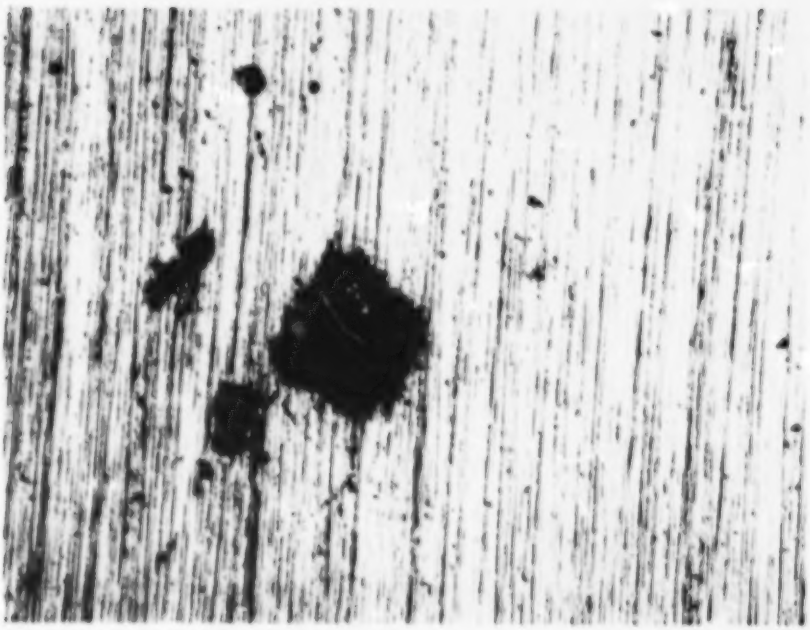

(b) Tube Surface 100x
(isolated pits)

FIGURE 23

SURFACE APPEARANCE OF AL6X TUBE SAMPLE FOLLOWING CYCLIC POTENTIODYNAMIC POLARIZATION (CPP) TESTING AT A SCAN RATE OF 0.25 V/HR AND INITIAL CONDITION OF 600 GRIT

168838 RD

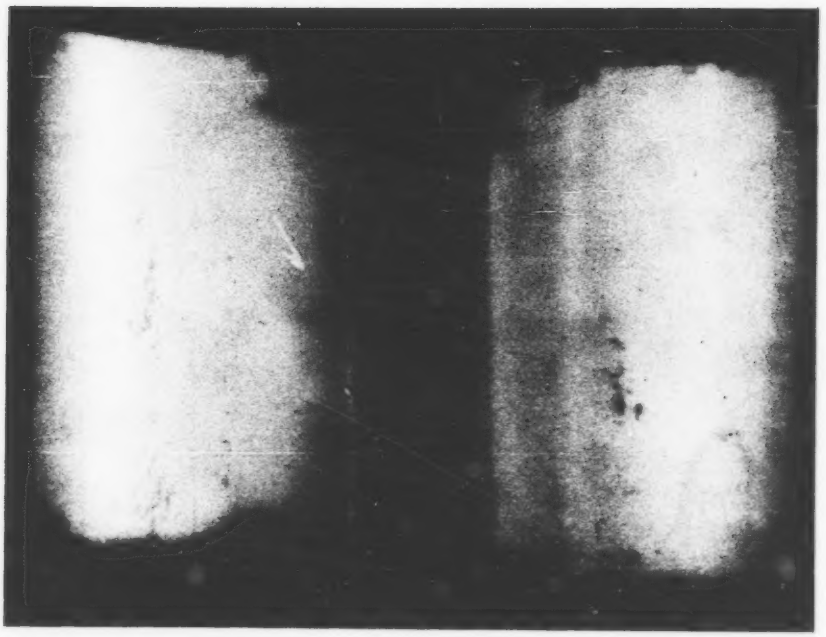

(a) Overall View 7.5x
(surface generally free of pitting)

(b) Tube Surface 100x
(small isolated shallow pits)

FIGURE 24

SURFACE APPEARANCE OF 904L TUBE SAMPLE FOLLOWING CYCLIC POTENTIODYNAMIC POLARIZATION (CPP) TESTING AT A SCAN RATE OF 0.25 V/HR AND INITIAL CONDITION OF 600 GRIT

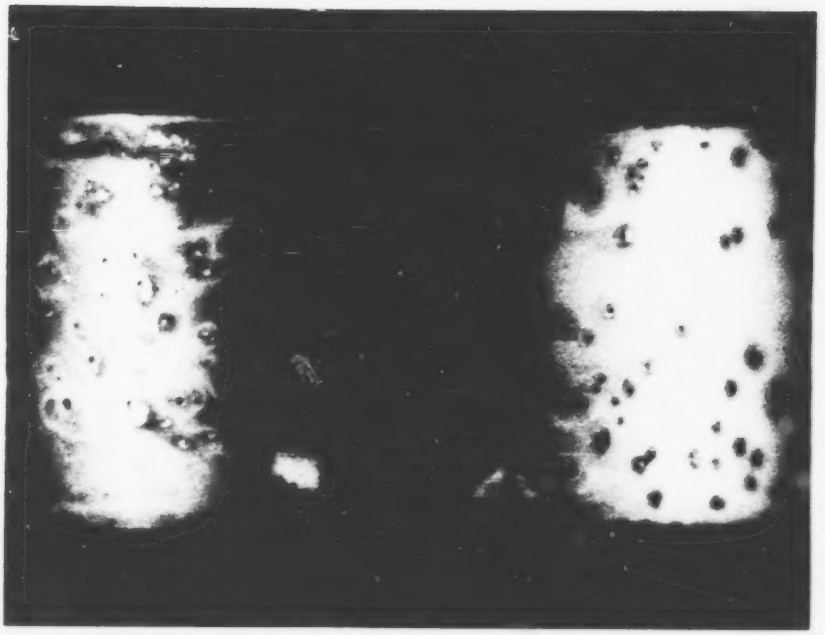

(a) Overall View 7.5x
(showing numerous well-developed hemispherical pits)

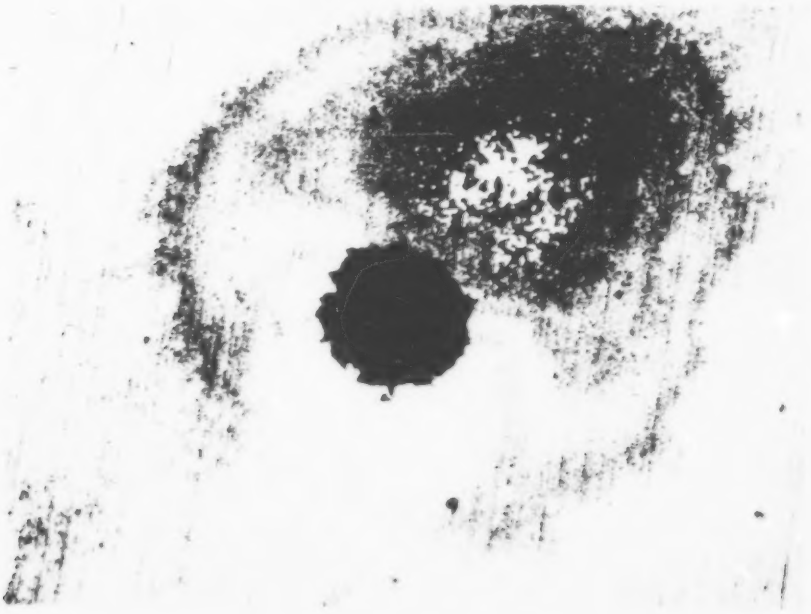

(b) Tube Surface 100x
(hemispherical pit)

FIGURE 25

SURFACE APPEARANCE OF S28 TUBE SAMPLE FOLLOWING CYCLIC POTENTIODYNAMIC POLARIZATION (CPP) TESTING AT A SCAN RATE OF 0.25 V/HR AND INITIAL CONDITION OF 600 GRIT

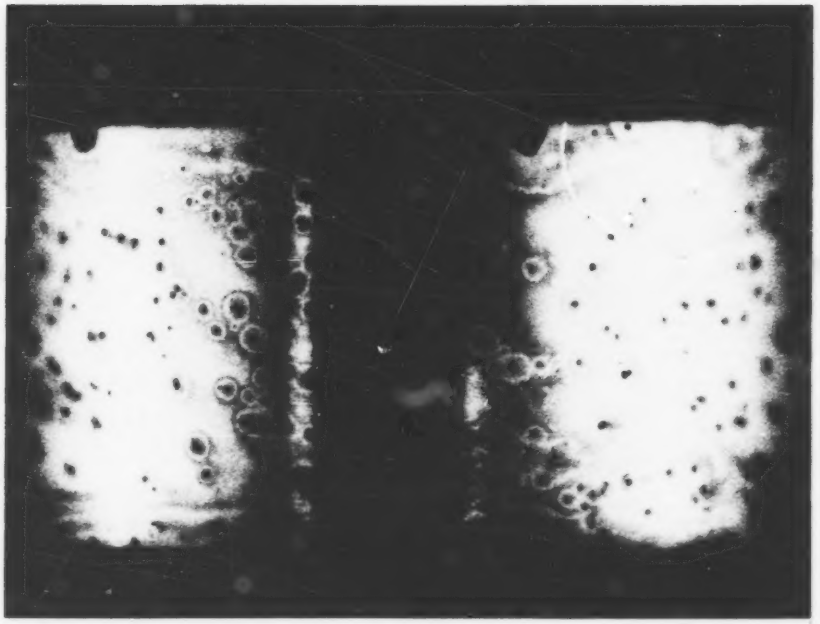

(a) Overall View 7.5x
(extensive pitting attack shown)

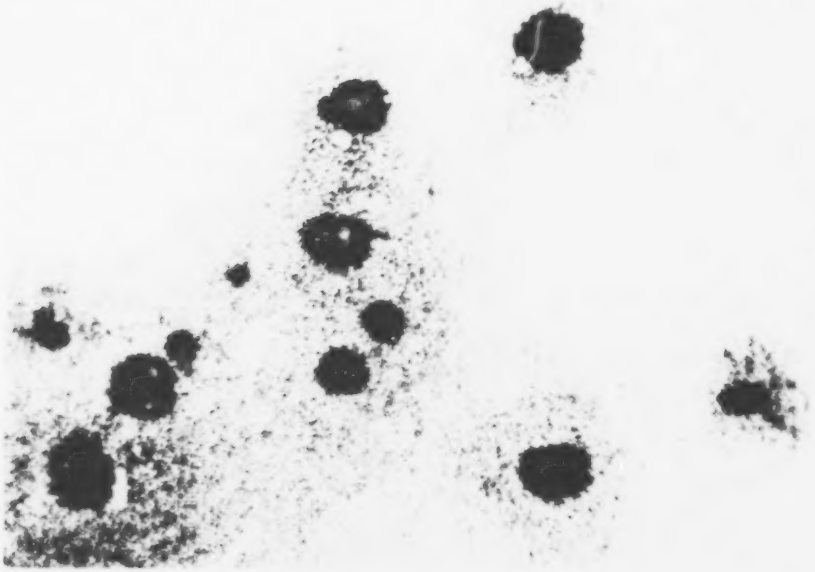

(b) Tube Surface 100x
(numerous pits and staining)

FIGURE 26

SURFACE APPEARANCE OF I825 TUBE SAMPLE FOLLOWING CYCLIC POTENTIODYNAMIC POLARIZATION (CPP) TESTING AT A SCAN RATE OF 0.25 V/HR AND INITIAL CONDITION OF 600 GRIT

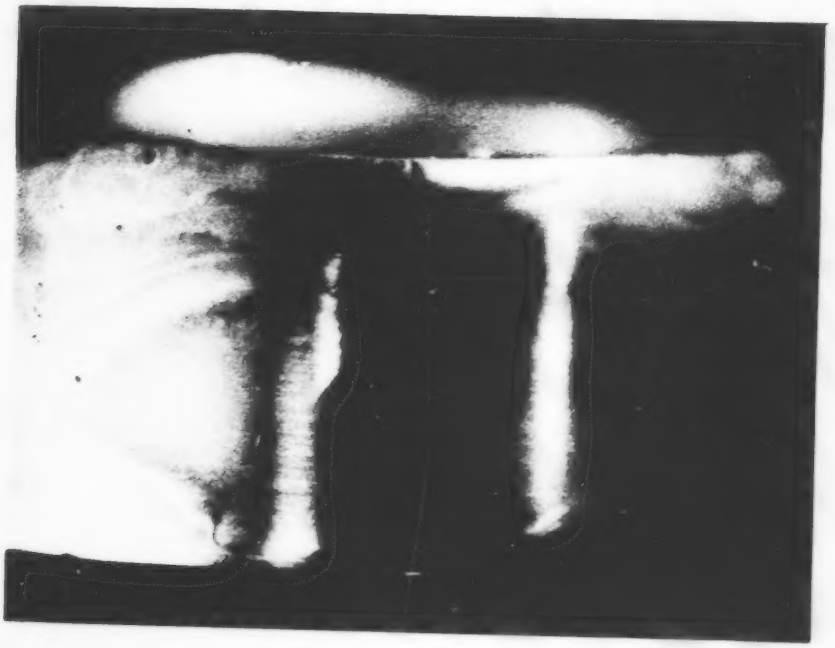

(a) Overall View 7.5x
(few shallow pits evident)

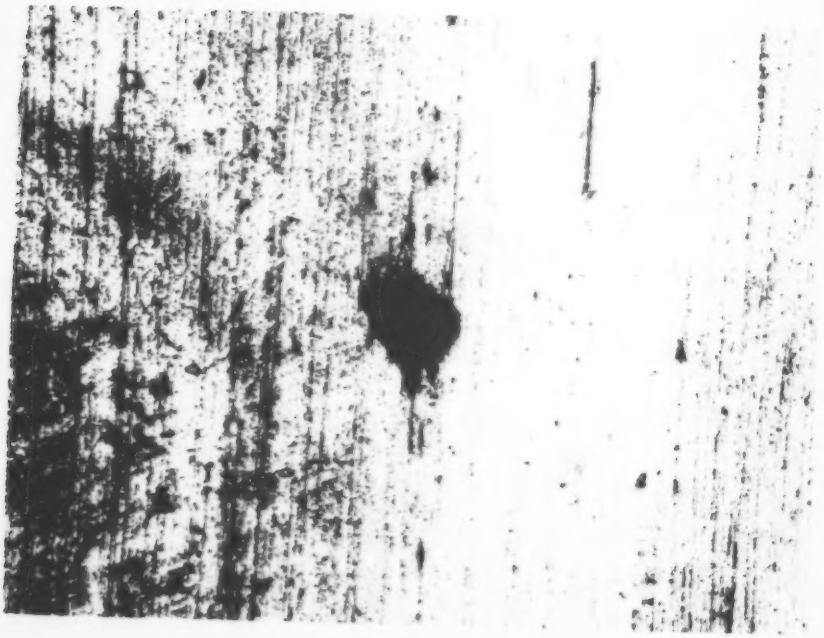

(b) Tube Surface 100X
(isolated hemispherical pit)

FIGURE 27

SURFACE APPEARANCE OF I800 TUBE SAMPLE FOLLOWING CYCLIC POTENTIODYNAMIC POLARIZATION (CPP) TESTING AT A SCAN RATE OF 0.25 V/HR AND INITIAL CONDITION OF 600 GRIT

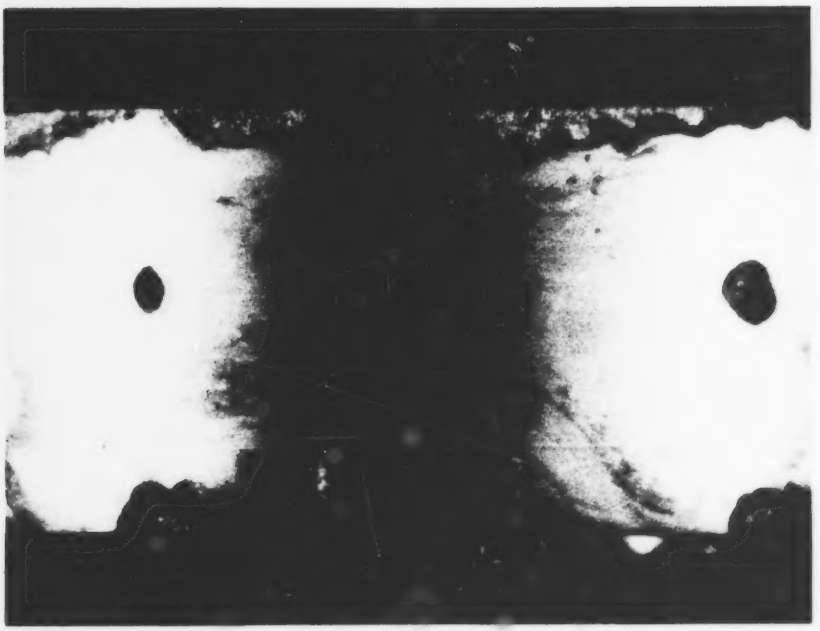

(a) Overall View 7.5x
(dealloying and some pitting)

(b) Tube Surface 100x
(showing pit)

FIGURE 28

SURFACE APPEARANCE OF M400 TUBE SAMPLE FOLLOWING CYCLIC POTENTIODYNAMIC POLARIZATION (CPP) TESTING AT A SCAN RATE OF 0.25 V/HR AND INITIAL CONDITION OF 600 GRIT

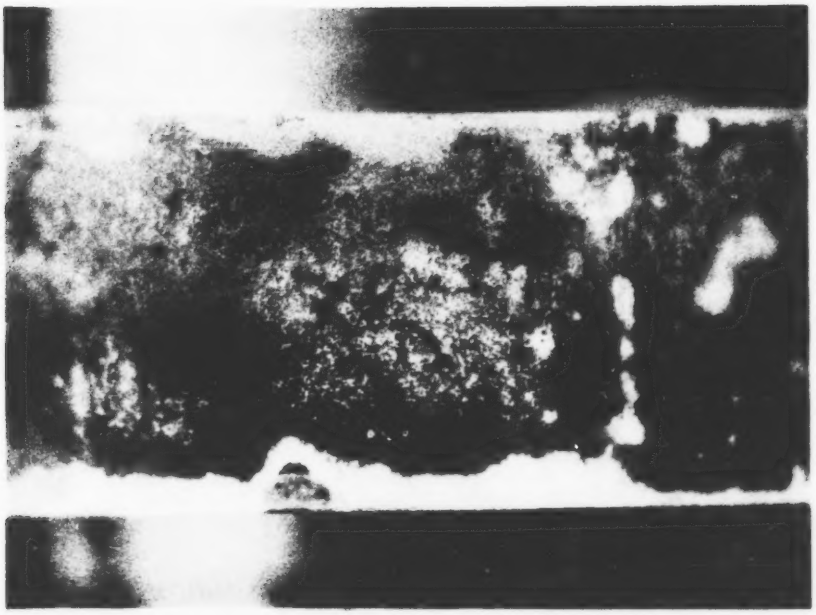

(a) Overall View 7.5x
(non-uniform general corrosion)

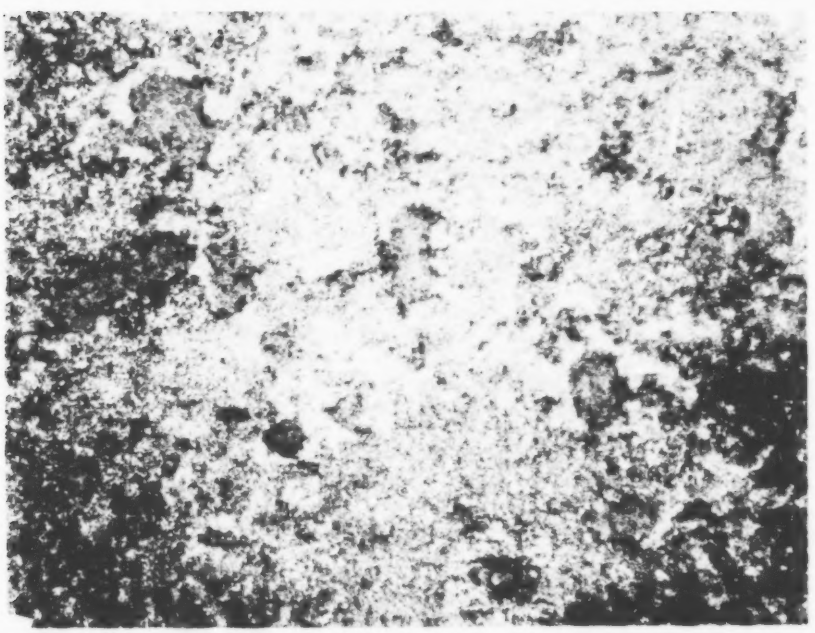

(b) Tube Surface 100x
(non-uniform general corrosion)

FIGURE 29

SURFACE APPEARANCE OF 70/30 TUBE SAMPLE FOLLOWING CYCLIC POTENTIODYNAMIC POLARIZATION (CPP) TESTING AT A SCAN RATE OF 0.25 V/HR AND INITIAL CONDITION OF 600 GRIT

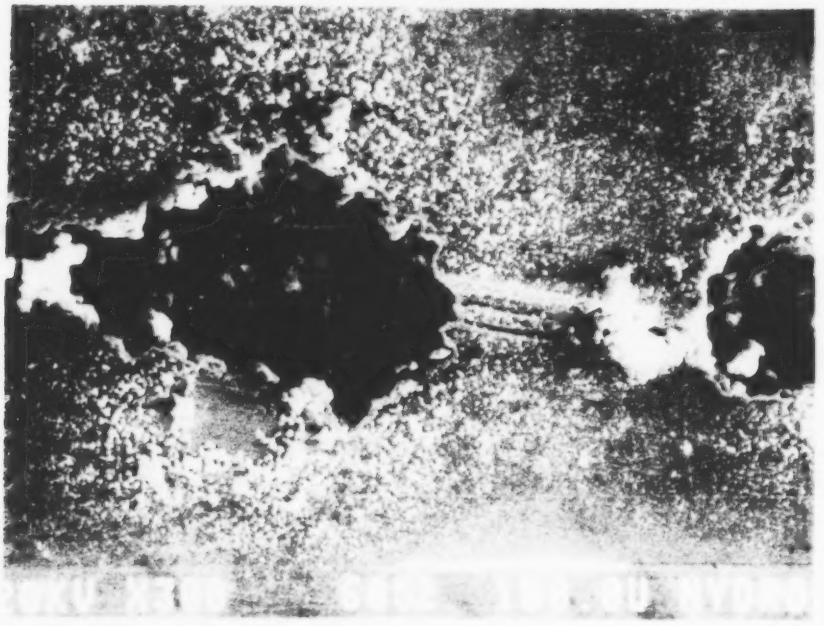

(a) 1825, 300X
(pit showing intergranular attack in base)

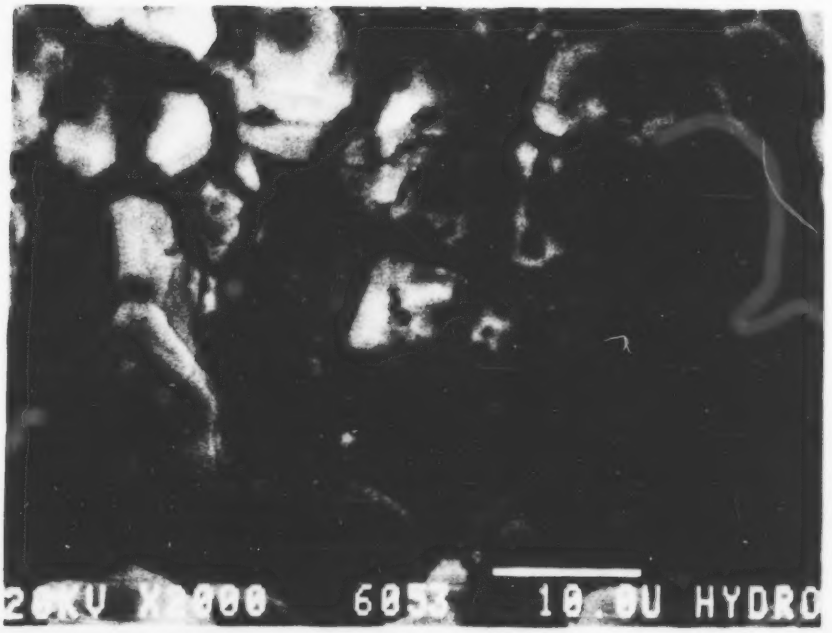

(b) 1825, Detail of Pit in (a) 200X
(intergranular attack)

FIGURE 30

DETAILED EXAMINATION OF PITS ARISING FROM CYCLIC POTENTIODYNAMIC POLARIZATION TESTING (SCAN RATE 0.25 V/HR, 600 GRIT)

(c) 1800, 300X
(pits showing undercutting)

(d) 1800, 150X
(pits showing undercutting)

(e) 1800, 300X
(intergranular attack)

FIGURE 30

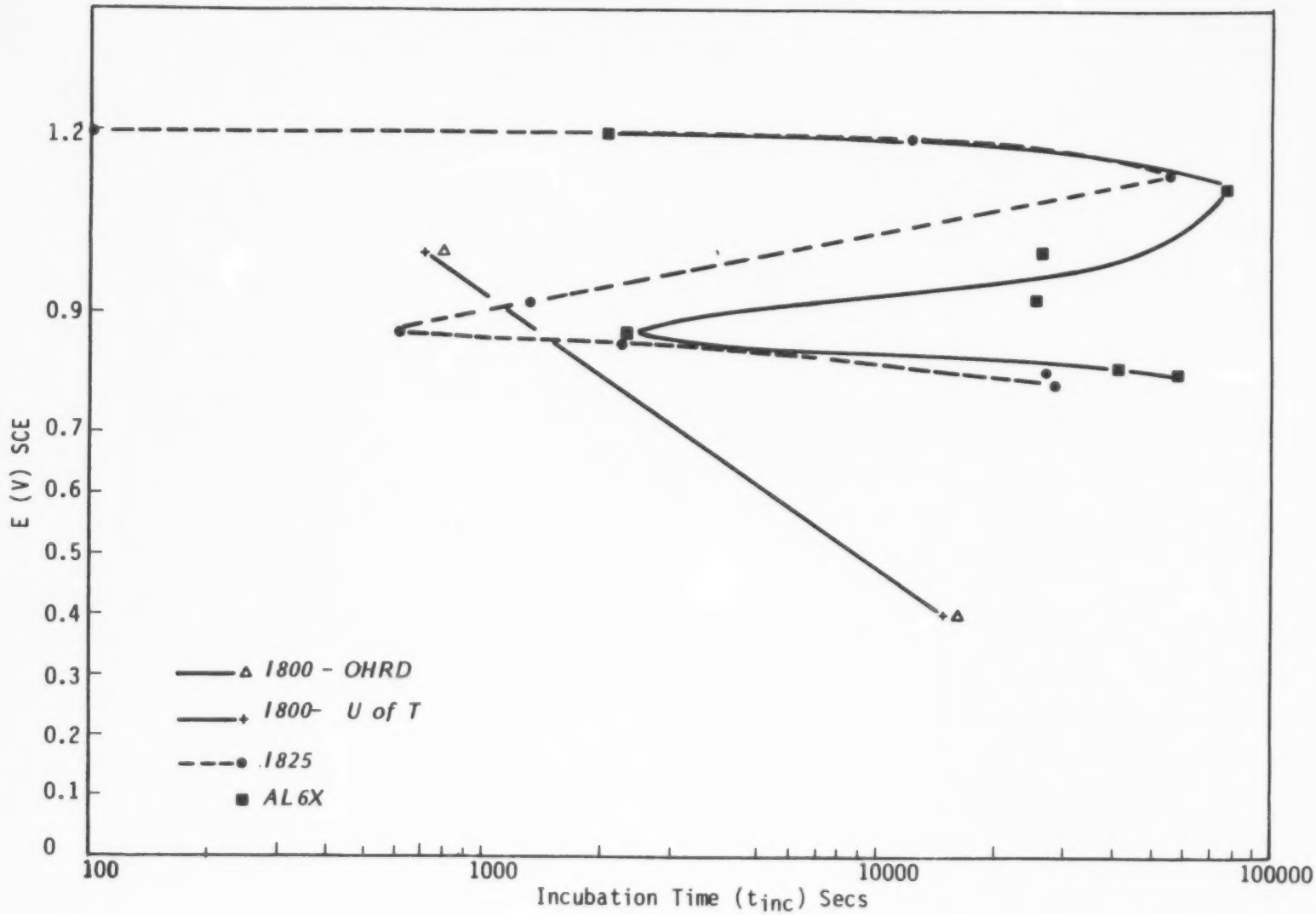

FIGURE 31

PIT INDUCTION TIMES (t_{inc}) VS APPLIED POTENTIAL (E)
FOR 1800, 1825 AND AL6X
(Note: Visual curve fitting based on experience with other materials - see Reference 30)

(a) 904L Isothermal, 40°C, 16w
(surface deposit covering pit)

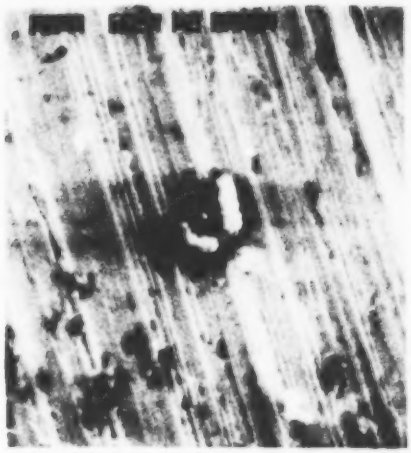

(b) S28 Isothermal, 40°C, 24w
(surface deposit)

(c) 1825 Isothermal, 40°C, 24w
(pits with surface deposit)

(d) 1800 Isothermal, 40°C, 16w
(surface deposits at
silt-water interface)

(e) M400 Isothermal, 40°C, 16w
(surface deposit)

(f) 70/30 Isothermal, 40°C, 16w
(surface deposit)

FIGURE 32

DETAILED EXAMINATION OF SAMPLES FOLLOWING
IMMERSION TESTING (SEE TABLE 7)

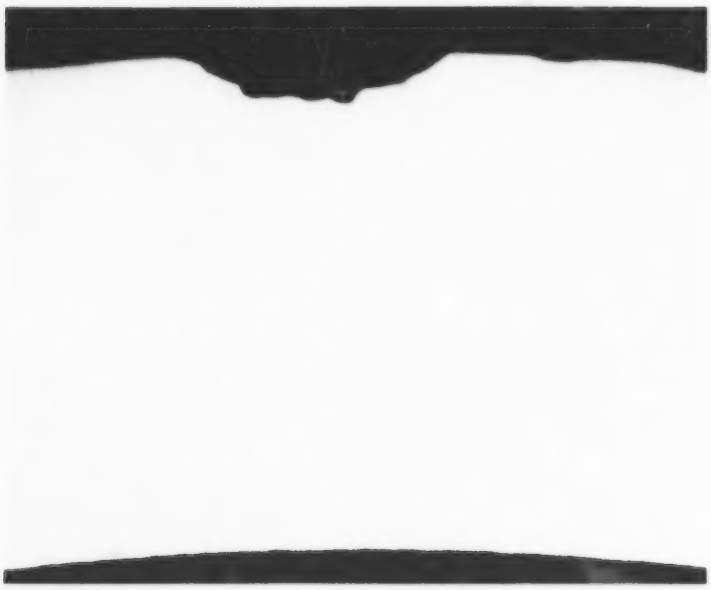

(g) 904L Heat Flux 24w, 40x
(Cross-Section of Pit)

(h) 1825 Heat Flux 8w, 100x
(Pit & Staining)

(i) 1800 Heat Flux, 24w, 15x
(Cross-Section Through Tube Wall at Pit)

FIGURE 32

DETAILED EXAMINATION OF SAMPLES FOLLOWING IMMERSION TESTING (SEE TABLE 7)

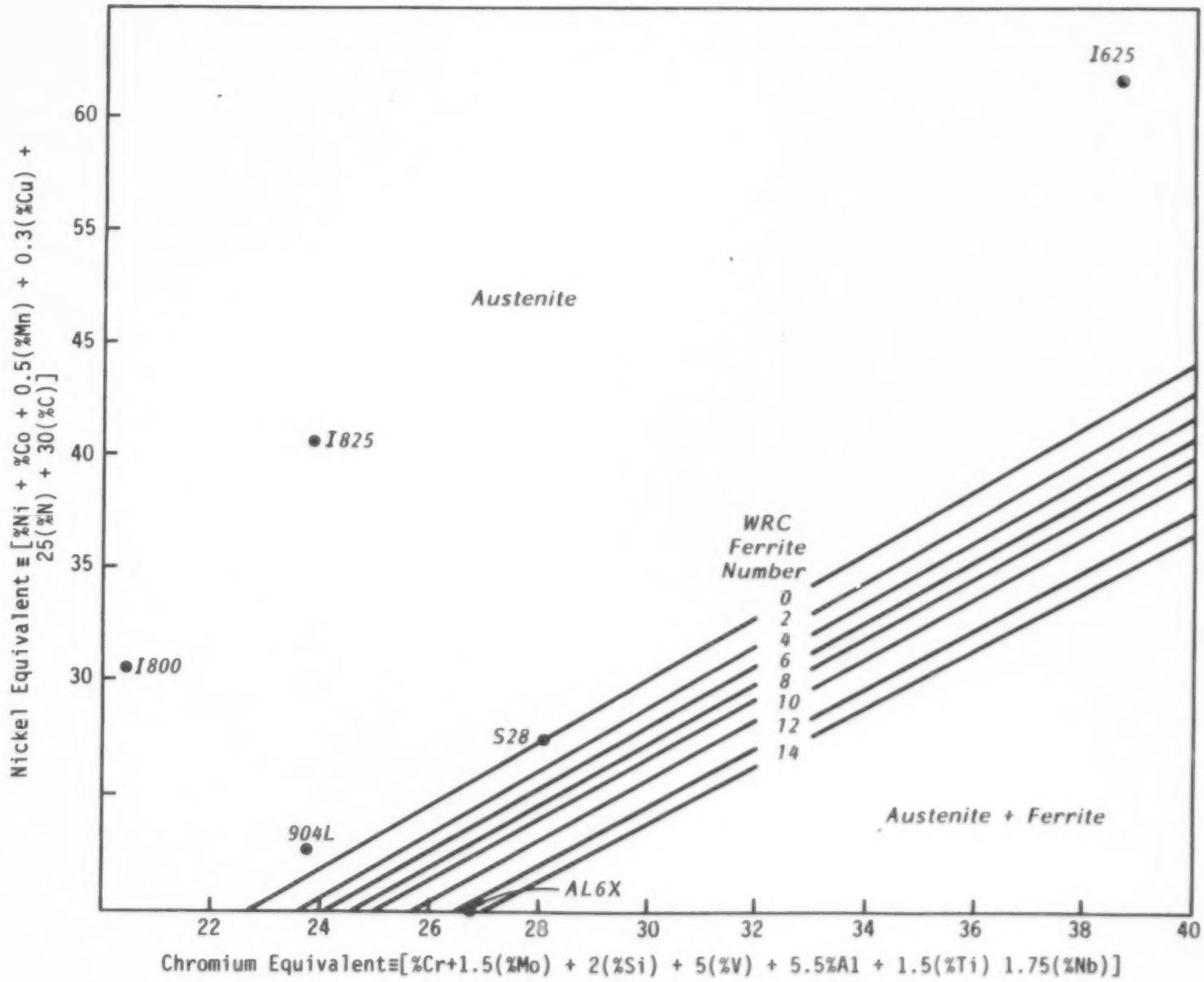

FIGURE 33

NICKEL AND CHROMIUM EQUIVALENTS FOR Fe-Cr-Ni (-Mo) AUSTENITIC ALLOYS
SCHNEIDER, H., FOUNDRY TRADE J., 1960, 108, P. 562

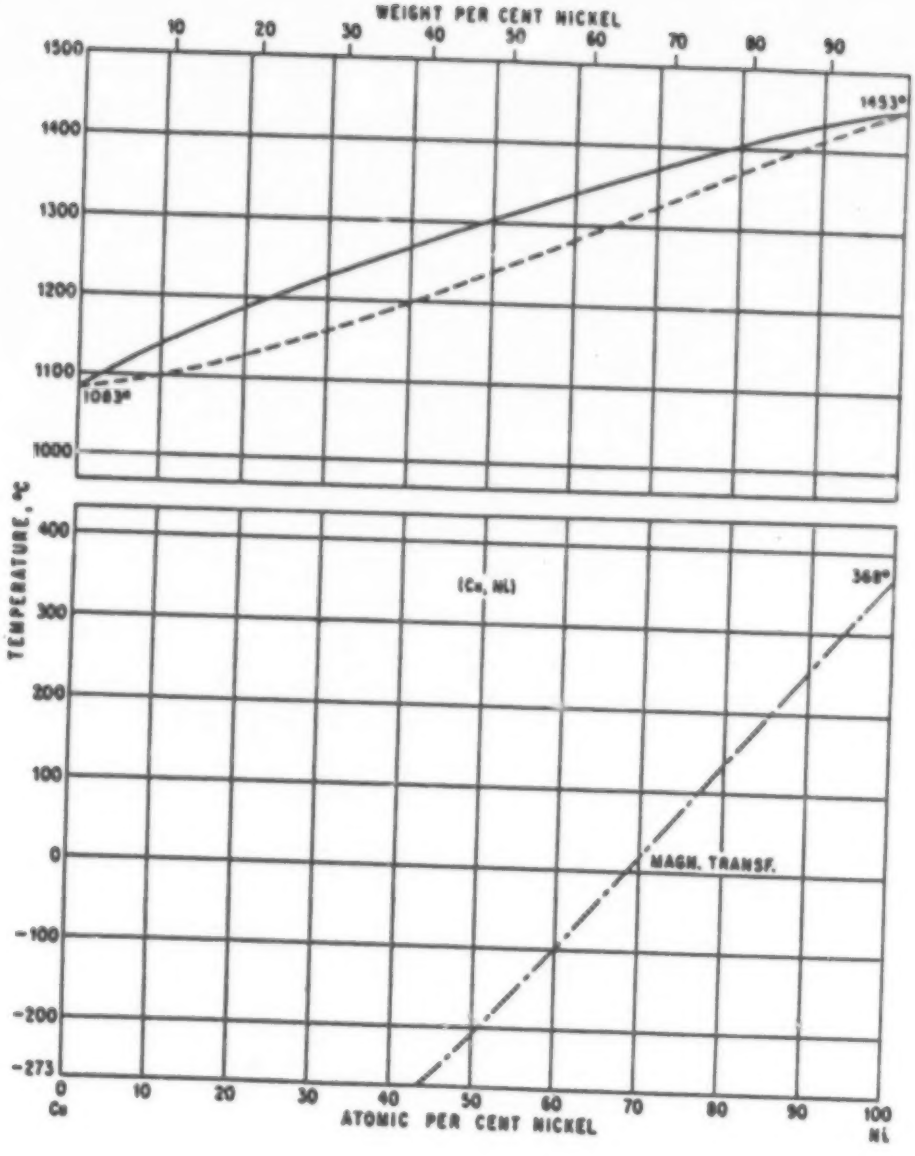

FIGURE 34

BINARY PHASE DIAGRAM Ni-Cu SYSTEM

REFERENCES

1. P. Lichtenberger, Memo to J. Brown, File No 04660, 84-06-01.

2. B. Warr, Memo to P. Lichtenberger, File N 827.2(T), 84-06-15.

3. N.D. Martin, Memo to B. Warr, 85-5-17.

4. R. Barton, Ontario Hydro Nuclear Plant HX Data, unpublished.

5. W. Babe, Presentation to Darlington NGS Staff, Darlington NGS 'A', Heat Exchangers 85-02-15.

6. E.T.C. Ho, "Failure ot Pickering Moderator HXs in Units 1 and 3", Ontario Hydro Research Division Report No 79-158-K.

7. G. Bellamy, "Condition of 70/30 Alloy Moderator HX Tubes, Unit 2, Pickering NGS 'A'", Ontario Hydro Research Division Report No M84-6-K.

8. G. Bellamy, "Pitting of Incoloy 800 Moderator HX Tubing, Unit 3, Pickering NGS 'A', Ontario Hydro Research Division Report No M83-173-K.

9. G. Bellamy, "Leakage of Moderator HX Tubing, Unit 3, Pickering NGS 'A', Ontario Hydro Research Division Report No M82-206-K.

10. G. Bellamy, "Pitting of Pickering NGS 'B' M400 Shutdown Cooler Tubing", Ontario Hydro Research Division Report No 84-352-K.

11. D.E. Williams et al, "The Statistical Approach to the Study ot Localized Corrosion", UK Atomic ENergy Authority AERE-R-10832, March 1983.

12. T. Shibata and T. Takeyama, Corrosion, 33, 243, (1977).

13. M. Urquidi and D.D. MacDonald, J.E.C.S., 132, 555, (1985).

14. M. Moriya, and M.B. Ives, Corrosion, 40, 105, (1985).

15. W.U. Yang et al, Corrosion Science, 24, 691, (1984).

16. T. Komada and J. Ambrose, Corrosion, 33, 155, (1977).

17. I.P. Ijsseling, Br. Corrosion J., 15, 51, (1980).

18. H.C. Man and D.R. Gabe, Corrosion Science, 21, 713, (1981).

19. M. Janik-Czachor et al, Br. Corrosion J., 15, 154, (1980).

20. Z. Szkborska-Smialowska, Corrosion, 27, 233, (1971).

21. A.J. Sendriks, "Corrosion of Stainless Steels", J. Wiley, NY, 1979, p. 63.

22. G. Bellamy, Ontario Hydro Research Division Report No 81-70-K.

23. S. Lawson, Memo to B. Warr, HX Materials Performance, File No 823.421(P), 83-10-21.

24. R. Tapping, T. Lavoie and B. Cheung, CRNL 2482, July 1983.

25. W.F. Heaton et al, J.I. Mech. E., (1979).

26. Climax Molybdenum Co., "Advanced Stainless Steels for Seawater Applications", Proc. Symp., University Piaccaza, Italy, Feb 28, 1980.

27. H. Schneider, Foundry Trade J., 108, 562, (1960).

28. M. Hansen, Constitution of Binary Alloys, McGraw-Hill 1958, ISBN 07-0260508.

29. G. Palumbo, "Pitting Corrosion of Incoloy 800 Report No 1, Pit Nucleation Processes in Lake Water Environments", University of Toronto, 83-9-21.

30. S.J. Thorpe, Ph.D. Thesis, University of Toronto, 1985, p. 121.

(a) x 200

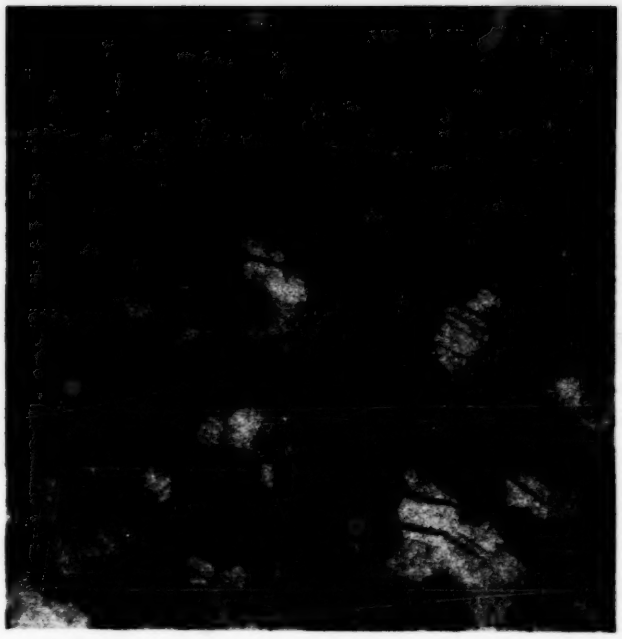

(b) x 200

Cross-Section Through Wall

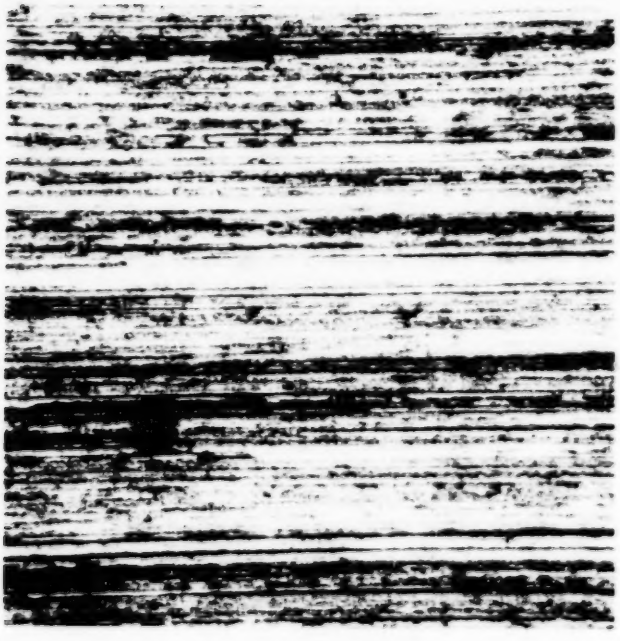

(a) x 100

(b) x 100

Plan View

APPENDIX 1 FIGURE 1

MICROSTRUCTURE AT SURFACE AND SURFACE CONDITION OF TUBE AND PLATE MATERIAL FOR Ti

(a) PLATE (b) TUBE

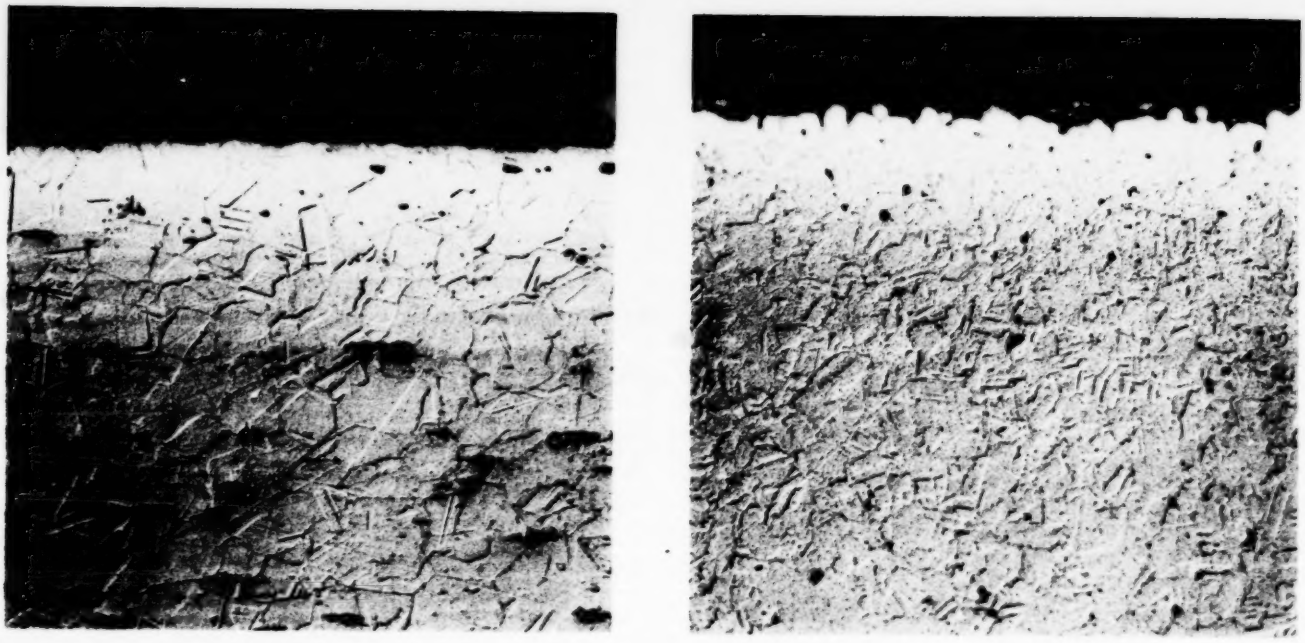

(a) x 250 (b) x 400

Cross - Section Through Wall

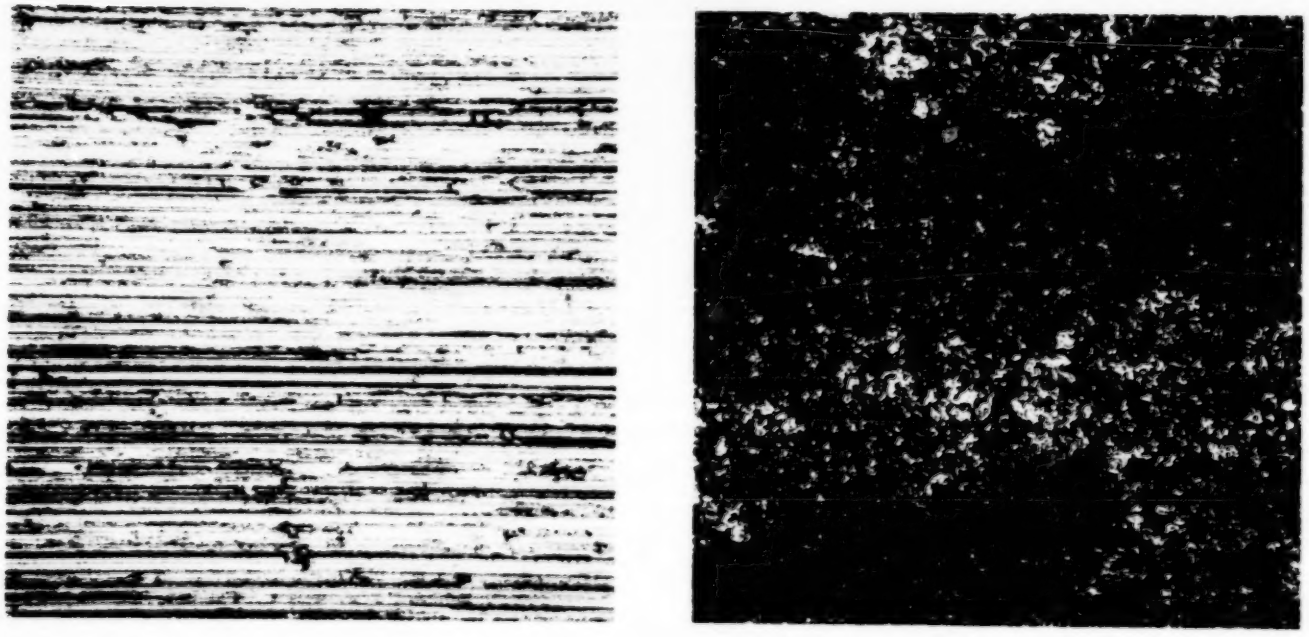

(a) x 100 (b) x 100

Plan View

APPENDIX 1 FIGURE 2

MICROSTRUCTURE AT SURFACE AND SURFACE CONDITION OF TUBE AND PLATE MATERIAL FOR 1625

(a) PLATE (b) TUBE

(a) x 200

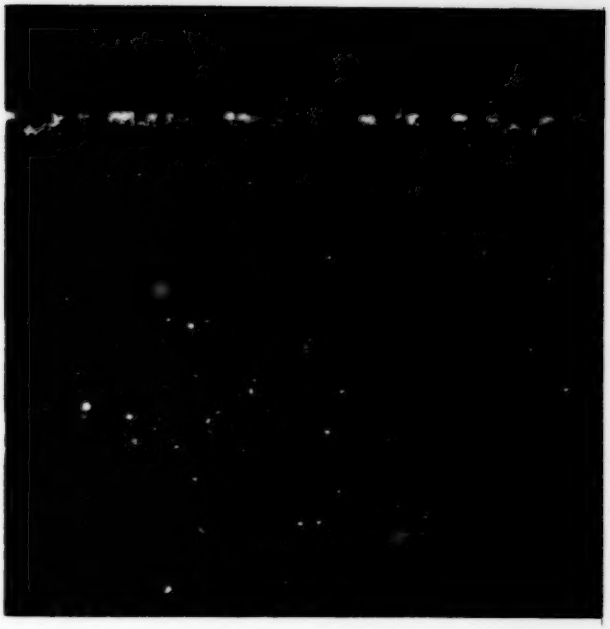

(b) x 200

Cross-Section Through Wall

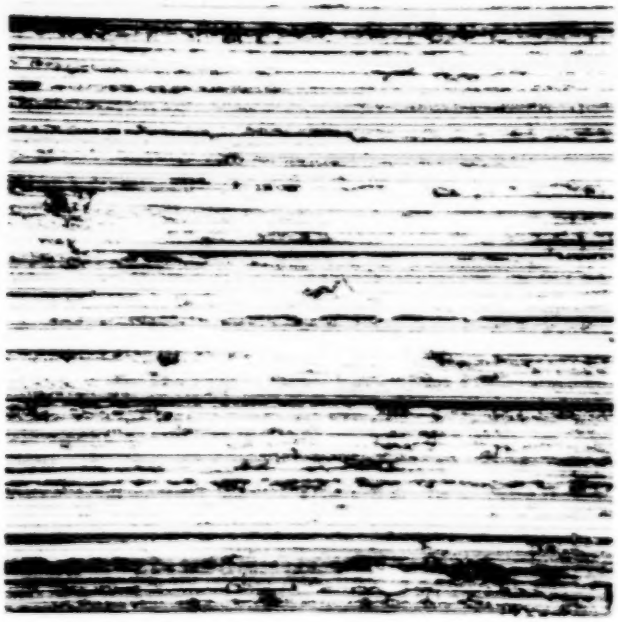

(a) x 100

(b) x 100

Plan View

APPENDIX 1 FIGURE 3

MICROSTRUCTURE AT SURFACE AND SURFACE CONDITION OF
TUBE AND PLATE MATERIAL FOR AL6X
(a) PLATE (b) TUBE

(a) x 200

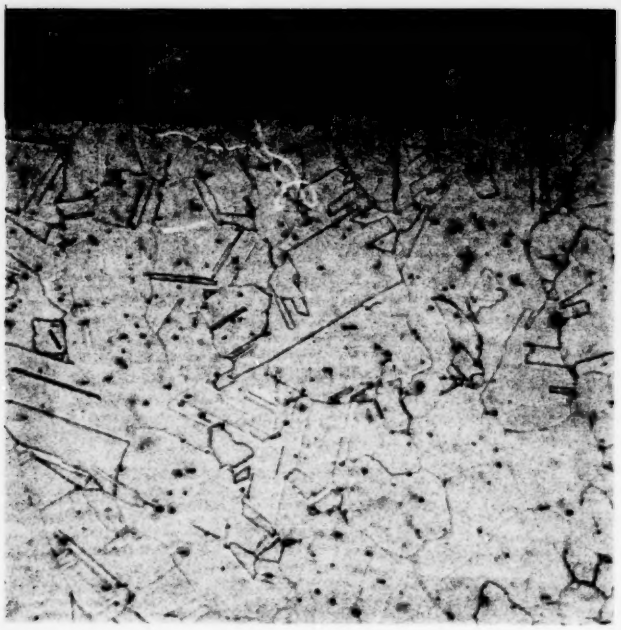

(b) x 200

Cross-Section Through Wall

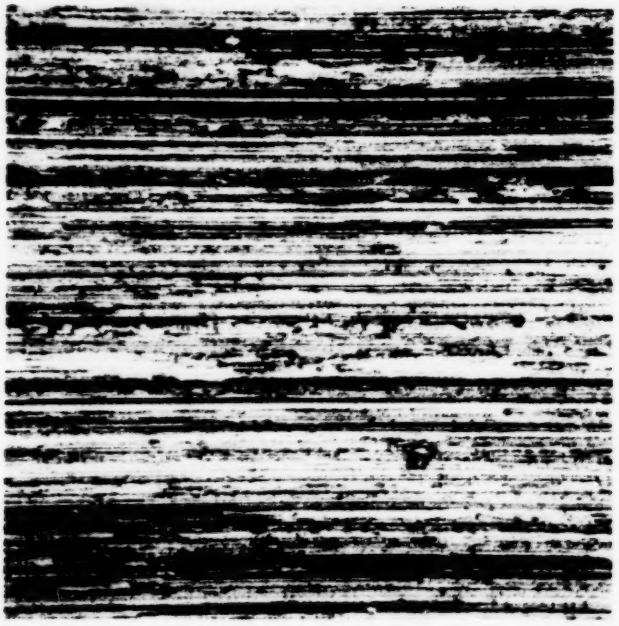

(a) x 100

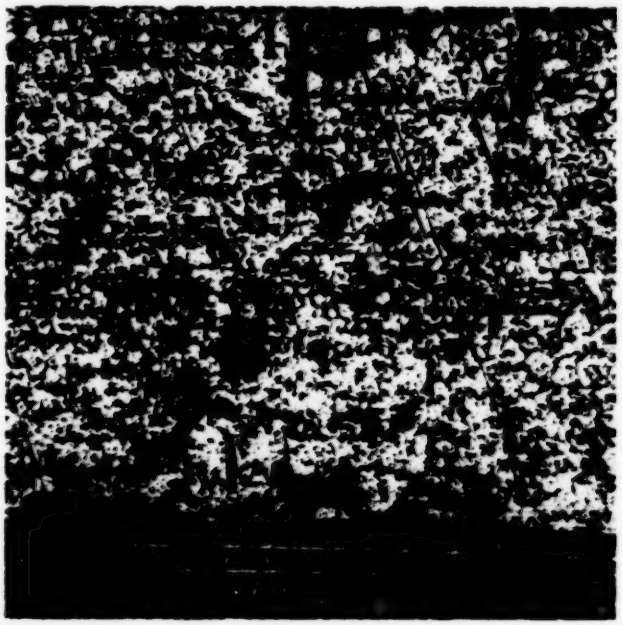

(b) x 100

Plan View

APPENDIX 1 FIGURE 4

MICROSTRUCTURE AT SURFACE AND SURFACE CONDITION OF TUBE AND PLATE MATERIAL FOR 904L
(a) PLATE (b) TUBE

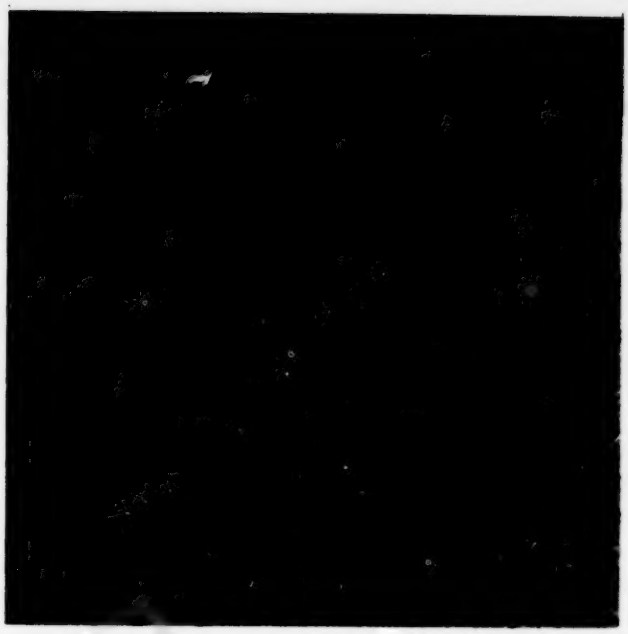

(a) x 200

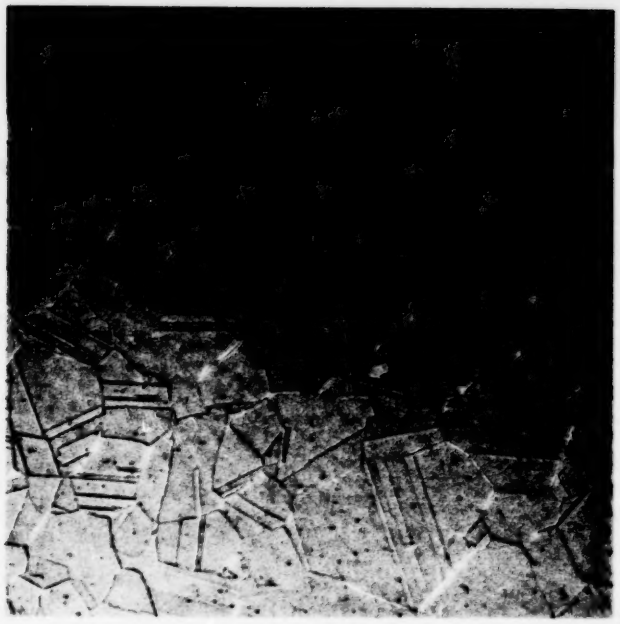

(b) x 200

Cross-Section Through Wall

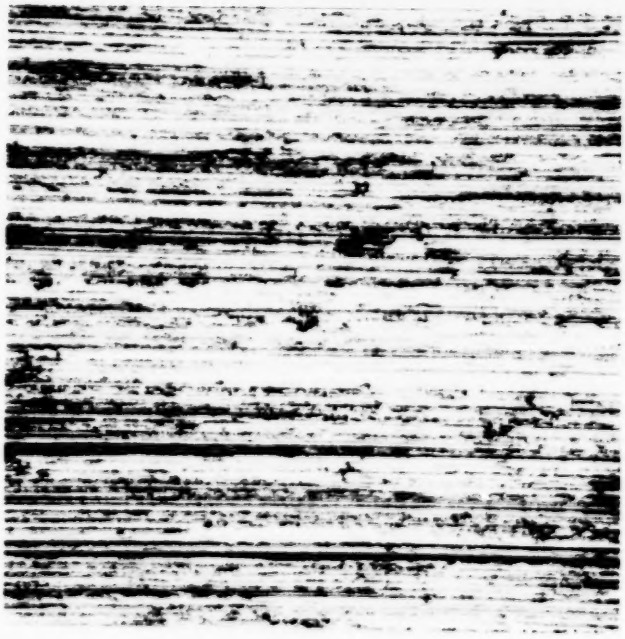

(a) x 100

(b) x 100

Plan View

APPENDIX 1 FIGURE 5

MICROSTRUCTURE AT SURFACE AND SURFACE CONDITION OF
TUBE AND PLATE MATERIAL FOR S28
(a) PLATE (b) TUBE

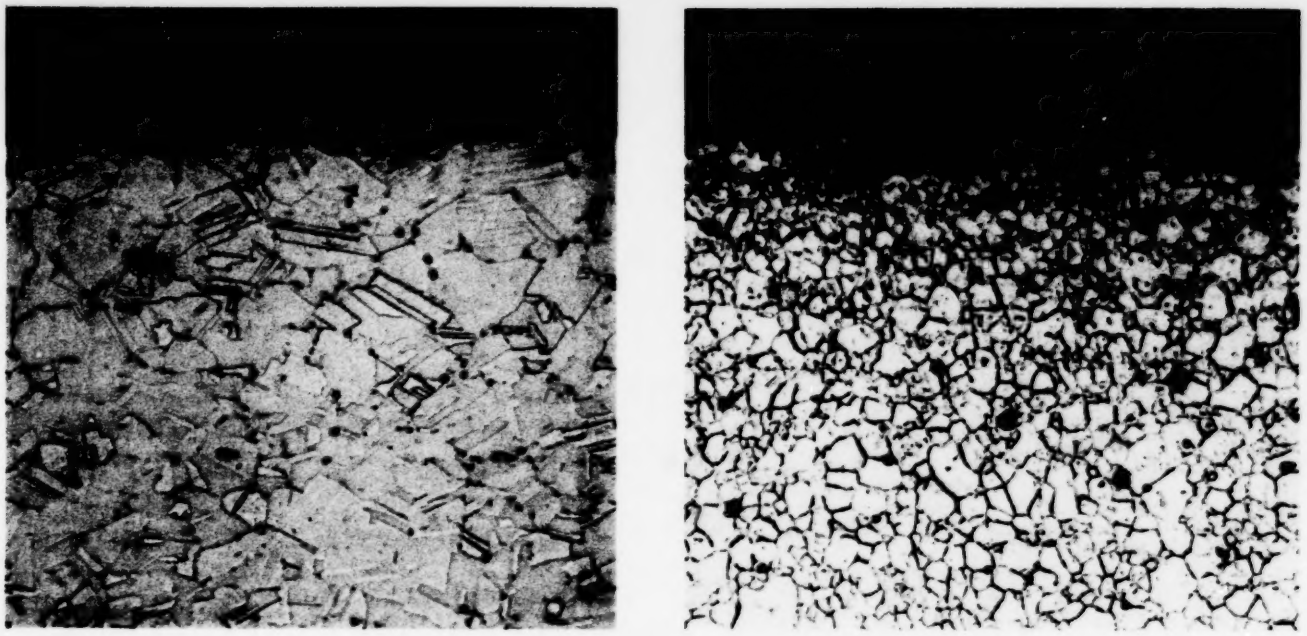

(a) x 400 (b) x 400

Cross-Section Through Wall

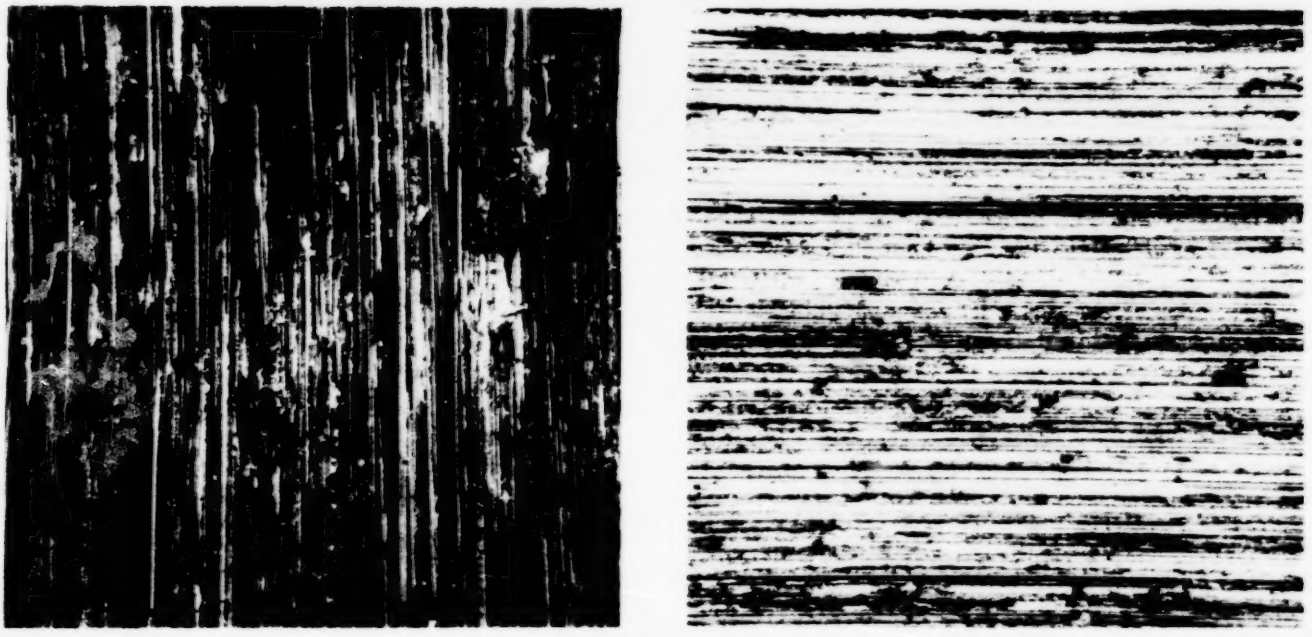

(a) x 100 (b) x 100

Plan View

APPENDIX 1 FIGURE 6

MICROSTRUCTURE AT SURFACE AND SURFACE CONDITION OF TUBE AND PLATE MATERIAL FOR I 825
(a) PLATE (b) TUBE

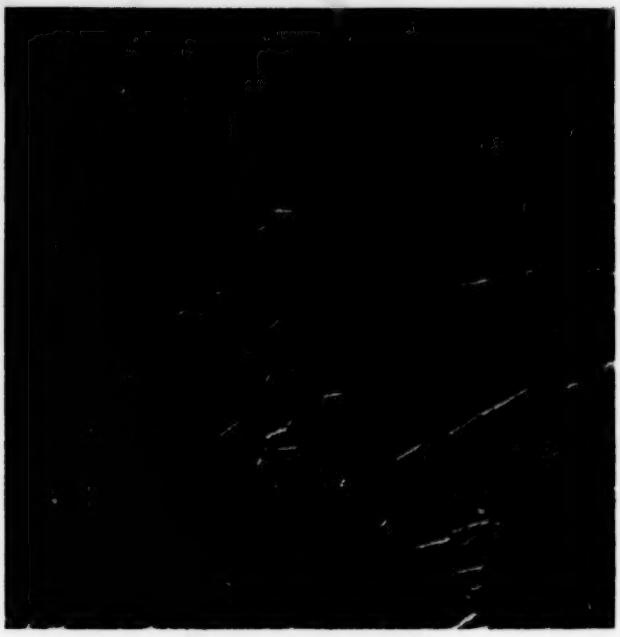

(a) x 400

(b) x 400

Cross-Section Through Wall

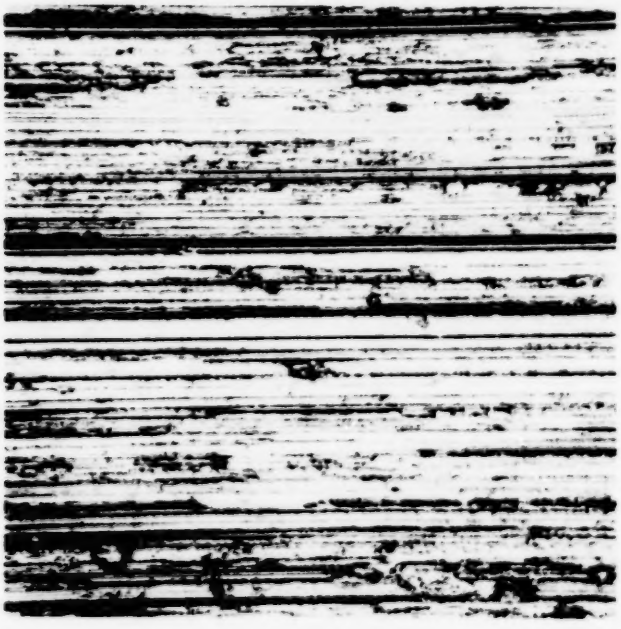

(a) x 100

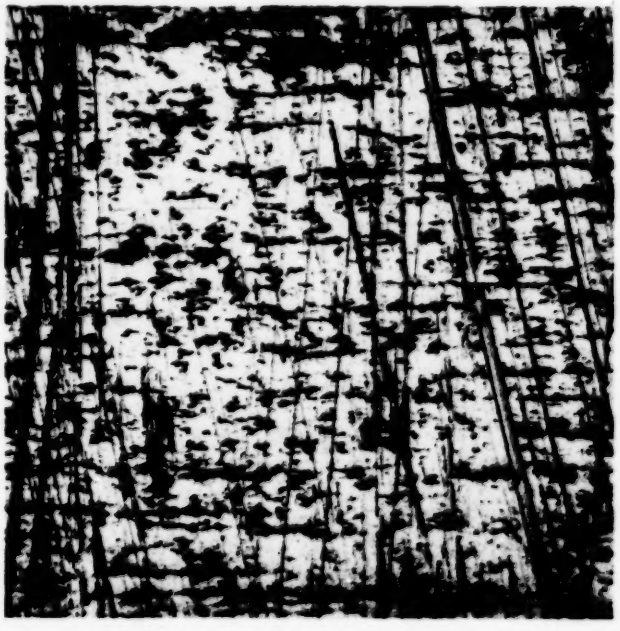

(b) 100

Plan View

APPENDIX 1 FIGURE 7

MICROSTRUCTURE AT SURFACE AND SURFACE CONDITION OF
TUBE AND PLATE MATERIAL FOR 1800
(a) PLATE (b) TUBE

(a) x 200

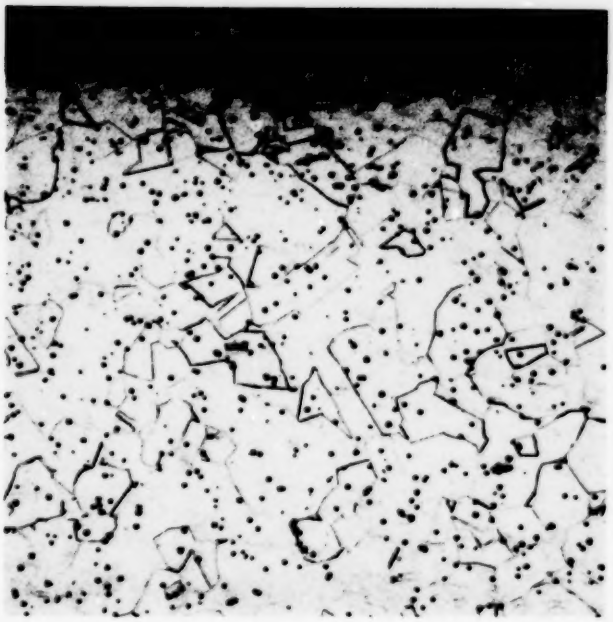

(b) x 200

Cross-Section Through Wall

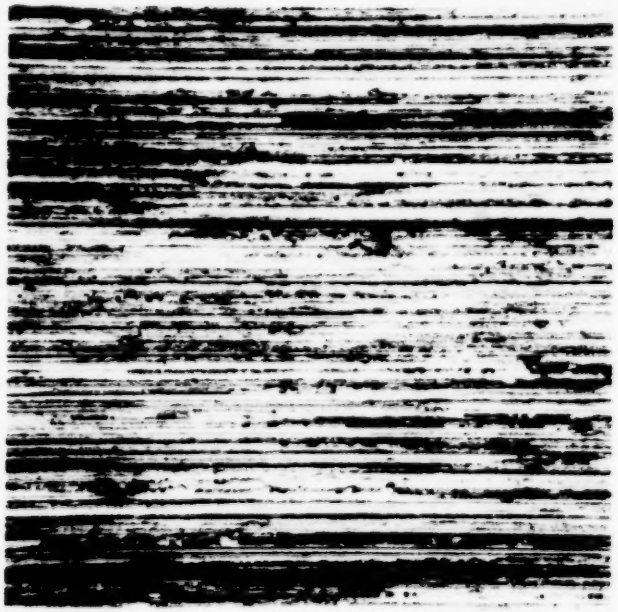

(a) x 100

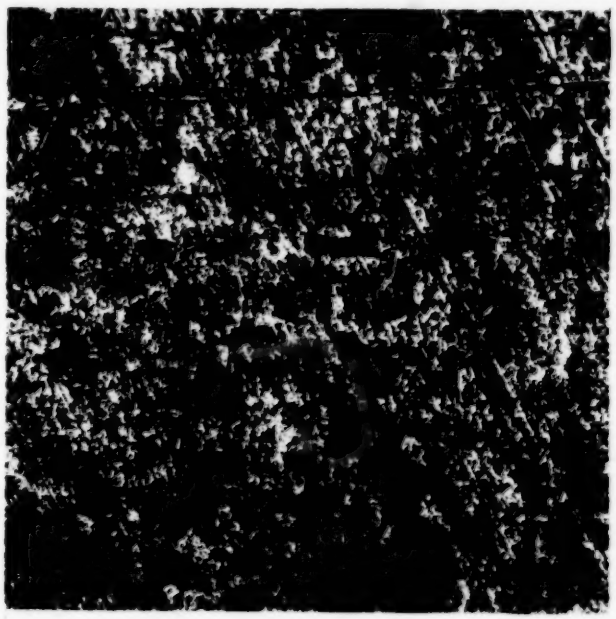

(b) x 100

Plan View

APPENDIX 1 FIGURE 8

MICROSTRUCTURE AT SURFACE AND SURFACE CONDITION OF TUBE AND PLATE MATERIAL FOR M400
(a) PLATE (b) TUBE

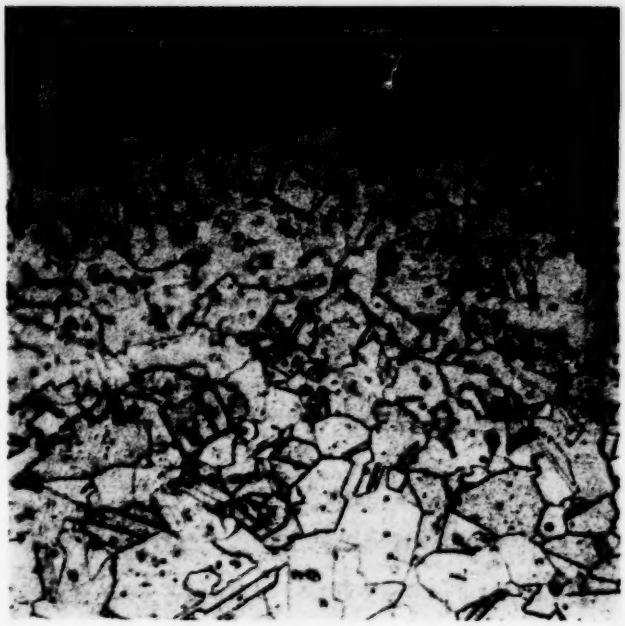

(a) x 400

(b) x 400

Cross-Section Through Wall

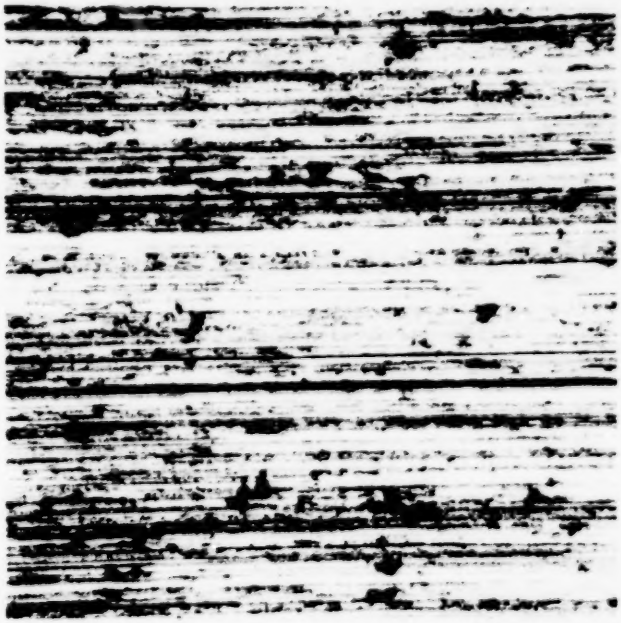

(a) x 100

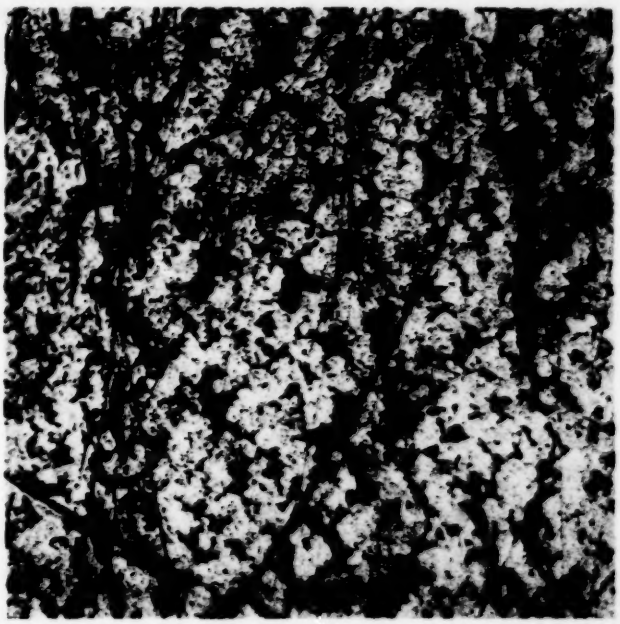

(b) x 100

Plan View

APPENDIX 1 FIGURE 9

MICROSTRUCTURE AT SURFACE AND SURFACE CONDITION OF TUBE AND PLATE MATERIAL FOR 70/30
(a) PLATE (b) TUBE